Transilvania
University
of Brasov
FACULTY OF
MECHANICAL ENGINEERING

THE 10TH INTERNATIONAL CONFERENCE ON ADVANCED COMPOSITE MATERIALS ENGINEERING

COMAT 2024

ISSN 2457 – 8541
ISSN – L 2457 - 8541

22-23 OCTOBER 2024
BRAŞOV, ROMANIA

Contents COMAT 2024

COMAT The 10th International Conference on ADVANCED COMPOSITE MATERIALS ENGINEERING

22-23 October 2024

THE ADVANTAGES OF MODERN DIMENSIONAL ANALYSIS IMPLEMENTING IN THE ADITIVE MANUFACTURING TECHNOLOGIES OPTIMIZATION

Zsolt Asztalos*[1], Maria-Luminita Scutaru[2], Sorin Vlase[3] , Renáta Ildikó Száva[4], Ioan Száva[5]

1. Transilvania University of Brasov, Brașov, Romania, zsolt.asztalos@unitbv.ro
2. Transilvania University of Brasov, Brașov, Romania, lscutaru@unitbv.ro
3. Transilvania University of Brasov, Brașov, Romania, svlase@unitbv.ro
4. Transilvania University of Brasov, Brașov, Romania, munteanurenata@yahoo.com
5. Transilvania University of Brasov, Brașov, Romania, eet@unitbv.ro

Abstract: *Nowadays the Additive Manufacturing (AM) represents a very promising manufacturing process, having several facilities and advantages in comparison with the classical manufacturing technologies. Also, one can underline that there are a huge number of unexplored directions, which assure for AM to becoming soon a very competitive manufacturing process, with undoubted low-cost-, reduced material consumption-, as well as optimal stiffness-, and competitiveness technology. In this sense, one of the less-explored ways represents exactly the involvement of the dimensional methods in gaining an optimal, high-competitive final product. Like this, instead of the real structural element, named prototype, the engineers will perform high-accuracy tests on the attached reduced-scale models, whose experimental results are extended to prototype by means of the deduced Model Law (ML). The authors, based on their previous theoretical as well as experimental investigations, offer a short overview of these advantages, based on Thomas Szirtes' approach of dimensional analysis, referred to below Modern Dimensional Analysis (MDA).*

Keywords: Additive Manufacturing (AM), Fuse Deposition Modelling (FDM), Geometric Analogy (GA), Theory of Similarity (TS), Modern Dimensional Analysis (MDA).

1. BRIEF OVERVIEW OF *AM*

Nowadays *AM* represents a very promising way to obtaining high quality-, cheap-, and low time-consumption-, as well as low pollution/waste products (unique components or spare parts, too). Since 1986, by Rapid Prototyping, the first complex products were obtained [1-4]. Later, the technology was applied not only for plastics, but also for plastic-metal, respectively only metal parts [5]. The Fuse Deposition Modelling (*FDM*), representing the authors' main field of analysis/investigation, was one of the earlier technologies [6-7]. It was followed by Power Bed Fusion processes, widely analyzed and applied [8-11]. The Sheet Lamination processes, which followed them, gained a huge and efficient application [12-15]. Nowadays, the Directed Energy Deposition,

respectively the Automated Fiber Placement techniques are widely and successfully applied [16-18]. The common casting technologies, combined with *AM*, offer several facilities and advantages both in obtaining complex final products and in improving their initial manufacturing process from point of view of cost, time, accuracy, waste amount, as well as durability. A fruitful combination of the plastic and metal layers, offers, mainly in the cases of the casting molds and cores manufacturing, new research directions. In these latter cases, due to the combination of the mechanical and thermal loadings, their stress-strain states become very complex and so, the involvement of the dimensional methods can represent a very promising modality/approach. It means that instead of the testing of the real structural element, named *prototype*, one can perform high-accuracy tests on an attached, reduced-scale one, named *model* [19-26]. It is well-known fact that in most cases, performing tests on the prototype is difficult, while on the model, they can be performed much easier, precisely, repeatable and cheaply. By the adequately deduced *ML*s, constituted strictly from dimensionless variables, one can extend the obtained results on model to the prototype, forecasting its (latter's) behaviors. In the following, the authors briefly review the main dimensional methods, together with their advantages and limits.

2. THE MAIN DIMENSIONAL METHODS AND THE PRINCIPLE OF *MDA* WITH ITS ADVANTAGES

In order to obtain easier and cheaper information on structural elements, as well as on large structures, mathematicians and engineers introduced the dimensional methods.

For the relatively simply cases the Geometric Analogy (*GA*) satisfies the imposed requirements. Here the geometric similarity is compulsory; it supposes rigorous proportionality of lengths, as well as angular equality for the prototype and the attached model. One can define homologous points, lines, surfaces and volumes; consequently, the attached model has a very limited flexibility with respect to the prototype. The Theory of Similarity (*TS*) solves a little bit more complex phenomenon, allowing both structural and functional similarity. In this case, the analyzed phenomena occurs so that, at homologous times, in homologous points, each involved η significant variable are described by distinct (separate)

$$S_\eta[-]=\frac{\eta_2}{\eta_1}=const. \tag{1}$$

constant ratio of the values, corresponding to model (η_2) and prototype (η_1).

The S_η dimensionless ratios are the so-called *scale factors*, which are always constant in time and space for the given phenomena; their number coincides with the involved variables' number.

In principle, instead of some solutions of complicated equations, one can apply relatively simply correlation between a reduced numbers of

$$\pi_j,\ j=1...n \tag{2}$$

dimensionless variables, which constitute the *ML*; at *TS*, they result by means of suitable grouping of the adequate terms of governing equations.

One has to mention, that the involvement of the above-mentioned *ML*s assure a significant diminishing of the measurement's volume.

For a large number of the dimensionless variables, the Classical Dimensional Analysis (*CDA*) was applied, based on the well-known Buckingham's π theorem.

At first sight, seems that *CDA* offers a relatively easy manner for analysis of complex phenomena. Upon closer analysis, we notice its main disadvantages, based between others on its difficulties in deducing the demanded/requested π_j, $j=1...n$ dimensionless variables.

One has to mention that for obtaining these π_j, $j=1...n$ dimensionless variables, *CDA* offers three main modalities, namely from:
the Buckingham's π theorem;
the partial differential equations applied to fundamental differential relations of the analyzed phenomenon, when the initial variables, by suitable grouping, offer these dimensionless quantities;
the complete, but in the same time the simplest equation(s) which describe the phenomena, which will be transformed into dimensionless forms, offering finally the desired π_j groups.

Consequently one can mention the main shortcomings of the *CDA*, namely:
the protocol in obtaining the desired set of π_j groups is rather chaotic, arbitrarily, and strongly depending on the ingenuity as well as of the involved specialist's experience;
for the involved specialist, there are required solid knowledge in the field of the analyzed phenomenon, as well as in higher mathematics, too;
only rarely (occasionally) can be obtained the complete *ML*, mainly due to the fact that there are only a limited number of the involved mathematical relations related to the phenomena;
for common engineers or specialists, involved in prototype-model correlation analysis, *CDA* dos not represents an easy approach.
Compared to this, the methodology developed by Szirtes [27-28], hereafter named Modern Dimensional Analysis (*MDA*), offers an efficient solution practically for all above-analyzed shortcomings.
Consequently, the *MDA* represents a simply, unitary, as well as particularly accessible methodology, with the following main advantages:
the involved specialist, instead of thorough connoisseur in the phenomenon as well as in higher mathematics, only has to identify the set of the involved variables, of course together with their dimensions, which have (or can present) a certain extent influence on the analyzed phenomena;
it has an unitary, simply and user-friend protocol, which assures at once to eliminate automatic all insignificant/irrelevant variables;
in all cases *MDA* assures obtaining the complete set of the π_j, $j=1...n$ dimensionless variables, as well as the complete *ML*; this is practically impossible the all afore-mentioned methods, excepting some particular cases;
this *ML* is very flexible, suitable for several particular cases, corresponding to simplified approaches of the phenomena;
by an a priori choosing/setting of the directly related variables to the conceived experimental investigations on model, hereafter named *independent variables*, *MDA* assures an additional flexibility, which represents a significant advantage,

non-existent in all the methods mentioned above; their a priori chose is possible/admitted both for the prototype and model;
this set (of the independent variables) assures defining the most suitable model, which will offer for the involved model the most simply, lower-cost testing conditions, safety, as well as repeatable experimental investigations;
The rest of the variables, hereafter named *dependent variables*, only for the prototype can be chosen a priori; their magnitudes for the model are strictly obtained by applying a given (suitable) element of the *ML*;
between the dependent variables there are also a small number of variables of the prototype, whose magnitude cannot be obtained more easily (with low cost or accessible experimental measurements) and whose determination is actually the purpose of this dimensional analysis; thus, these afore-mentioned prototype's variables are obtained by applying the *ML*;
furthermore, *MDA* removes the restriction of the geometric similarity of the model with the prototype, e.g. the shape of the cross-sections can be different at the model from the prototype; in this case, instead of selecting/choosing as independent variables the cross-sectional dimensions, one will substitute them by the I_z second order moment of inertia of cross-section;
if the material is considered as independent variable, choosing by mean of E Young modules, than one can accept different material for the model, respectively for the prototype;
in the case of choosing instead of them the $E \cdot I_z$ flexural stiffness (rigidity), than neither the shape of the cross-section, nor the type of material must be identical in the prototype and model; the single request/condition remaining that their

$$S_{E \cdot I_z} = \frac{E_2 \cdot I_{z,2}}{E_1 \cdot I_{z,1}} \tag{3}$$

scale factor to remain the same (to be constant), with the afore-mentioned indexing (2- for model and 1-for prototype).
Of course, this evaluation can be continued, but only these, afore-mentioned facilities underline the suitability of *MDA* in *AM* process optimization.

3. CONCLUSIONS

Based on the authors' previous theoretical and experimental investigations, including *ML*s' validation for different structural elements manufactured by *AM* [29-31], one can conclude the followings:
The *MDA* offers several incontestable facilities, starting from choosing different materials up to adopting different shape of cross-sections for prototype and model;
It represents a simply, unitary, as well as particularly accessible methodology;
the involved specialist, instead of thorough connoisseur in the phenomenon as well as in higher mathematics, only has to identify the set of the involved variables, of course together with their dimensions, which have (or can present) a certain extent influence on the analyzed phenomena;
it assures at once to eliminate automatic all insignificant/irrelevant variables;
in all cases *MDA* assures obtaining the complete set of the π_j, $j = 1...n$ dimensionless variables, as well as the complete *ML*; this is practically impossible the all afore-mentioned methods, excepting some particular cases;

this *ML* is very flexible, suitable for several particular cases, corresponding to simplified approaches of the phenomena;
the deduced *ML* for a complex phenomenon it can serve to obtain particular cases, with more simply and cheapest models;
in addition, the deduced *ML* for a given structural element, allows its application (extension) to complex structures, made of these structural elements, by taking into account the homologous points of the structure in relation to the basic structural element.
All of these advantages can be followed in the authors' previous mentioned works. Among the following goals of the authors is the analysis of complex structures, made of several materials (plastic combined with metals), obviously through *AM* technology, with immediate application to molds for casting unique pieces, respectively of complex shapes.

REFERENCES

[1] Anderson, D. M., Design for manufacturability & concurrent engineering: How to design for low cost, design in high quality, design for lean manufacture, and design quickly for fast production. CIM press, 2004.

[2] Boyard, N., Rivette, M., Christmann, O., Richir, S., "A design methodology for parts using additive manufacturing," in High Value Manufacturing: Advanced Research in Virtual and Rapid Prototyping: Proceedings of the 6th International Conference on Advanced Research in Virtual and Rapid Prototyping, 2013.

[3] Gibson, I., Rosen, D.W., Stucker, B., "Additive Manufacturing Technologies," pp. 17–40, 2010.

[4] Jasiuk, I., Abueidda, D.W., Kozuch, C., Pang, S.Y., Su, F.Y., McKittrick, J., An Overview on Additive Manufacturing of Polymers. JOM 2018, VL 70, IS 3, pp.275-283, DI 10.1007/s11837-017-2730-y

[5] Bai, L. et al., Additive Manufacturing of Customized Metallic Orthopaedic Implants: Materials, Structures, and Surface Modifications, Metals 2019, 9, 1004; doi: 10.3390/met9091004.

[6] Mertkan, I.A., Tezel, T., Kovan, V., Surface and Dimensional Quality of Thermoplastics Manufactured by Additive Manufacturing-based Hybrid Manufacturing, Research Square, DOI: https://doi.org/10.21203/rs.3.rs-2229678/v1

[7] Micali, L.M., Characterisation of Mechanical Properties of 3D Printed Continuous Carbon Fibre Reinforced Composites, PhD thesis, Politecnico di Torino, Italy, 2018

[8] Leicht, A., Rashidi, M., Klement, U., Hryha, E., Effect of process parameters on the microstructure, tensile strength and productivity of 316l parts produced by laser powder bed fusion. Materials Characterization, 159:110016, 2020.

[9] Miyagi, M., Wang, J., Keyhole dynamics and morphology visualized by insitu X-ray imaging in laser melting of austenitic stainless steel. Elsevier, Journal of Materials Processing Technology, 282, 116673 (2020).

[10] M. Nikzad, S. H. Masood, I. Sbarski, A. Groth, "A Study of Melt Flow Analysis of an ABS-Iron Composite in Fused Deposition Modelling Process," vol. 14, no. June, pp. 29–37, 2009.

[11] Parandoush, P., Lin, D., A review on additive manufacturing of polymer-fibre composites. COMPOSITE STRUCTURES 2017, VL 182, pp.36-53, DI 10.1016/j.compstruct.2017.08.088.

[12] Ponche, R., Kerbrat, O., Mognol, P., Hascoet, J. Y., "A novel methodology of design for Additive Manufacturing applied to Additive Laser Manufacturing process," Robot. Comput. Integr. Manuf., vol. 30, no. 4, pp. 389–398, 2014.

[13] Sing, S.L., Yeong, W.Y., Process-Structure-Properties in Polymer Additive Manufacturing. POLYMERS 2021, VL 13, IS 7, AR 1098, DI 10.3390/polym13071098

[14] Thompson, M. K. et al., "CIRP Annals - Manufacturing Technology Design for Additive Manufacturing : Trends , opportunities , considerations , and constraints," CIRP Ann. - Manuf. Technol., vol. 65, no. 2, pp. 737–760, 2016.

[15] Vayre, B., Vignat, F., Villeneuve, F., "Designing for Additive Manufacturing," Procedia CIRP, vol. 3, pp. 632–637, Jan. 2012.
[16] Ye, J., Khairallah, S.A., Rubenchik, A.M., Crumb, M.F., Guss, G., Belak, J., Matthews, M.J., Energy coupling mechanisms and scaling behaviour associated with laser powder bed fusion additive manufacturing. Advanced Engineering Materials, 21(7):1900185, 2019.
[17] Zhao, C., Parab, N.D., Li, X., Fezzaa, K., Tan, W., Rollett, A.D., Sun, T., Critical instability at moving keyhole tip generates porosity in laser melting. Science, 370(6520):1080–1086, 2020.
[18] *** "ASTM International, WK 38342: New Guide for Design for Additive Manufacturing".
[19] Baker, W. et al., Similarity Methods in Engineering Dynamics, Elsevier, Amsterdam, 1991.
[20] Barenblatt, G. I., Scaling, Self-similarity, and Intermediate Asymptotics. Cambridge, UK: Cambridge University Press, 1996.
[21] Barenblatt, G. I., Scaling, volume 34. Cambridge University Press, 2003.
[22] Bhaskar, R.; Nigam, A., Qualitative Physics using Dimensional Analysis. Artificial Intelligence, 1990, 45(1-2), pp.73-111, 10.1016/0004-3702(90)90038-2
[23] Bridgman, P.W., Dimensional Analysis, Encyclopaedia Britannica. Encyclopaedia Britannica, Chicago, pp. 439–449, 1969.
[24] Butterfield, R., Dimensional analysis revisited, Proc. Instn. Mech. Engrs. Vol 215 Part C, ImechE, pp. 1365-1375, 2001.
[25] Buckingham, E., On Physically Similar Systems: illustrations of the use of dimensional equations, Physical Review, 1914, 4(4), 2nd Series, p. 345.
[26] Calvetti, D., Somersalo, E., Dimensional analysis and scaling. The Princeton Companion to Applied Mathematics, Princeton University Press, Princeton, NJ, USA, pages 90–93, 2015.
[27] Szirtes, Th. The Fine Art of Modelling, SPAR Journal of Engineering and technology, 1992, 1,p. 37.
[28] Szirtes, Th. Applied Dimensional Analysis and Modelling, McGraw-Hill, Toronto, 1998
[29] Asztalos, Zs., Modern Dimensional Analysis implemented in spare parts' analysis obtained by Rapid Prototyping, Diploma work, Transylvania University of Brasov, 2021.
[30] Asztalos, Z.; Száva, I.; Vlase, S.; Száva, R.I. Modern Dimensional Analysis Involved in Polymers Additive Manufacturing Optimization. Polymers 2022, 14, 3995. https://doi.org/10.3390/polym14193995
[31] I. Száva, S. Vlase, M.L.Scutaru, Zs. Asztalos, B.P. Gálfi, A. Șoica, S. Șoica, Dimensional Methods Used in the Additive Manufacturing Process, https://doi.org/10.3390/polym15183694Published: 07 September 2023 in Polymers

COMAT The 10th International Conference on ADVANCED COMPOSITE MATERIALS ENGINEERING

Transilvania University of Brasov
FACULTY OF MECHANICAL ENGINEERING

22-23 October 2024

STUDY ON NEW CONCEPT OF AIRCRAFT FRAME - PAX CROSSBEAM CONNECTION

Bencze Andrei*[1], Buican George[2]

1. University Transilvania of Brașov, Brașov, Romania, andrei.bencze@unitbv.ro
2. University Transilvania of Brașov, Brașov, Romania, buican.george@unitbv.ro
*Corresponding author: andrei.bencze@unitbv.ro

Abstract: *The paper is presenting a study on a new concept of an aircraft frame to passenger floor crossbeam connection. The current standard in the industry consists in a fastened joint (large bolt field) between the aircraft frame's web and the web of the crossbeam profile. This extremely rigid connection also transfers, on top of the axial loads, bending moments between the parts, which leads to high stresses and strains in the area. In order to mitigate these high local loads, the parts require increased stiffness, leading to increased weight. The new proposed concept consists of an articulated connection that transfers only axial loads, while the bending moments are not transferred any more. A Finite Element Analysis (FEA) is carried out for both standard and new concept, on isotropic materials (metallic) components. Results (deformations, stress and strains) are compared in order to determine the new concept behavior.*

Keywords: *new concept, frame-crossbeam connection, composite materials, stress, strain*

1. INTRODUCTION

The main two goals in the aviation industry are to increase the safety of flight (which is already at a high level) and to reduce the costs. Both of these goals are followed from the beginning of the design phase and into the operational phase, until the end of the aircraft life cycle.

In general, most components are already optimized in terms of weight to cost ratio, while reducing the weight is one of the main driving factors accounted in the final cost. Nevertheless, there are highly stressed areas and components that need additional material to sustain the loads from the worst possible case.

This leads to additional weight that increase the manufacturing and operational costs and reduce the maximum passenger and cargo capacity.

One of these highly loaded areas is the connection between the passenger (noted as Pax) Crossbeam and the Frame, as marked in Fig. 1.

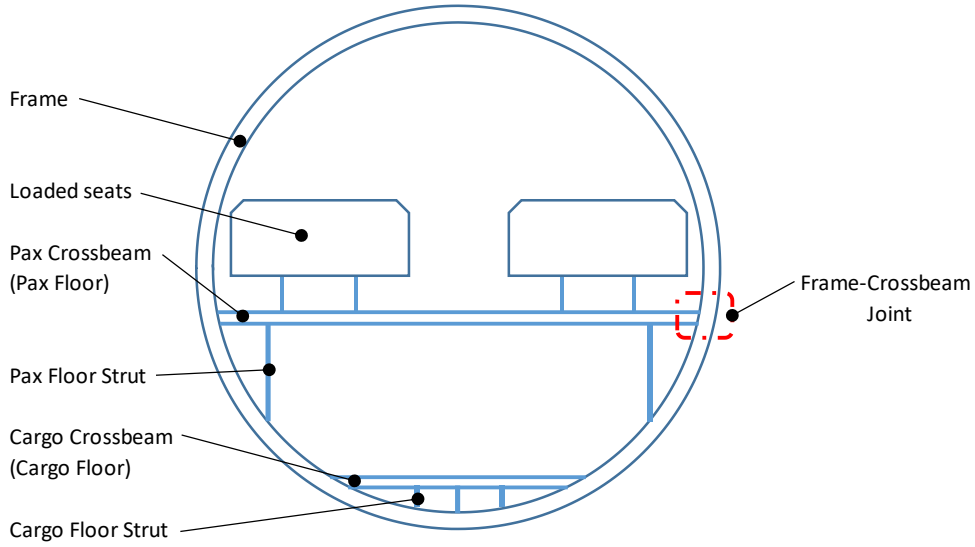

Figure 1: Typical passenger aircraft section (single aisle)

The current standard in the industry consists in a fastened joint (large bolt field) between the aircraft frame's web and the web of the crossbeam profile [1], as presented in Fig. 2. This extremely rigid connection, on top of the axial loads, also transfers the bending moments between the parts, which leads to high stresses and strains in the area. In order to mitigate these high local loads, the parts require increased stiffness, leading to increased weight.

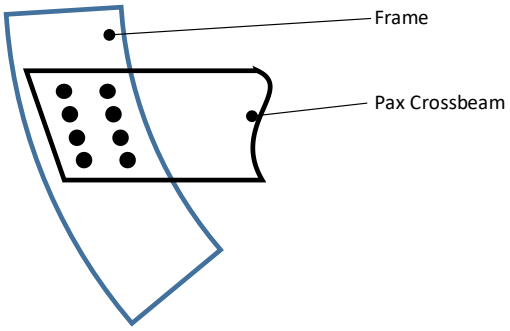

Figure 2: Typical passenger aircraft Frame to Pax. Crossbeam Bolted Joint

In this paper is proposed a new concept of an aircraft frame to passenger floor crossbeam connection. The new proposed concept consists of an articulated connection that transfers only axial loads, while the bending moments are not transferred any more. A Finite Element Analysis (FEA) is carried out for both standard and new concept, on isotropic materials (metallic) components. Results (deformations, stress and strains) are compared in order to determine the new concept behavior.

2. INITIAL ASSUMPTIONS AND MATHEMATICAL MODEL

As described above, this paper is trying to assess the loads transferred from the passenger floor crossbeam into the frame. An initial mathematical approach is done to compare the transferred loads in both cases: the current case with the crossbeam bolted onto the frame and the proposed case with an articulated connection.

For the classical connection, the crossbeam is considered clamped at one side (frame side) and supported at the other side. Vertical and horizontal loads are applied in the middle of the beam.

For the articulated connection, the crossbeam is considered articulated at the frame side and supported at the other side. Same loads are applied as for the classical connection model.

In order to calculate the reactions from both models in Fig. 3, the classical equilibrium equations are used [2]. Additionally, for the classical joint model, since the equation system is undetermined, the Castigliano's Theorem [3] is used. All equations are presented in (1). Results (reactions in points A and B) are presented in (2).

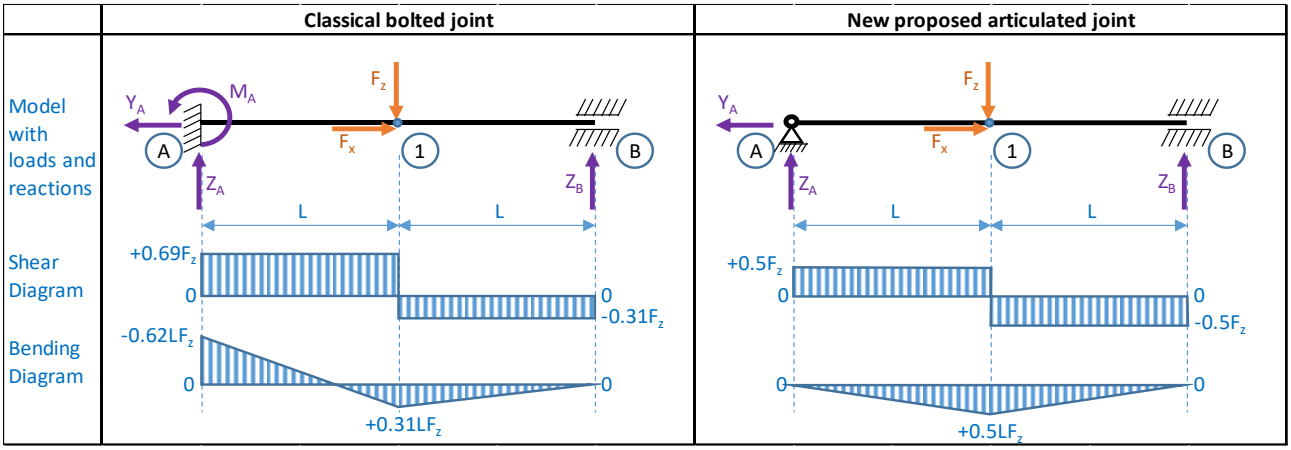

Figure 3: Simplified mathematical model and loading diagrams

	Classic bolted joint	**New proposed articulated joint**
Static equilibrium equations $\sum F_y = 0$, $\sum F_z = 0$, $\sum M_x = 0$	$X_A = F_y$ $Z_A + Z_B = F_z$ $M_A - F_z \cdot L + Z_B \cdot 2L = 0$	$X_A = F_y$ $Z_A + Z_B = F_z$ $F_z \cdot L - Z_B \cdot 2L = 0$
Castigliano's Theorem $\sum \frac{M(y)}{E \cdot I} \cdot \frac{\partial M(y)}{\partial Z_B} = 0$	for vertical displacement of point B ($v_B = 0$) $\int_0^L \frac{Z_B \cdot y}{E \cdot I} \cdot y\, dy + \int_0^L \frac{Z_B \cdot (L+y) - F_y \cdot y}{E \cdot I} \cdot (L+y) dy = 0$	-

(1)

Classic bolted joint	**New proposed articulated joint**
$X_A = F_y$; $M_A = 0.62\, L \cdot F_z$ $Z_A = 0.69\, F_z$; $Z_B = 0.31\, F_z$	$X_A = F_y$; $M_A = 0$ $Z_A = 0.5\, F_z$; $Z_B = 0.5\, F_z$

(2)

3. FINITE ELEMENT MODEL

In order to assess and evaluate the new proposed articulated joint, a FE Model is created. The model is a loads model (GFEM – Global FEM) with coarse elements. Pre and post-processing are carried out in MSC Patran 2019, while the processing is done with MSC Nastran 2019, using solution 101 (linear static).

Therefore, a five frame bays zone (5 times the length between 2 consecutive frames) from a constant single aisle aircraft section is used. The boundary conditions from the first frame are not affecting the results extracted from the middle of the model (at the third frame).

The model is created once for the classic frame-crossbeam joint, and once for the new hinged joint. The loads and the corresponding 9 load cases are defined in such a way that the results cover a wide range of different interactions.

3.1. FE Model Description

In Fig. 4 is presented the 5 frame bays length aircraft constant cylindrical section. The model contains all the main parts of a classical passenger aircraft section: skin with longitudinal reinforcements (stringers) and radial reinforcements (frames), the passenger floor with the longitudinal rails, transversal crossbeams and the floor panels, the Z-struts that supporting the passenger floor, and the cargo floor with similar components as the main floor.

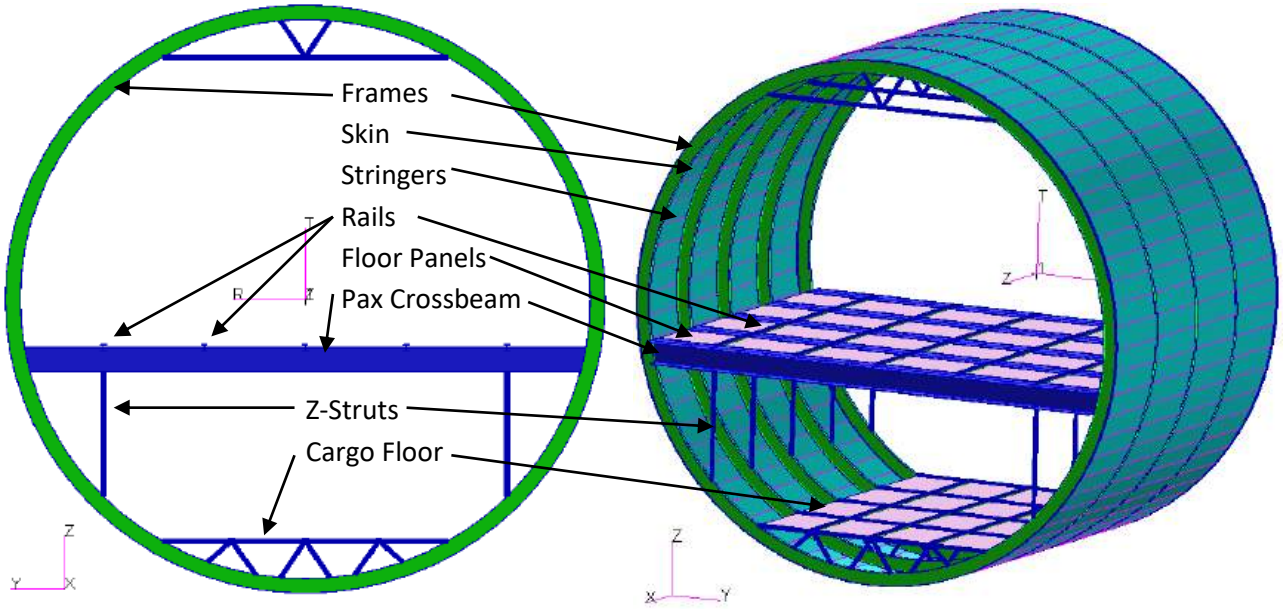

Figure 4: FE Model of the single aisle aircraft (5 frame bays length)

The model is meshed with:

- 1D beam elements for: stringers, frames free and attached flanges, all rails and struts, crossbeams upper and lower flanges,
- 2D shell elements for: skin, floor panels, frame web, crossbeam web.

All parts are considered to be metallic (aluminum alloys) with different thicknesses. For the scope of this model, which is to compare results between two concepts, the materials and properties are of secondary interest.

The boundary conditions consists of fixing all degrees of freedom for all the nodes on the first frame through an MPC (Multi Point Constraint) RBE2 (Rigid Body Element).

Additionally, 9 load cases are defined, based on the special load cases used in the aerospace industry (double internal pressure, emergency landing with up / down / sideways accelerations [4]) and some load cases with load combinations.

3.2. FE Model Results

Each of the two models (classic joint and hinge at the frame – crossbeam connection) was analyzed at all 9 defined load cases. Figure 5 presents in parallel some of the results (deformation, stress etc.), while in Figures 6 and 7 are presented as graphs the compared results for the Frame's Outer Flange (flange attached to skin) and for the Frame's Inner Flange respectively.

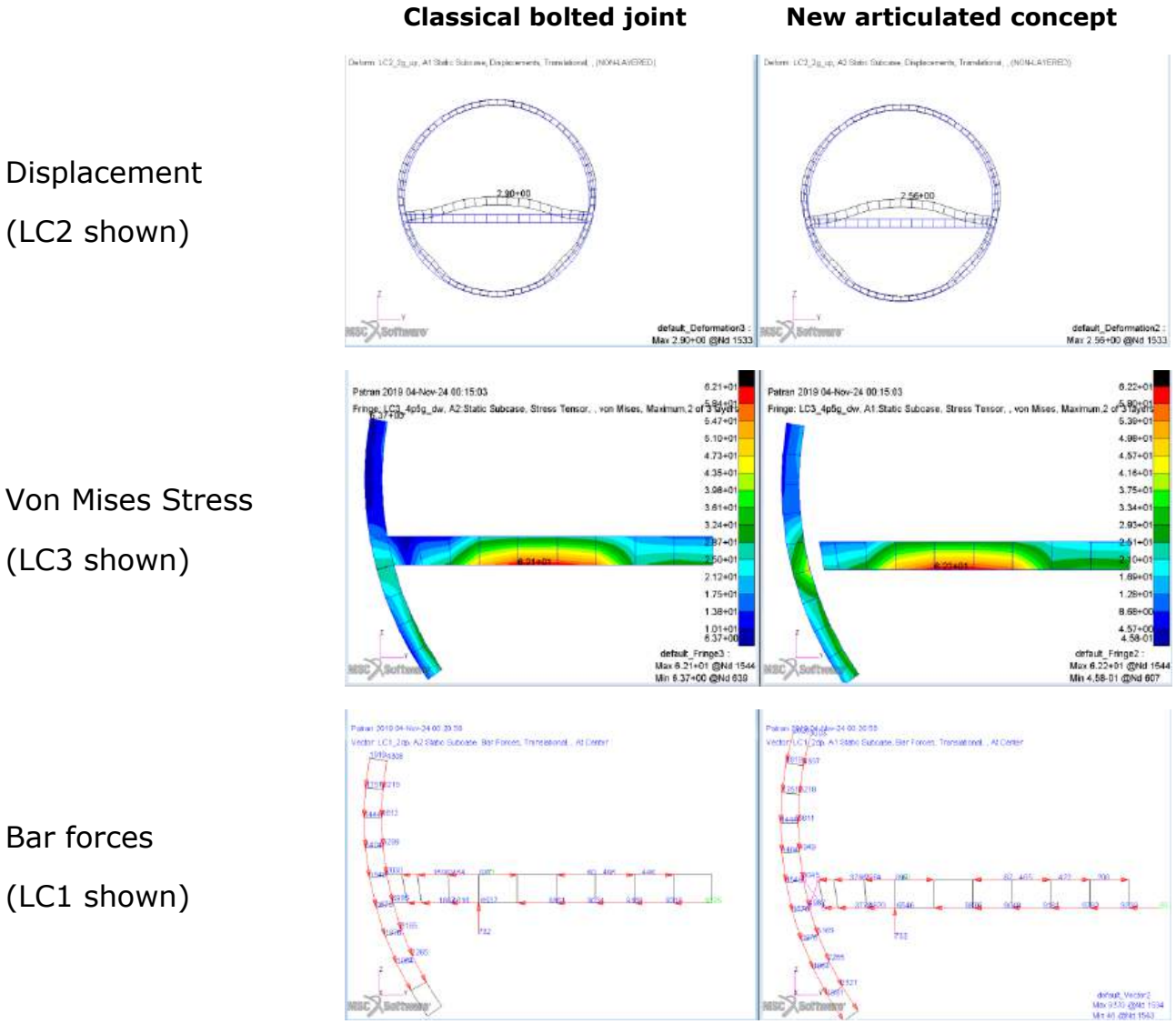

Figure 5: FE Results – comparison between the two analyzed concepts

As seen in the examples presented in Figure 5, on the frame side are relevant differences between the two analyzed concepts.

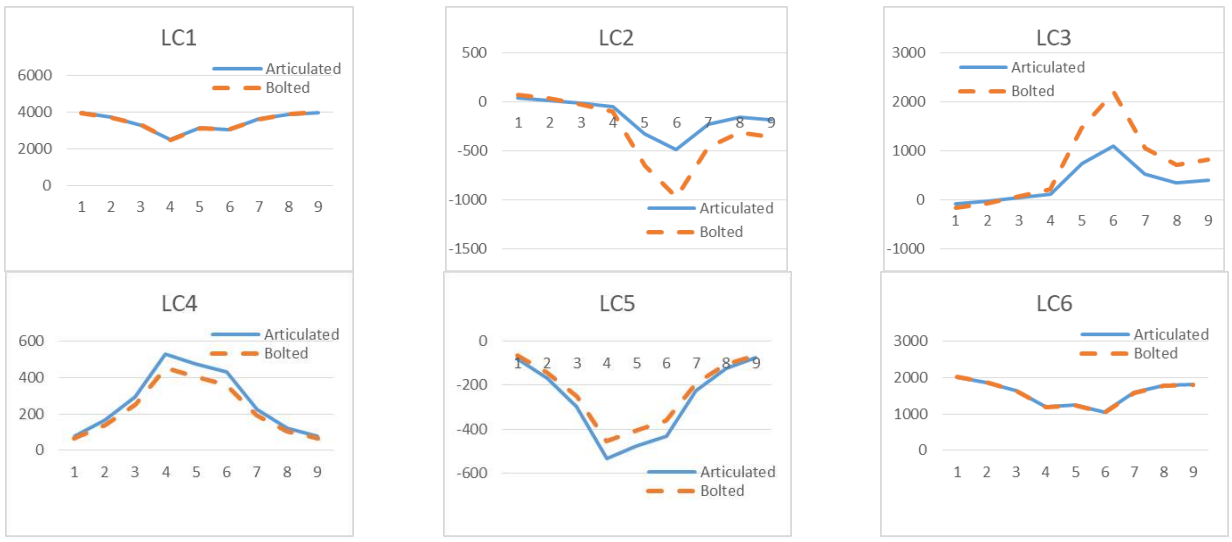

Figure 5: FE Results – Axial load in the beam elements modelling the Frame's Outer Flange

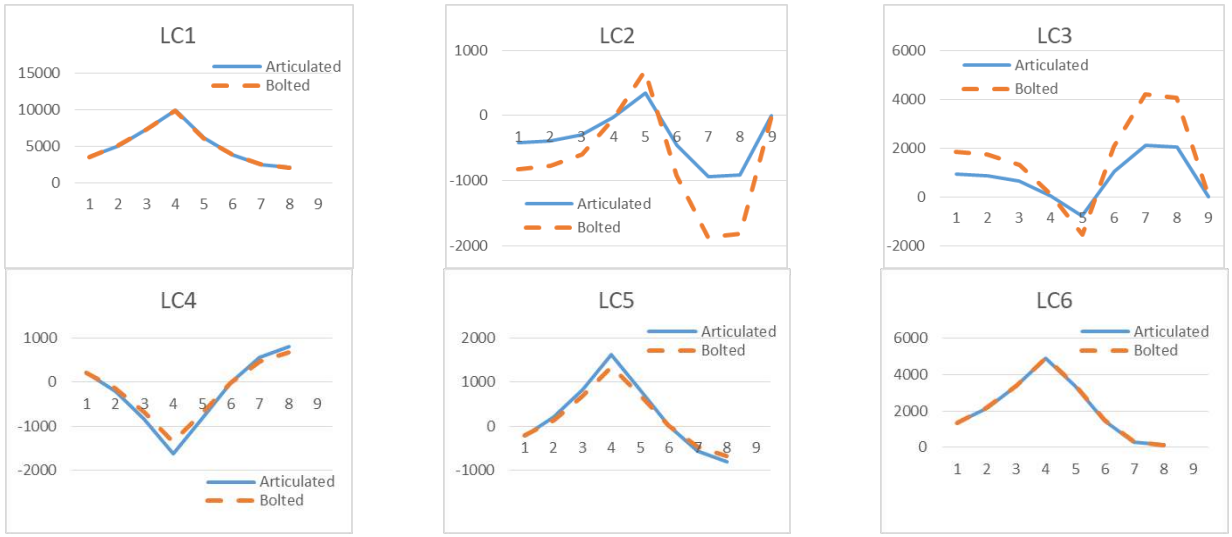

Figure 5: FE Results – Axial load in the beam elements modelling the Frame's Inner Flange

4. CONCLUSIONS

As can be observed in the compared results between the classical bolted joint and the new hinged concept, the way how the frame is connected to the crossbeam affects the load path and the load transfer. With the new concept, the loading of the frame's flanges (outer and inner) is reduced even with 50% in the area of the connection for some load cases, while at the pressurized load cases, the differences are small. At higher distances from the connection, the load differences are also small.

These results prove that the new concept could reduce the loading of the parts in some configurations. Additional work should follow to improve the modeling.

BIBLIOGRAPHY

[1] Megson THG, Aircraft Structures for Eng. Students 6th Ed., Elsevier, Cambridge, 2017
[2] Hibbeler R, Engineering Mechanics: Statics 14th Ed., Pearson, 2015
[3] Budynas RG, Roark's Formulas for Stress and Strain, 9th Ed., McGraw-Hill Ed., 2020
[4] Evolution of Air Force Crash Load and Cargo Restraint Req., EN-SB-10-002-Appendix A

COMAT The 10th International Conference on ADVANCED COMPOSITE MATERIALS ENGINEERING

Transilvania University of Brasov
FACULTY OF MECHANICAL ENGINEERING

22-23 October 2024

EXPERIMENTAL STUDY OF THE TENSION MECHANICAL PROPERTIES OF PETG AND PLA MATERIALS USED IN 3D PRINTING

Bencze Andrei*[1], Stanciu Anca[2]

1. University Transilvania of Brașov, Brașov, Romania, andrei.bencze@unitbv.ro
2. University Transilvania of Brașov, Brașov, Romania, anca.stanciu@unitbv.ro
*Corresponding author: andrei.bencze@unitbv.ro

Abstract: *This paper investigates the mechanical behavior of 3D-printed Polyethylene Terephthalate Glycol (PETG) and PLA (Polylactic Acid). The aim of this study is to provide information on how the tension mechanical properties of 3D-printed PETG and 3D-printed PLA are affected by the irregularities in the printing material and from the printing process, using samples with the infill parameter set to 100%. PETG and PLA exhibited elastoplastic behavior during tension tests, characterized by an initial linear elastic region followed by plastic deformation before fracture. Obtained results indicate that samples made with PLA exhibit superior mechanical properties compared to those made with PETG, but also with important variations between samples from the same material.*

Keywords: *tension test; mechanical properties, 3D printing material, stress, strain*

1. INTRODUCTION

During the last decades, the 3D printing technology started to become more available, affordable and more used, and started to replace the traditional manufacturing methods, which was more expensive and time consuming. This is even truer when discussing about prototypes, parts with complex geometry, test components with variable dimensions or features etc. This advantages are useful in many industries as automotive, aerospace, architecture and constructions etc.

Modern 3D printing technology can use different materials in different forms (solid, powder, melt, and liquid) and presents a variety of strength levels.

Fused deposition modelling (FDM™) is one of the most used 3D printing technologies, while is relatively cheap and reliable.

The 3D printing FDM process is using a thermoplastic filament which is melted and extruded through a nozzle. The size of the nozzle determines the thickness of the printed layers, printing time tolerances. The mechanical properties of printed parts are influenced by processing conditions, including temperature, layer thickness and speed [1].

Tensile experiments have been performed to compare FDM materials, contributing in understanding the mechanical behavior and performance of different these printed polymers. The mechanical properties of FDM-printed polymers are affected by layer thickness, orientation angles, and air gaps.

One of the most popular, affordable, and used thermoplastic materials currently available are polylactic acid (PLA) and polyethylene terephthalate glycol (PETG). Other available materials have some limitations: high extrusion temperatures, low mechanical modulus, toxic chemicals, high density etc.

Despite the variety of filaments available, comprehensive information on their properties is often limited and is given for the raw material, while the mechanical characterization of printed samples is insufficient. Further research is needed to develop test standards based on the material's intended use [1].

Therefore is necessary to conduct tests on samples to determine the material's mechanical properties. The aim of this presented study is to investigate the variation of material properties with the irregularities found in the printing wire and in the printing process.

2. MATERIAL DESCRIPTION

The Prusament PLA (polylactic acid) by Prusa Polymers (Prague, Czech Republic), is suitable for a multitude of applications, but its main purpose is for small and large 3D extrusion based FDM printing of functional and mechanical parts. It is biodegradable, easy to print and very strong, while having a low thermal expansion coefficient (reduced warping). It supports only wet sanding and is not suitable for outdoor application due to temperature restrictions.

The Prusament PETG (polyethylene terephthalate glycol) by Prusa Polymers (Prague, Czech Republic), is suitable for a multitude of applications, but its main purpose is for 3D extrusion based FDM printing of functional and mechanical parts. Thanks to good layer adhesion it is also suitable for waterproof prints. It supports also both dry and wet sanding. Compared to other similar materials, PETG is more heat resistant, more flexible and less brittle.

The properties of the selected materials are summarized in Table 1.

Table 1. Properties of PETG and PLA

Properties	**PETG**	**PLA**
Melting point [^{o}C]	245 to 260	150 to 160
Injection mould temperature [^{o}C]	200-255	178-248

Density [g/cm^3]	1.27	1.25
Crystallinity	3-11%	<10%
Melt flow [g/min]	0.8	0.6

3. SAMPLES PREPARATION

For this study, the test samples are produced using the Original Prusa i3 MK3S 3D printer. Printing parameters for PETG and PLA filaments were selected as presented in Table 2.

Table 2. Properties of PETG and PLA

Printing properties	**PETG**	**PLA**
Bed temperature [°C]	60	60
Layer thickness [mm]	0.15	0.15
Infill density	100%	100%
Fan speed	100%	100%
Deposition speed [mm/s]	200	200
Deposition temp [°C]	250	245
Extruder temperature [°C]	230-240	215
Print speed for perimeters [mm/s]	50	50
Print speed for infill [mm/s]	56	56

The test sample geometry (see Fig. 1):

- total length L = 84 mm,
- minimum cross-section width w = 10 mm,
- cross-section thickness t = 4 mm (total thickness),
- minimum cross-section area A = 40 mm2.

A density of 100% means that all available volume in one ply (each ply has a constant thickness, therefore a volume) is filled with material.

Orientation 0 means that the fibers (filament laid by the printing head) are aligned with the test sample's longitudinal direction, Fig.1

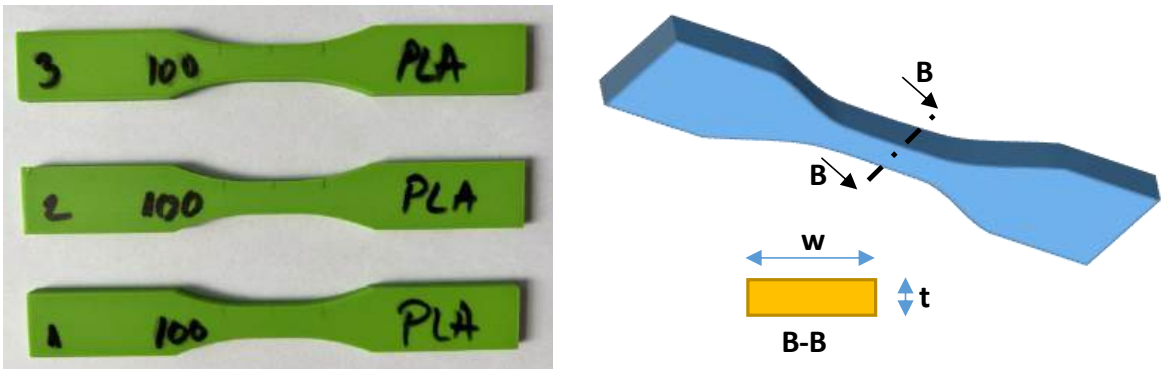

Figure 1: Printed test samples (example for PLA) and geometry

4. TRACTION TEST SETUP

The traction test was performed with an LS100Plus Universal Materials Testing Machine (100 kN maximal applied force), produced by Lloyd Instruments, Great Britain, as presented in Fig. 2.

Other parameters of the test machine: test speed accuracy: <0.2%; maximum travel: 840 mm; load resolution: <0.01% of the used force cell; extension resolution: <0.1 micron; force cell: XLC-100K-A1; analysis software: NEXYGENPlus Data Analysis Software.

The test sample is clamped on both ends. While one end is fixed, the other is pulled away, leading to the elongation of the test sample.

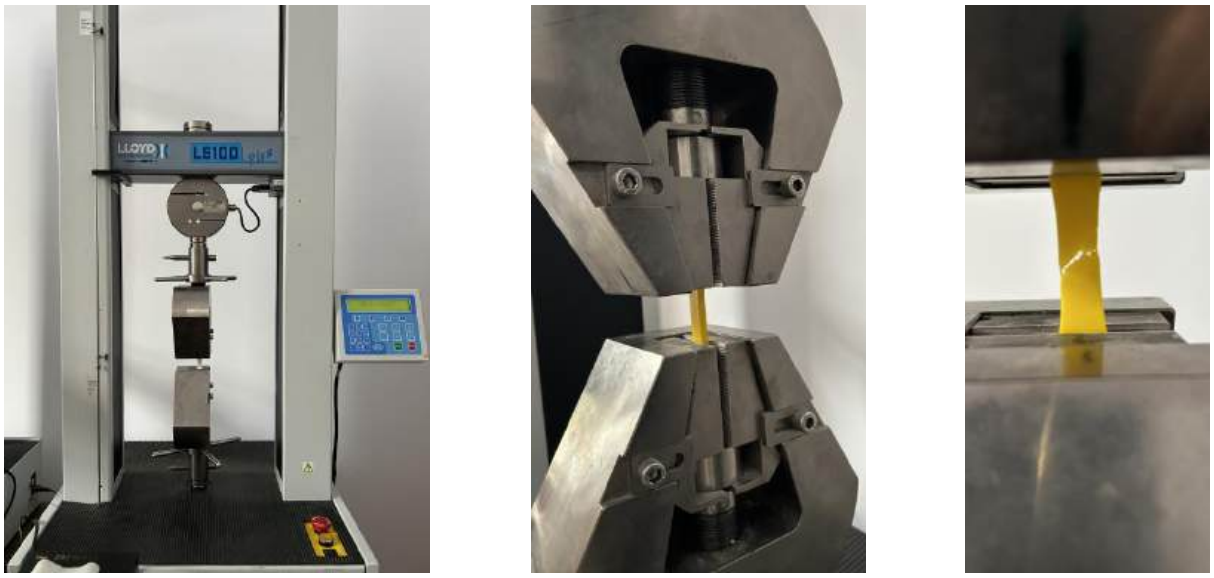

Figure 2: Traction test machine LS100Plus and traction test until failure

The machine direct outputs are: applied force F measured in [N] (incremented from 0 until it reach material failure) and extension Δl measured in [mm], as presented in Fig. 3. Knowing the geometry and the machine outputs, the material strength properties for tension (σ_y yield stress, σ_u ultimate stress, ε strain, E longitudinal elasticity modulus) can be computed.

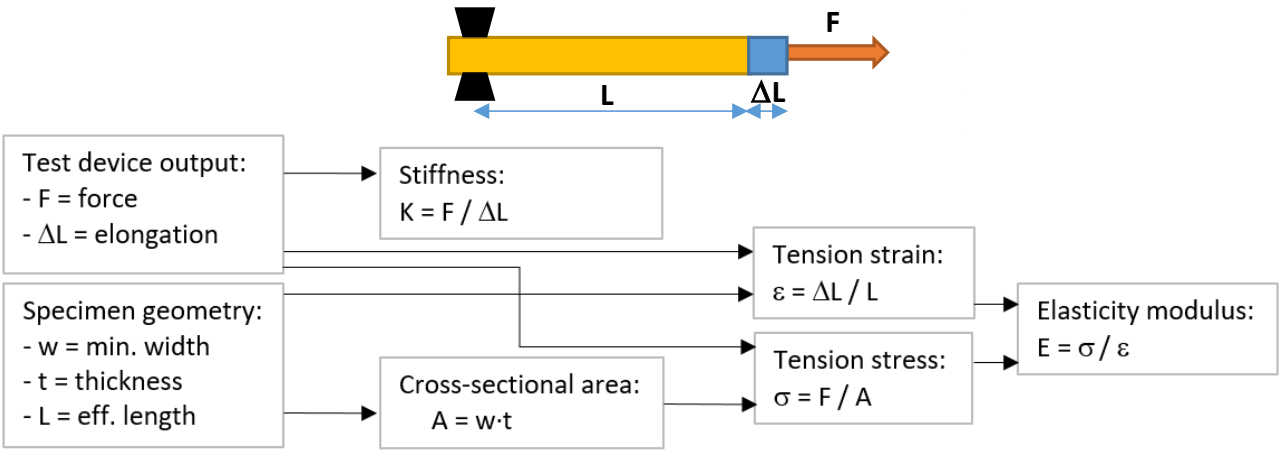

Figure 3: Traction machine outputs and calculated tension strength parameters

5. RESULTS AND DISCUSSIONS

Test samples present a linear elastic region (important for applications) and then transition into a plastic behavior, where remnant deformations occur. The extension then increases until failure, but the material's loading capabilities decrease abruptly.

Some of the tested samples are shown in Fig.4. The typical PETG and PLA material behavior (stress-strain curve) is presented below in Fig. 5.

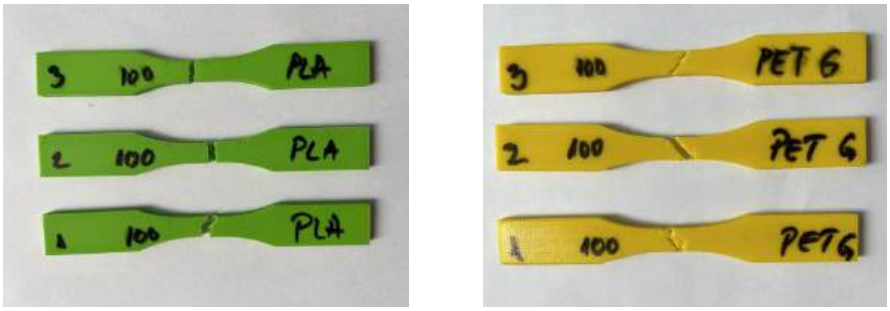

Figure 4: PLA / PETG tested samples after tension failure

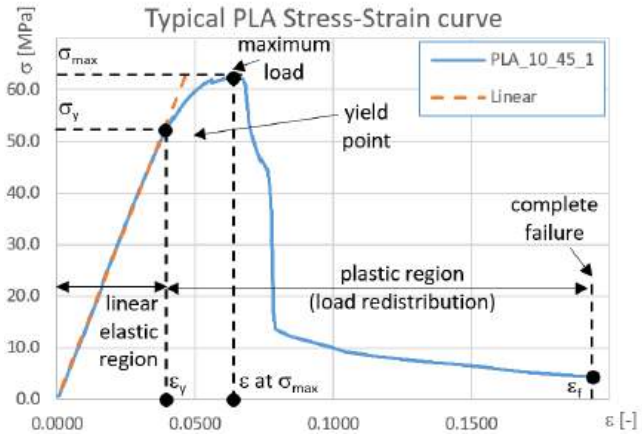

Figure 5: Typical material behavior - stress-strain curve (PLA shown, PETG similar)

As presented in Fig. 5, the maximum loading (σ_{max}) occurs just before failure. The rupture is quick, and the load capability of the part is decreasing rapidly since the sectional area that can carry loads is continuously reducing.

But, even if the part has not failed in the region just before the peak, remnant deformations occur. These deformations will make the part not to function correctly. The material can still be unpredictable, and in this situation, this value cannot be taken into account as an allowable limit because cracks can appear at the level of the structure, passing into the plastic region [2].

Thus, for engineering, a more relevant material parameter is the yield stress σ_y. Up until this point, the stress-strain varies almost linear and will not produce remnant deformations. The traction test results, for each sample type from PETG and PLA, are presented in Fig. 6. The analysis of the average values was followed to ensure the stability of the printed material, without changes occurring in the material. The traction test material parameters for each sample and as average are presented in Table 3 and Table 4.

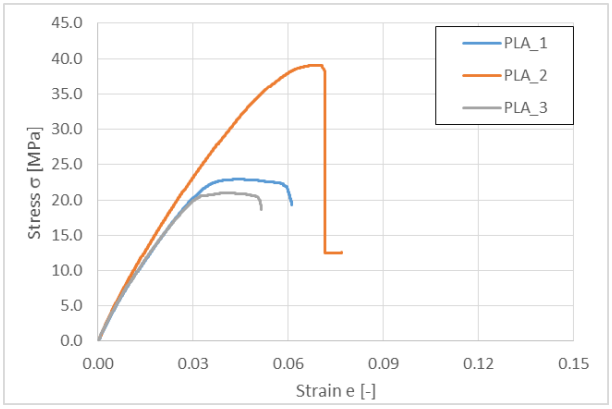

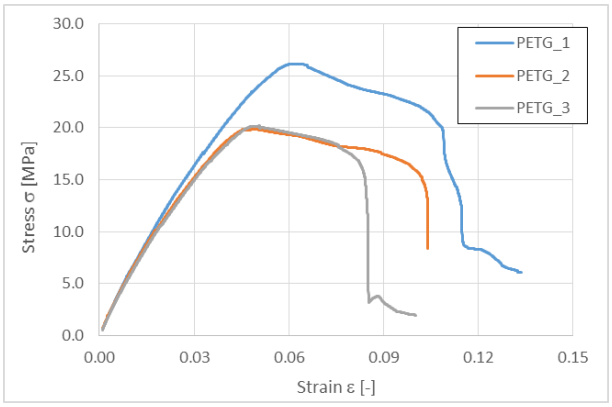

Figure 6: PLA (left) and PETG (right) - Material properties variation due to irregularities

Table 3. Properties of PETG and PLA

Test sample	Values at Yield Point				Values at Maximum Load / Stress			
	σ_i [MPa]	E [MPa]	K [N/m]	ε [%]	σ_i [MPa]	E [MPa]	K [N/m]	ε [%]
PLA_1	24.1	766	1276	0.0315	39.1	581	968	0.0525
PLA_2	12.9	757	1262	0.0171	20.9	529	882	0.0284
PLA_3	14.1	740	1233	0.0191	22.9	518	863	0.0318
Avr	17.1	754	1257	0.0225	27.6	543	904	0.0376

Table 4. Properties of PETG and PLA

Test sample	Values at Yield Point				Values at Maximum Load / Stress			
	σ_i [MPa]	E [MPa]	K [N/m]	ε [%]	σ_i [MPa]	E [MPa]	K [N/m]	ε [%]
PETG_1	16.3	546	910	0.0298	26.1	434	724	0.0496
PETG_2	12.3	539	898	0.0229	19.9	400	667	0.0381
PETG3	12.5	521	868	0.0239	20.2	397	662	0.0398
Avr	13.7	535	892	0.0255	22.1	411	684	0.0425

6. CONCLUSIONS

As observed above, the computed material strength properties for tension present a high variation (20%-40%). These are due to a multitude of factors from the entire process, starting with the irregularities in the wire material, the microscopic problems and small local differences in the actual 3D printing process, the differences in temperature between the printed layers and how this is affecting the bonding between the layers etc. All of these factors are adding, and in some instances, the differences in results could be high.

Therefore, in the design phase of the components made from these materials (PLA and PETG), a lower allowable value should be used and in addition a higher safety factor should be considered to cover for the above mentioned factors.

BIBLIOGRAPHY

[1] Solomon IJ. et al. A review on the various processing parameters in FDM. Mater Today Proc 2021

[2] Garg, A et al. An insight to the failure of FDM parts under tensile loading: Finite element analysis and experimental study. Int. J. Mech. Sci. 2017

COMAT The 10th International Conference on ADVANCED COMPOSITE MATERIALS ENGINEERING

Transilvania University of Brasov
FACULTY OF MECHANICAL ENGINEERING

22-23 October 2024

Viscous–elastic properties of varnished wood

Gall R. [1], Stanciu M.D. [*1], Savin A. [1,2]

1. Transilvania University of Brașov, Brașov, Romania, roxana.gall@student.unitbv.ro, mariana.stanciu@unitbv.ro
2. National Institute of Research and Development for Technical Physics, B-dul Dimitrie Man-geron, 47, Iași, Romania, asavin@phys-iasi.ro

[*]Corresponding author: mariana.stanciu@unitbv.ro

Abstract: *The varnish together with the wooden support forms a new layered mechanical system that has viscous-elastic properties different from the individual components. The work aims to investigate these properties through mechanical dynamical analysis, studying the influence of the wood species, the main direction, the type of varnish on the storage modulus, loss modulus and damping. The results showed that the wood species, the type of varnish (oil-based varnish and alcohol varnish), the thickness of the varnish film influence the viscous-elastic behavior at different stress frequencies.*

Keywords: *wood, viscous-elastic properties, varnish*

1. INTRODUCTION

Wood is a natural polymer made up of materials with a crystalline structure (cellulose), an amorphous structure (lignin) and a mixed structure (hemicelluloses and holocelluloses). As a result, the viscous-elastic behavior of wood over time can be modeled as a rheological model that takes into account elastic and plastic deformation, viscous-elastic creep, hygro-expansion deformation, Kelvin–Voigt element-wise mechano-sorptive strain tensor according to [1]. There are numerous approaches regarding the viscous-elastic behavior of wood from different species [3–5]. There are numerous approaches regarding the viscous-elastic behavior of wood from different species. An important problem in the acoustics of musical instruments is the system formed by wood and lacquer film, since, unlike unvarnished wood, the new system presents a different vibro-acoustic behavior because of the change in mechanical properties [6–8]. Determining the viscous-elastic parameters of varnished wood involves different measurement methods, among them, the

dynamic mechanical analysis (DMA) which is a technique to analyze the mechanical response to the vibrational forces produced by the cyclically applied mechanical load. The dynamic properties of the wood are important because they characterize the material during the vibrations of the musical instruments, compared to the statically determined properties. The techniques for determining the dynamic modulus (MOED) and damping (tan δ) are based either on vibrational tests with non-contact force, or on damping methods (with impact), or with forced vibrations maintained with direct contact between the force and the wooden sample [8–13]. The purpose of the study was to characterize the dynamic behavior of the resonance wood through mechanical analysis in dynamic mode, determining the storage modulus, the loss modulus and damping for spruce wood samples varnished with oil-based varnish and spirit varnish.

2. MATERIALS AND METHOD

The varnished spruce wood samples were cut from a varnished plate (1), in longitudinal (2) and radial (3) direction of wood as can be seen in Figure 1a. The dimensions of samples for dynamical mechanical analysis (DMA) were: 50 mm (length) x 10 mm (width) x 5 mm (thickness). In Table 1 are presented the types of studied samples and coding. The experimental set-up of DMA consists in applying of an oscillating force at different frequencies (f=1Hz; 5Hz; 10Hz; 50Hz), at constant temperature at 30°C. The spruce wood samples were subjected to three points bending (Fig. 2b). The magnitude of bending load was 6 N. The equipment used is DMA 242C Netzsch equipment.

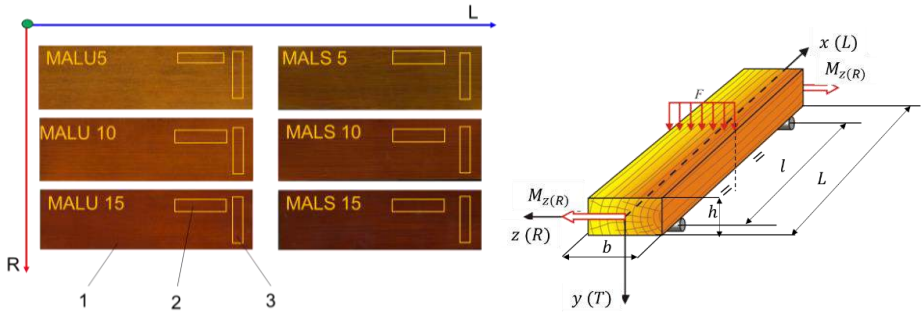

Figure 1: Experimental set-up: a) The samples in longitudinal (2) and radial (3) direction of wood extracted from varnished spruce plate (1); b) the bending loading of sample

Table1. Physical features of varnished samples

Sample	Wood direction	No. of varnish layers	Code	No. of samples
Spruce with oil-based varnish	Longitudinal	5	MALU5L	4
		10	MALU10L	4
		15	MALU15L	4
Spruce with oil-based varnish	Radial	5	MALU5R	4
		10	MALU10R	4
		15	MALU15R	4
Spruce with spirit varnish	Longitudinal	5	MALS5L	4
		10	MALS10L	4
		15	MALS15L	4
Spruce spirit varnish	Radial	5	MALS5R	4
		10	MALS10R	4

	15	MALS15R	4

3. RESULTS AND DISCUSSION

Figures 2 and 3 illustrate the simultaneous evolution of the storage modulus, loss modulus and damping in the case of spruce samples cut longitudinally and radially, varnished with 5, 10, 15 layers, subjected to different loading frequencies. It is observed that the storage modulus tends to increase over time, and the loss modulus to decrease in accordance with loading frequencies.

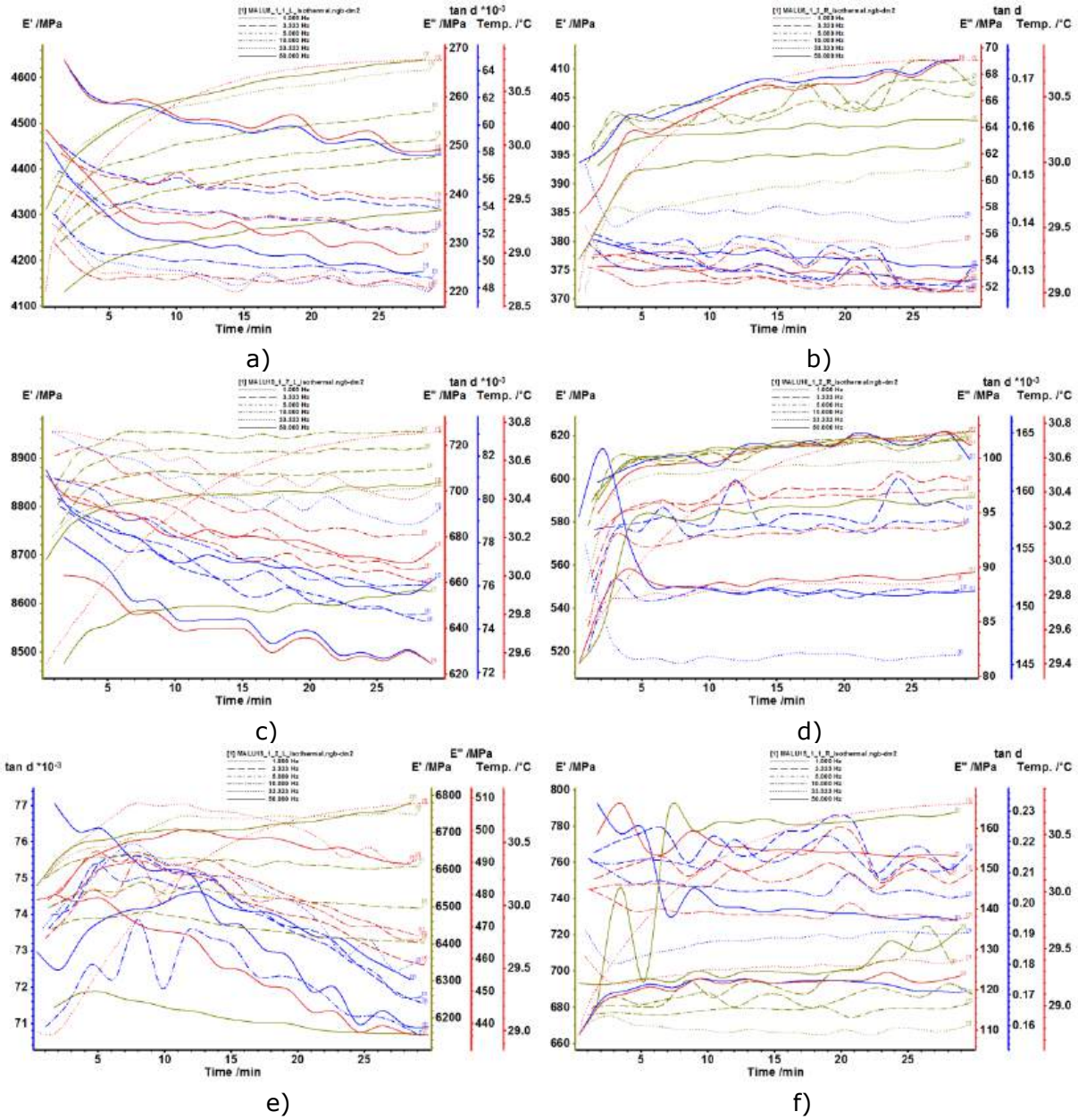

Figure 2: The variation of storage modulus, loss modulus and damping tand in case of spruce samples with oil-based varnish: a) longitudinal direction, 5 layers; b) radial direction, 5 layers; c) longitudinal direction, 10 layers; d) radial direction, 10 layers; e) longitudinal direction, 15 layers; f) radial direction, 15 layers.

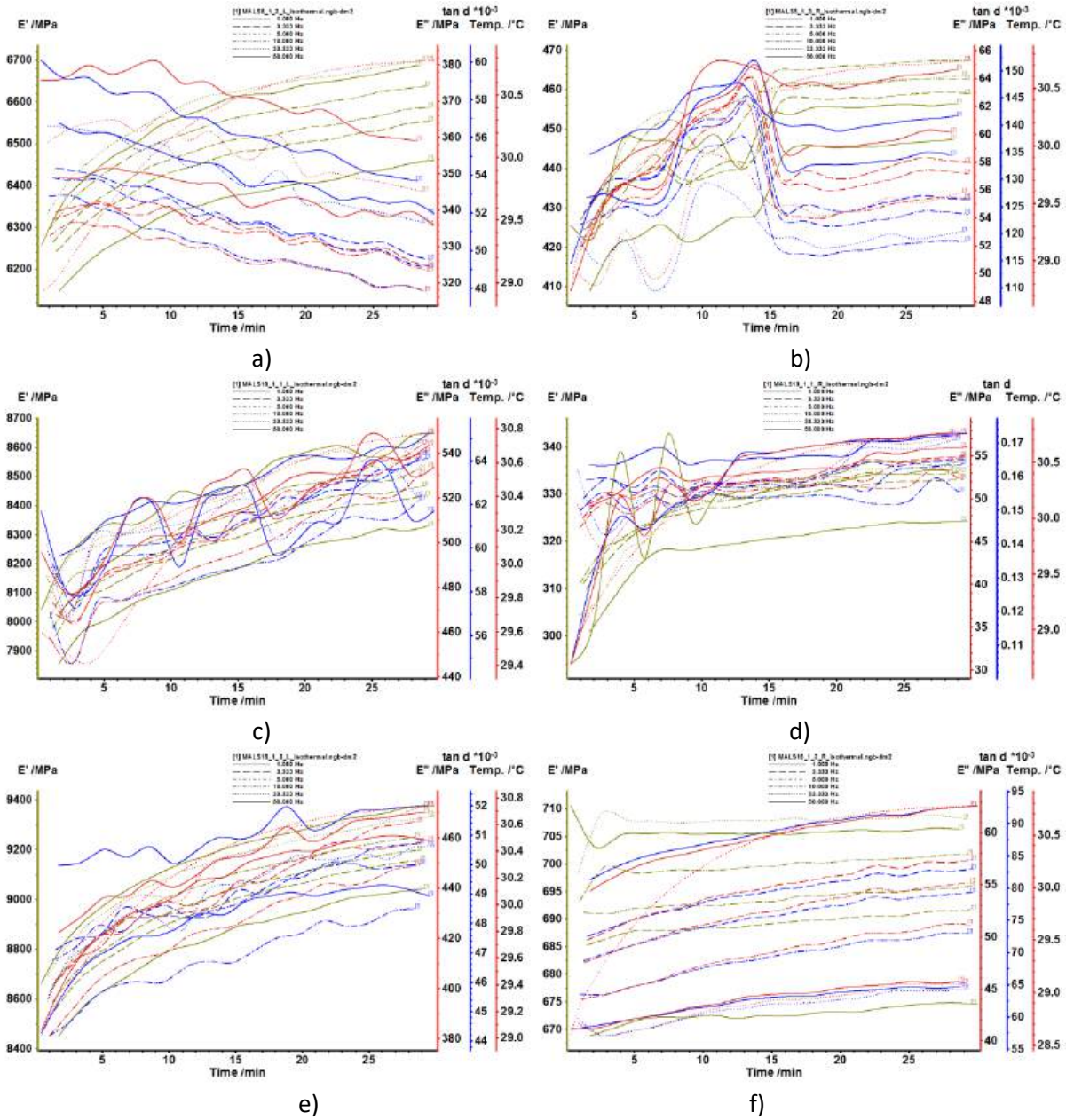

Figure 3: The variation of storage modulus, loss modulus and damping tand in case of spruce samples with spirit varnish: a) longitudinal direction, 5 layers; b) radial direction, 5 layers; c) longitudinal direction, 10 layers; d) radial direction, 10 layers; e) longitudinal direction, 15 layers; f) radial direction, 15 layers.

For the quantitative analysis of the changes in the viscous-elastic properties of the samples, the values of the storage modulus, loss modulus and damping were extracted at the initial moment (t_0) and at the final moment, after the 30 minutes of loading (t_{30}). Comparisons and trends of storage modulus with increasing loading frequencies are shown in Figure 4. It is observed that the behavior of the samples differs depending on the direction of the spruce wood fibers (longitudinal and radial), but also depending on the type of varnish applied. In the case of spruce wood varnished with oil-based varnish, the conservation modulus shows lower values compared to spirit varnish, but the differences from one application frequency to another are more pronounced (Figure 4a). Thus, the samples varnished with spirit varnish register the greatest changes (increases) of the storage modulus after exposure to

different loading frequencies (approx. 6 - 7% for 5 layers, approx. 7 - 8.5% for 10 layers and between 8 - 9.5% for 15 layers) (Figure 4b). The samples with 5 layers, regardless of the type of varnish, have a similar behavior. Instead, the samples with 10 layers and 15 layers show peaks at the frequency of 3.33 Hz, in the case of samples with oil-based varnish and decreases in the case of samples with spirit, and at the frequency of 33.3 Hz, the behavior is reversed (Figure 4c,d).

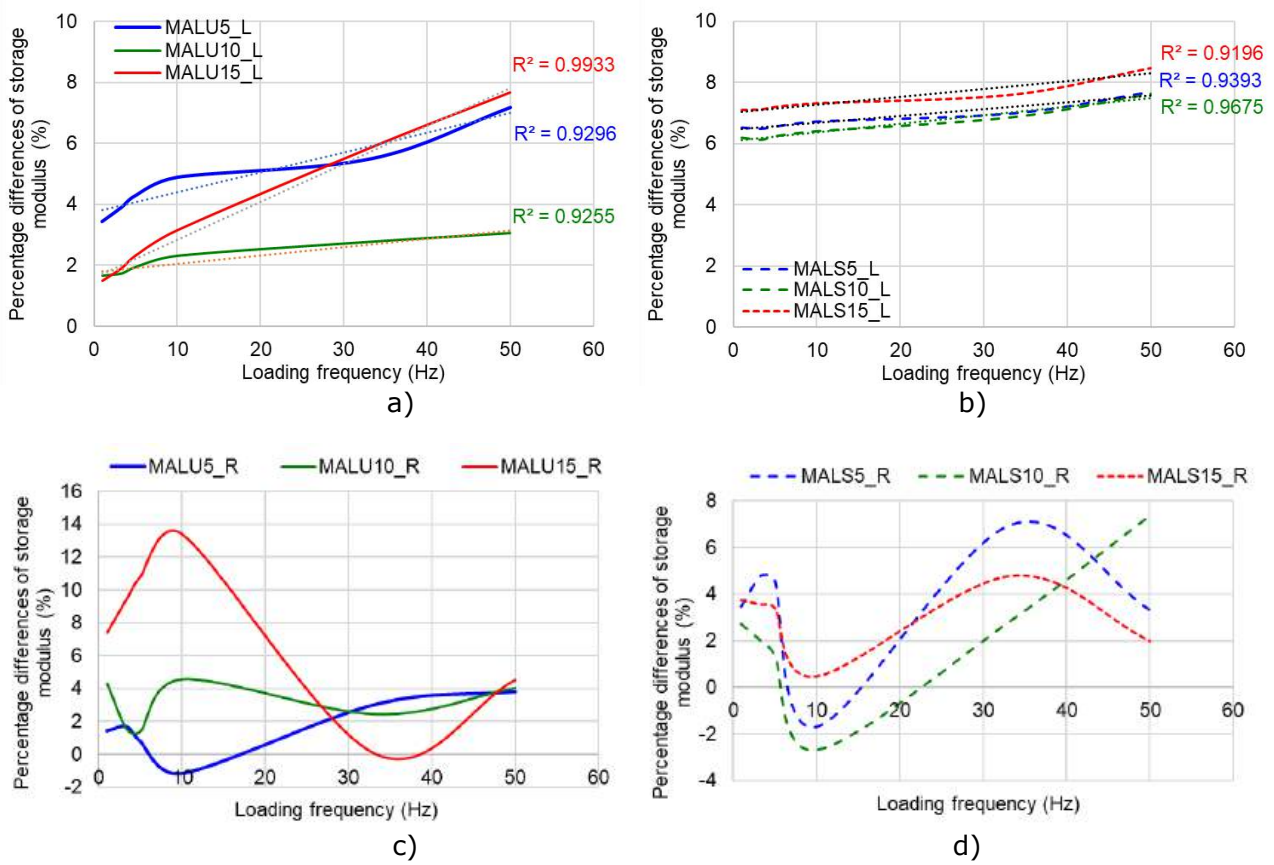

Figure 4: The variation of storage modulus, in case of spruce samples: a) oil-based varnish, longitudinal direction; b) spirit varnish, longitudinal direction; c) oil-based varnish, radial direction; d) spirit varnish, radial direction.

The loss modulus tends to decrease with increasing loading time in the longitudinal samples, varnished with oil-based varnish, registering the extreme values for 10 layers (Figure 5a). In the other samples, the tendency of the viscous modulus is to increase after exposure to dynamic loading (Figures 5b,c,d). In the radial direction, the type of varnish and the thickness of the varnish film determine the viscous behavior of the material. Thus, the loss modulus for the samples with oil-based varnish increases with the increase in the thickness of the varnish layer, while for the samples with spirit varnish, the loss modulus decreases with the increase in the thickness of the film (Figure 5, c and d). The ratio of the loss modulus to the storage modulus represents the logarithmic damping or decrement (tand). This is a sensitive indicator of mechanical or thermal conditions during the input of mechanical energy that is dissipated as heat through internal friction. During the vibrations of the violin plates, this energy dissipation occurs in the wood in the longitudinal and radial direction. In Figure 6, the variation of damping is presented.

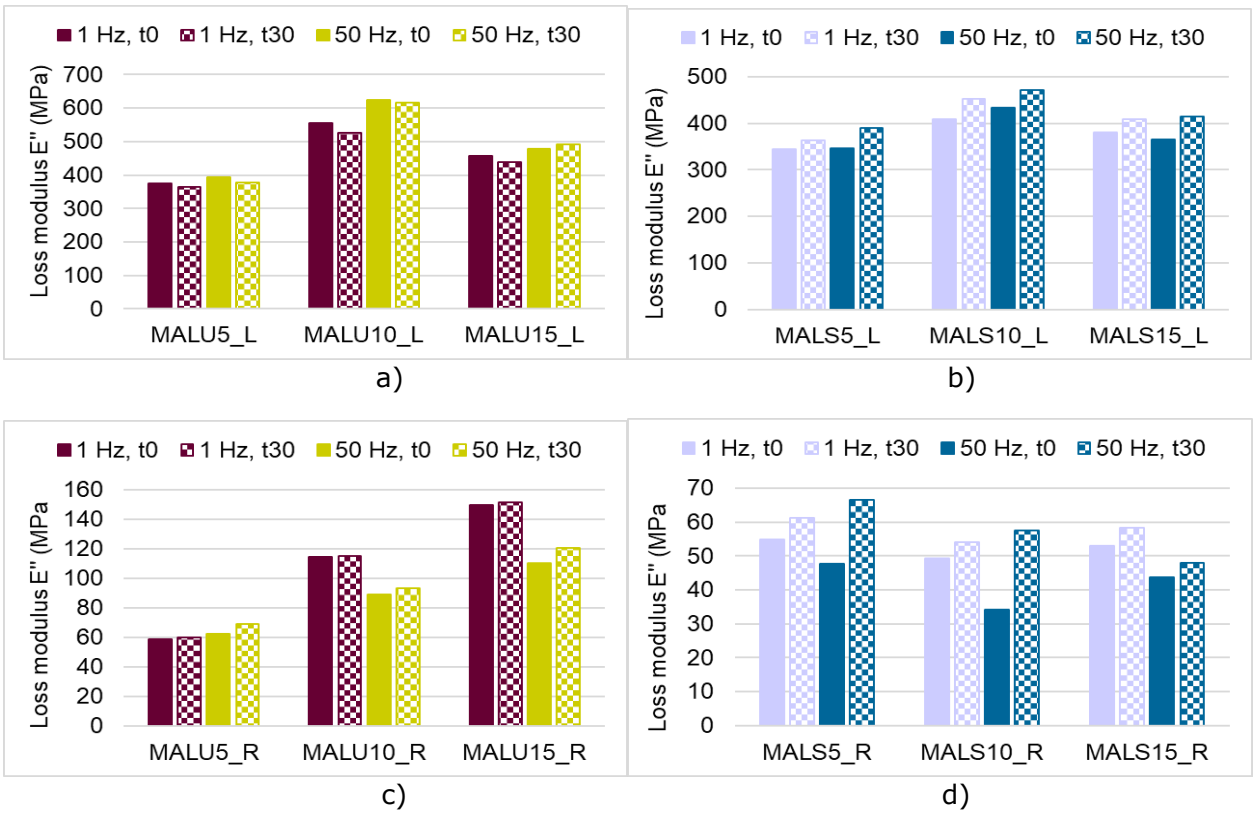

Figure 5: The variation of loss modulus, in case of spruce samples: a) oil-based varnish, longitudinal direction; b) spirit varnish, longitudinal direction; c) oil-based varnish, radial direction; d) spirit varnish, radial direction.

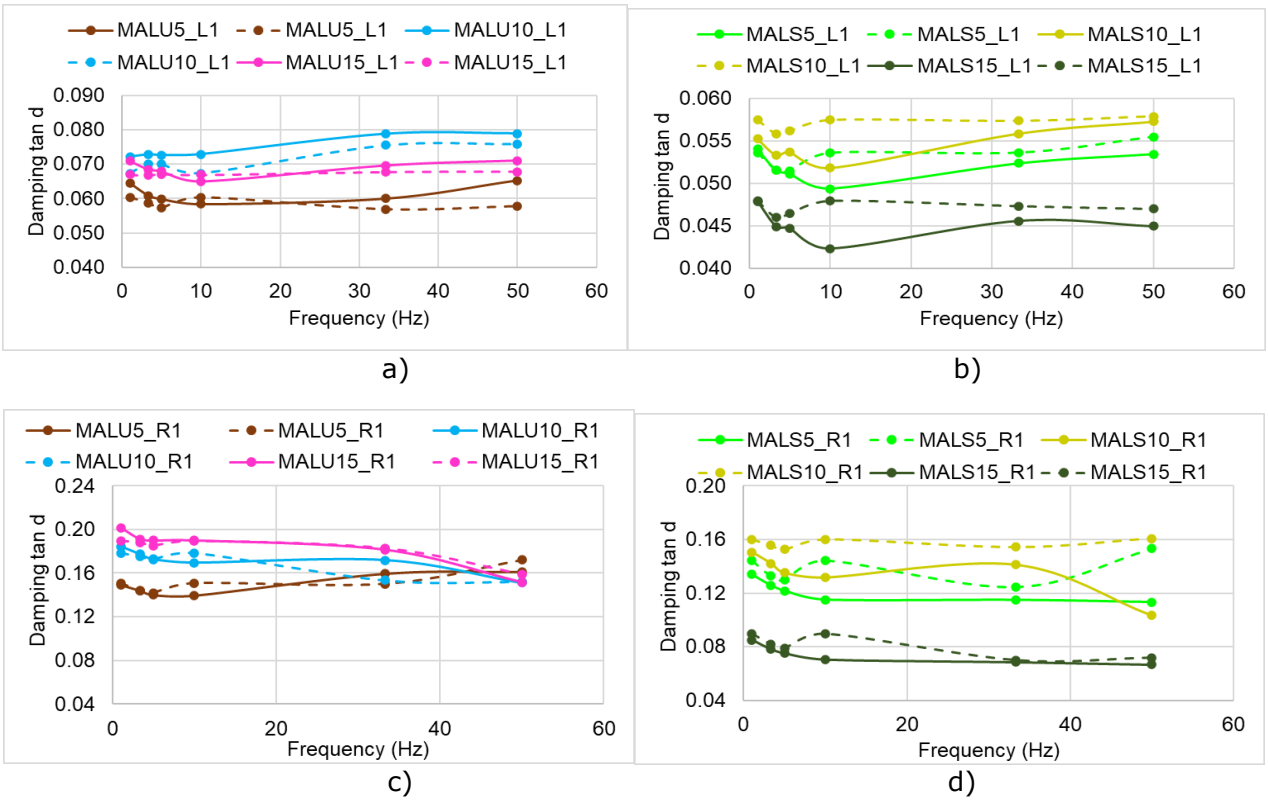

Figure 6: The variation of damping, in case of spruce samples: a) oil-based varnish, longitudinal direction; b) spirit varnish, longitudinal direction; c) oil-based varnish, radial direction; d) spirit varnish, radial direction.

4. CONCLUSIONS

In conclusion, the paper focused on the analysis of the viscous-elastic response of the resonance spruce wood varnished with different types and thicknesses of varnish, the results obtained being relevant to both musical instrument manufacturers, musical instrument varnish manufacturers, instrumentalists and researchers. Varnishes applied to the plates of musical instruments influence the acoustics of the instrument by changing the properties of the wood, for example mass, stiffness and damping as they are amorphous polymers with high molecular weight below their glass transition temperature. According to [14, 15], it can be observed that in the case of samples with oil-based varnish, the increase in internal friction precedes the increase in stiffness, being more pronounced in the radial direction than in the longitudinal direction. Samples with spirit varnish show a lower damping compared to the other type of varnish, but higher in the radial direction than in the longitudinal direction. A similar behavior for both types of varnishes is observed in relation to the number of layers. The highest damping occurs for samples with 10 layers of varnish.

ACKNOWLEDGEMENT

This research was supported by a grant of the Ministry of Research, Innovation and Digitization, CNCS/CCCDI – UEFISCDI, project number 61PCE/2022, PN-III-P4-PCE2021-0885, ACADIA – Qualitative, dynamic and acoustic analysis of anisotropic systems with modified interfaces.

BIBLIOGRAFIE

[1] Hassani, M.M., Wittel, F.K, Hering, S., Herrmann, H.J. Rheological model for wood, Computer Methods in Applied Mechanics and Engineering, 283, 1032-1060, 2015.

[2] Kawahara, K., Ando, K. & Taniguchi, Y. Time dependence of Poisson's effect in wood IV: influence of grain angle. J Wood Sci 61, 372–383, 2015. https://doi.org/10.1007/s10086-015-1477-8

[3] Hofer, U., Pichler, C., Maderebner, R. et al. Lomnitz-type viscoelastic behavior of clear spruce wood as identified by creep and relaxation experiments: influence of moisture content and elevated temperatures up to 80 °C. Wood Sci Technol 53, 765–783, 2019. https://doi.org/10.1007/s00226-019-01099-8

[4] Trcala, M., Suchomelová, P., Bošanský, M. et al. A constitutive model considering creep damage of wood. Mech Time-Depend Mater 28, 163–183, 2024. https://doi.org/10.1007/s11043-024-09679-3.

[5] Lämmlein S L, Van Damme B, Mannes D, Schwarze F, Willis M R, Burgert I Vi-olin varnish induced changes in the vibro-mechanical properties of spruce and maple wood. Holzforschung, 74(8), 765-776, 2020, https://doi.org/10.1515/hf-2019-0182

[6] Stanciu M D, Cosnita M, Gliga G V, Gurau L, Timar C M, Guiman M V, Năstac S M, Roșca I C, Bucur V, Dinulică F Tunable Acoustic Properties Using Different Coating Systems on Resonance Spruce Wood. Adv. Mat. Interfaces, 1, 2300781, 2024, https://doi.org/10.1002/admi.202300781.

[7] Gall, R. Stanciu, M.D., Savin, A., Campean, M., Gliga, V.Gh. The influence of the type of varnish on the viscous-elastic properties of maple wood used for musical instruments, 11th Hardwood Conference Proceedings, Sopron, Hungary, 30-31 May 2024, Eds.

Róbert Németh, Christian Hansmann, Holger Militz, Miklós Bak, Mátyás Báder, University of Sopron Press, 426 – 434, 2024
[8] Bucur V. Acoustics of wood, 2nd ed.; Springer, Germany, Berlin, 2006.
[9] Danihelova A, Spisiak D, Reinprecht L, Gergel T, Vidholdov Z, Ondrejka V. Acoustic properties of Norway spruce wood modified with staining fungus (Sydowia polyspora). BioResources 14(2), 3432-3444, 2019. https://doi.org/10.15376/biores.14.2.3432-3444
[10] Brémaud, I. Acoustical properties of wood in string instruments soundboards and tuned idiophones: Biological and cultural diversity. J. Acoust. Soc. Am. 131(1), 807-818, 2012, DOI: 10.1121/1.3651233
[11] Nop, P., Cristini, V., Tippner, J., Zlámal, J., Vand, M.H., Šeda, V. Dynamic Properties of Wood Obtained by Frequency Resonance Technique and Dynamic Mechanical Analysis, Wood and Fiber Science, 55(2), 131-142, 2023.
[12] Obataya, E., Ono, T., Norimoto, M. Vibrational properties of wood along the grain. J. Mater. Sci. 35(12), 2993-3001, 2000. DOI: 10.1023/A:1004782827844
[13] Crețu, N., Roșca, I.C., Stanciu, M.D. et al. Evaluation of Wave Velocity in Or-thotropic Media Based on Intrinsic Transfer Matrix. Exp Mech 62, 1595–1602, 2022. https://doi.org/10.1007/s11340-022-00889-9.
[14] Schelleng J.C. Acoustical Effects of Violin Varnish. The Journal of the Acoustical So-ciety of America. 44(5), 1175 – 1183 (1968
[15] Minato K, Akiyama T, Yasuda R, Yano H. Dependence of vibrational properties of wood on varnishing during its drying process in violin manufacturing. Holzforschung 49(3), 222–226 (1995). https://doi.org/10.1515/hfsg.1995.49.3.222

COMAT The 10th International Conference on ADVANCED COMPOSITE MATERIALS ENGINEERING

Transilvania University of Brasov
FACULTY OF MECHANICAL ENGINEERING

22-23 October 2024

Method to recycle corrugated cardboard in eco-friendly composites

Mohammad Hassan Mazaherifar [*1], Camelia Coșereanu [1], Cristina Maria Timar[1], Sergiu Valeriu Georgescu [1]

[1] Faculty of Furniture Design and Wood Engineering, Transilvania University of Brasov, B-dul Eroilor, nr. 29, 500036 Brasov, Romania, E-mail: mohammad.mazaherifar@unitbv.ro, cboieriu@unitbv.ro, cristinatimar@unitbv.ro, sergiu.georgescu@unitbv.ro

[*]Corresponding author: mohammad.mazaherifar@unitbv.ro

Abstract: *This study aims to explore a sustainable method for recycling corrugated cardboard into eco-friendly composites and their potential uses in different applications. Two types of composites made from recycled cardboard (printed and unprinted) were produced and compared in terms of density, dimensional stability, modulus of elasticity (MOE), modulus of rupture (MOR), internal bonding strength (IB), thermal conductivity, and sound absorption. Samples made from unprinted cardboard demonstrated better overall performance in terms of density, thermal insulation and sound absorption. In contrast, composite B, derived from printed cardboard, exhibited greater strength. The findings suggest these materials can be viable alternatives for thermal insulation panels and acoustic panels.*

Keywords: *Cardboard, Recycling, Composite, Thermal insulation, Sound absorption.*

1. INTRODUCTION

The effective insulation of buildings plays a key role in reducing global energy consumption. Building insulation serves as a passive energy-saving technique, significantly improving energy efficiency. Insulation materials are essential across a variety of applications, due to their versatile properties such as high specific surface area, and low density. Currently, many insulation materials are derived from inorganic or synthetic materials such as expanded polystyrene [1] and polyurethane [2] with harmful environmental effects, so actually, there is a growing interest in eco-friendly alternatives [3]. Corrugated cardboard is a

widely used material composed of multiple layers of paperboard. In light of the environmental implications, recycling practices have gained importance [4], and cardboard fibers can be recycled up to 25 times. According to FAO reports, global annual cardboard production exceeds 50 million metric tons, with 90% of this being recycled [5]. Cardboard consists primarily of cellulose fibers derived from wood pulp. It contains approximately 52.02% cellulose, 6.79% hemicellulose, and 10.43% lignin, 15.71% ash and 15.05% other additives, which improve its overall performance. The fibers have an average length of 192 µm and a width of 53 µm. With a relatively low density, low cost and high recyclability, cardboard is a promising solution, as it helps to reduce energy consumption, minimize waste and promotes sustainability by aligning with circular economy principles [6,7]. Experimental research has explored various applications of recycled cardboard [8-10], except foam panels made of recycled cardboard, which remains underexplored [11].
In this study, recycled cardboard was used to develop and manufacture two types of green composites with low densities. The physical and mechanical properties of the samples were evaluated to understand their behavior.

2. MATERIAL AND METHODS

2.1 Composite panels manufacturing

Under laboratory conditions, two distinct composites were produced using defibrated fibers obtained from unprinted and printed cardboard. The fibers were mixed with sodium bicarbonate (wt.10%), yeast (wt.5%) and water. The mats were heated in a mold at a temperature of 150°C for 15 hours, followed by a gradual cooling. For each type, a total of four panels with final sizes of 320 mm x 250 mm x 12 mm were obtained. The densities of the composites were of 152.73 kg/m³ and 138.83 kg/m³ for unprinted (U-cardboard) and printed cardboard (P-cardboard) respectively (Figure1).

Figure 1: Composites made of recycled cardboard.

2.2 Physical properties

Water absorption (WA) and thickness swelling (TS) were evaluated in accordance with [12] by immersing five samples (sized to 50 mm x 50 mm) in

a water bath maintained at 20°C for 24 hours. The sizes and weights of the samples were recorded before immersion, and after 2 and 24 hours. The thermal conductivity coefficient (λ) of the samples was automatically calculated with Fourier's Law with a Netzsch HFM436 Lambda equipment (Netzsch, Selb, Germany), according to [13,14] standards. The heat transfer was assessed between a hot plate (heated up to 20°C) and a cold plate (with temperatures rising from -10°C to 15°C). The sound absorption properties of the specimens were evaluated using a Kundt's impedance tube, across a frequency range of 50 to 1390 Hz, with a test sound level set at 75 dB. For each composite, two specimens were tested.

2.3 Mechanical properties

The mechanical testing procedures were conducted in accordance with relevant European standards [15-17].
The modulus of elasticity (MOE), modulus of rupture (MOR) and internal bonding (IB) strength perpendicular to the board plane were evaluated using a Zwick Roell Z010 Universal Testing Machine (Ulm, Germany) equipped with a 10,000 N capacity load cell.

2.4 Microscopic evaluation

Stereo-microscopy analysis was carried out using a NIKON SMZ 18-LOT2 microscope (Nikon Corporation, Tokyo, Japan) to examine the fiber structures and gaps within the composite materials, with particular attention given to fiber adhesion. Images were taken at magnifications of 60×, and 180×.

2.5 Statistical analysis

Statistical analysis was performed using Microsoft Excel to compute the standard deviation, with a 95% confidence interval and a significance threshold of 0.05 ($p < 0.05$). Additionally, Minitab software was employed to conduct two-sample t-tests, comparing the mean values of the MOR, MOE, IB, WA, TS, and λ.

3. RESULT AND DISCUSSION

Table 2 displays the physical and mechanical properties of the samples.

Table 2. Properties of the panels

Panel type	Density kg/m³	λ, W/mK	WA, %		TS, %		MOE, N/mm²	MOR, N/mm²	IB, N/mm²
			2h	24h	2h	24h			
U-cardboard	152.7 (7)	0.053 (0.001)	590.2 (31.1)	597.3 (29.5)	7.08 (1.90)	9.99 (1.87)	42.78 (13.4)	0.23 (0.08)	0.063 (0.17)
P-Cardboard	138.8 (17)	0.055 (0.002)	568.2 (31.2)	597.8 (36.5)	8.22 (3.76)	12.07 (2.06)	41.32 (13.4)	0.30 (0.09)	0.061 (0.3)

The values in the parenthesis represent the standard deviation.

3.1 Physical properties

The WA results indicates that U-cardboard absorbs moisture faster than P-cardboard composite, which may be attributed to coatings typically applied to printed materials, which can reduce the moisture uptake. The similar values after 24 hours suggest that long-term water absorption capacity converges, indicating that both types can reach a saturation point after prolonged exposure. The high values of WA are typical for materials with low densities, which exhibit higher moisture uptake due to their greater internal voids [18]. The greater TS value for P-cardboard may be explained by the presence of inks and coatings that can alter the structural integrity of the composite.
Both materials demonstrated low thermal conductivity coefficient, the characteristic of good insulating materials (Figure 2)

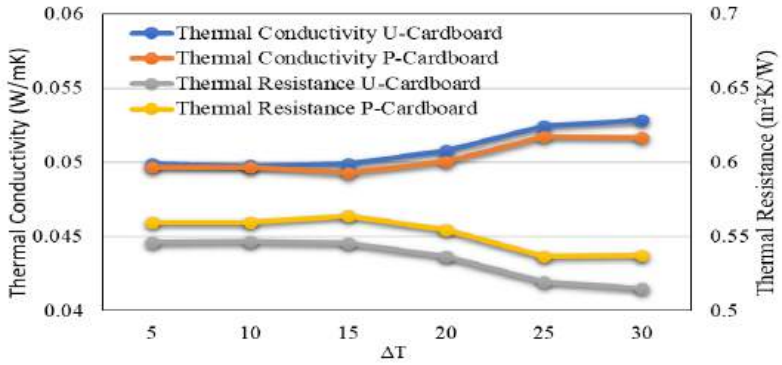

Figure 2: Thermal insulation parameters

The higher thermal conductivity observed in the P-cardboard composite can be attributed to its lower density compared to the U-cardboard composite.
On average, both U-cardboard and P-cardboard exhibited impressive sound absorption coefficients of approx. 0.85, demonstrating their effectiveness in mitigating mid-frequency noise (Figure 3). U-cardboard maintained this coefficient over the frequency range of 600 Hz to 900 Hz, with a peak of 0.88 at 800 Hz, whilst the P-cardboard maintained it in a slightly narrower range of 600 Hz to 800 Hz, with a peak of 0.87 at 675 Hz.

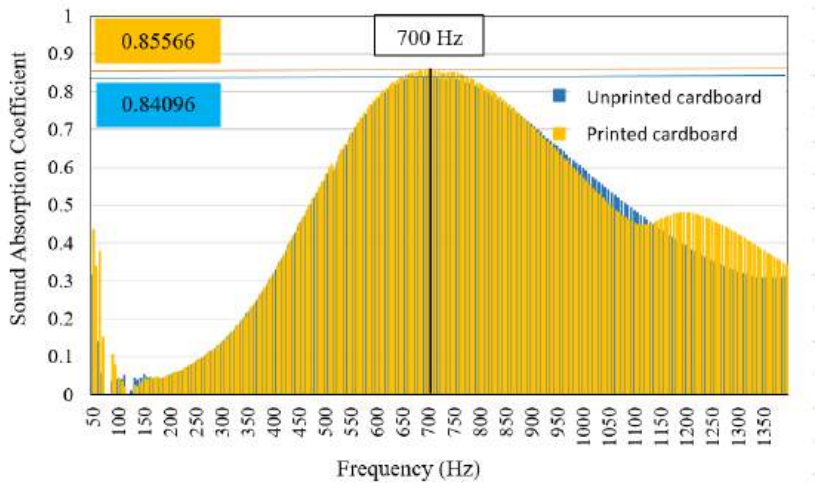

Figure 3: Sound absorption coefficient at various frequencies.

3.2 Mechanical properties

Both composites demonstrated similar trends in mechanical behavior. U-cardboard exhibited a slightly higher MOE compared to the P-cardboard, proving to be stiffer and more resistant to bending deformation. In contrast, P-cardboard displayed a higher MOR, which suggests that it can withstand greater stress before failure, likely due to the reinforcing effect of printing inks and coatings, as found also by other researchers [19]. The IB of the two composites was nearly identical, indicating that they have similar features regarding the internal bonding and proves the conclusion from [20], stating that the IB of fiber-based composites is more strongly influenced by the fiber network itself than by the surface treatments.

3.6 Microscopic investigation

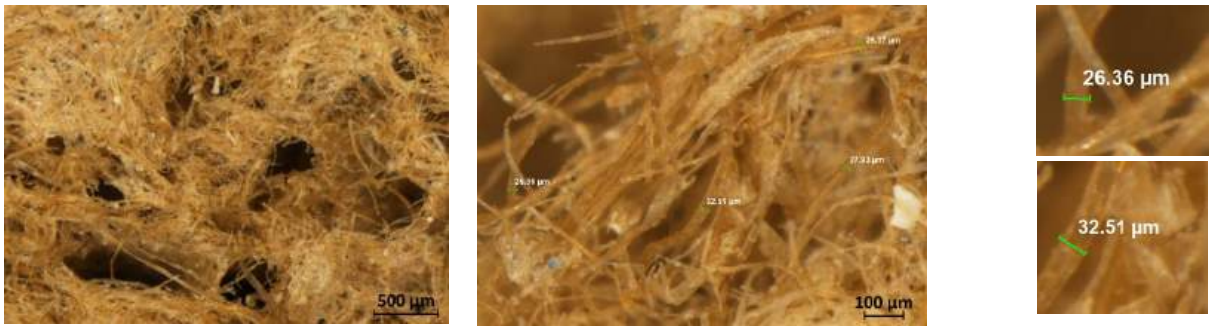

a. b. c.

Figure 4: Microscopic images of the U-composite; a. magnification 60×; b. magnification 180×; details of the fiber measurements from b. image.

The images in Figure 4 illustrate the porous structure of the composites with defined dimensions of the cardboard fibers, complying with the literature in the field [21]. Pore sizes of the composites are correlated to the utilization of sodium bicarbonate and yeast, resulting in numerous and larger pores for both composite structures and proves the high porosity volumes of 87% and 86% for U-cardboard and P-cardboard, respectively.

4. Conclusion

When referring to WA and TS, both materials ultimately reach similar levels of saturation and swelling after extended exposure. In terms of thermal insulation, U-cardboard composite provides slightly better thermal insulation compared to P-cardboard, but both of them exhibited impressive sound absorption coefficients of approximately 0.85, value that recommend them for environments where sound clarity is crucial, such as recording studios and performance venues, where no high MOE, MOR and IB are needed. However, the statistical analysis revealed no significant differences in the tested physical and mechanical properties between the two types of samples at a 95%

confidence level. These results suggest that both materials could be effectively used in a range of applications, including those requiring acoustic treatments or lightweight insulation composites.

REFERENCES

[1] Yucel K., Basyigit C., Ozel C. Thermal insulation properties of expanded polystyrene as construction and insulating materials, 15th Symposium in Thermophysical Properties 2003, p. 54-66.

[2] Kausar A. Polyurethane composite foams in high-performance applications: A review. Polymer-Plastics Technology and Engineering. 2018,57(4):346-69.

[3] Benallel A., Tilioua A., Ettakni M., Ouakarrouch M., Garoum M., Hamdi M.A.A., Design and thermophysical characterization of new thermal insulation panels based on cardboard waste and vegetable fibers. Sustain. Energy Technol. Assess. 2021,48:101639.

[4] Xie M., Qiao Q., Sun Q., Zhang L., Life cycle assessment of composite packaging waste management-a Chinese case study on aseptic packaging. Int J Life Cycle Assess. 2013,18:626-35.

[5] FAO, World production cardboard. Food and Agriculture Organization, 2021.

[6] Virtanen Y., Nilsson S., Environmental impacts of waste paper recycling, Routledge 2013.

[7] Venkatesan S., Afroz M., Navaratnam S., Gravina R., Circular-economy-based approach to utilizing cardboard in sustainable building construction. Buildings, 2023,13(1):181.

[8] Mahdi S., Xie T., Venkatesan S., Gravina R., Mechanical characterisation and small-scale life-cycle assessment of polypropylene macro-fibre blended recycled cardboard concrete. Construction and Building Materials, 2023,409:133902.

[9] Mc Cracken A., Sadeghian P., Corrugated cardboard core sandwich beams with bio-based flax fiber composite skins. Journal of Building Engineering, 2018, 20:114-22.

[10] Sair S., Mandili B., Taqi M., El Bouari A., Development of a new eco-friendly composite material based on gypsum reinforced with a mixture of cork fibre and cardboard waste for building thermal insulation. Compos. Commun., 2019,16:20-4.

[11] Jensen M.S., Alfieri P.V., Design and manufacture of insulation panels based on recycled lignocellulosic waste. Clean. Eng. Technol., 2021,3:100111.

[12] ISO 16983:2003, Determination of Swelling in Thickness after Immersion in Water.

[13] ISO 8301:1991, Thermal insulation. Determination of Steady-State Thermal Resistance and Related Properties.

[14] EN 12664:2001, Thermal performance of building materials and products - Determination of thermal resistance by means of guarded hot plate and heat flow meter methods - Dry and moist products of medium and low thermal resistance.

[15] ISO 16978:2003, Wood-based panels. Determination of modulus of elasticity in bending and of bending strength.

[16] EN 326-1:1994, Wood-Based Panels. Sampling, Cutting and Inspection. Part 1: Sampling and Cutting of Test Pieces and Expression of Test.

[17] EN 319:1993, Particleboards and Fibreboards: Determination of Tensile Strength Perpendicular to the Plane of the Board.

[18] Ouakarrouch M., Bousshine S., Bybi A., Laaroussi N., Garoum M., Acoustic and thermal performances assessment of sustainable insulation panels made from cardboard waste and natural fibers, Applied Acoustics, 2022,199:109007.

[19] Jonoobi M., Ghorbani M., Azarhazin A., Zarea Hosseinabadi H., Effect of surface modification of fibers on the medium density fiberboard properties. Eur. J. Wood Wood Prod., 2018, 76:517-24.

[20] Van den Oever M., Bos H., Van Kemenade M., Influence of the physical structure of flax fibres on the mechanical properties of flax fibre reinforced polypropylene composites, Appl. Compos. Mater., 2000, 7:387-402.

[21] Chinga-Carrasco, G., Cellulose fibres, nanofibrils and microfibrils: The morphological sequence of MFC components from a plant physiology and fibre technology point of view. Nanoscale Res. Lett., 2011, 6:1-7.

COMAT

The 10th International Conference on ADVANCED COMPOSITE MATERIALS ENGINEERING

Transilvania University of Brasov
FACULTY OF MECHANICAL ENGINEERING

30-31 October 2024

ADVANCES OF COMPOSITE MATERIALS IN COMPACTION EQUIPMENTS FABRICATION. A REVIEW

Miron D.S., Debeleac C.N.*, Nechita P., Căpățână G.F., Dobrescu C.F., Calu M.

"Dunarea de Jos" University of Galati, Engineering and Agronomy Faculty in Braila, Research Center for Mechanics of Machines and Technological Equipments, Braila, Romania, carmen.debeleac@ugal.ro
*Corresponding author: carmen.debeleac@ugal.ro

Abstract: *In this paper, the authors address an actual aspect regarding the introduction into manufacturing of parts of compactors made of advanced composite materials. In this sense, types of materials, their technical requirements, examples of component elements whose traditional material has been replaced by composite materials are presented. The benefits of implementing these materials in the current manufacture of compactors have been quantified according to the statements of the major manufacturers of equipments for compaction.*
Keywords: *compactor equipment, advanced composite materials, requirements, benefits*

1. INTRODUCTION

Nowadays, advanced composite materials are widely used in various applications such as aerospace, automotive, wind energy etc. due to superior strength-to-weight ratios, corrosion resistance and customizable properties [1,2,3]. The use of advanced composite materials in manufacturing of equipments for terrain compaction (Figure 1) significantly influences their performance and efficiency and implicitly the technological processes in which they are incorporated on construction sites [4,5].

Figure 1: Examples of compaction equipments:
a) Roller machine; b) Rammer; c) Vibratory plate; d) Mini roller.

Common composite materials used in the manufacture of parts into compactors structure (as rollers, rammers or vibratory plates) are [6-9]:

- Fiber-Reinforced Polymers (FRP) as: carbon fiber-reinforced polymer (CFRP), glass fiber-reinforced polymer (GFRP), aramid fiber-reinforced polymer (AFRP) that offer high strength-to-weight ratios, corrosion resistance, and durability;

- Kevlar Reinforced Composites with epoxy, rubber, polypropylene, and thermoplastic materials, used where impact resistance is crucial, providing protection against wear and tear while maintaining a lightweight structure;

- Natural Fiber-Reinforced Composites (NFRC) using wood, Kenaf, rice, flax, hemp etc. offering a balance of good mechanical properties and sustainability, as environmentally friendly alternatives to synthetic fiber composites.

The important aspects that influence decision-making regarding the change of materials [10] in the construction of compactors equipment are the following:

a) The complexity of the compaction machines is an important criterion that must be considered when designing vibratory systems (requiring strict control of technological parameters, such as frequency, amplitude of vibrations [11-14]) with component elements made of composite materials.

b) The sensitivity of the material to the intensively dynamic work regime of the technological equipment can lead to the shortening of the life of the respective components because of the damage of the fibers or the resin used [15,16].

c) Integrating new materials into existing production lines can be challenging, requiring consideration of costs and compatibility with older compaction equipment [17-19].

2. TECHNICAL REQUIREMENTS

New composite materials often have different thermal, mechanical, and chemical properties compared to traditional materials. This affects how they interact with existing equipment, particularly compaction tools, which might not be designed for the specific needs of these materials, changing the lifetime [20], adding heating elements [21,22], enhancing precision controls [22]. For the mechanical characterization and damage diagnosis of advanced composite materials, non-destructive techniques based on the propagation of high-frequency sound waves through materials are used to detect internal characteristics, measure material properties and identify structural damage [23,24].

The component parts of mini equipment for vibratory compaction made of composite materials have the following constructive and visual characteristics:

a) textured appearance, especially those made of carbon fiber, if they are not covered with a layer of paint.

b) versatility in choosing the constructive form, designing curved shapes, with smooth edges and an ergonomic design, which gives a modern and aerodynamic appearance.

c) light weight because these materials are lighter than steel, resulting in a slim but robust construction.

d) lifespan of components made from composite materials is longer compared to those made from conventional materials.

In particular, the beneficial aspects of manufacturing some parts of the constructive assembly of the usual compaction equipment from composite materials will be exemplified. It is known that the chassis or main frame provides structural support for all other components of the compactor. The material from which it is made is based on composites with glass fiber or carbon fiber. Thus, the use of composite materials reduces the overall weight of the equipment, making it easier to handle and transport from one job to another, without compromising its structural strength. The drum or base plate are the component of the equipment that come into direct contact with the ground or other materials that require compaction. These are typically made of either steel or cast iron, but it can be made is based on glass fiber or carbon fiber composites, conferring high resistance to abrasion compared to traditional materials and reducing the transmission of unwanted vibrations to the user operator. The insulation mount reduces the transmission of vibrations from the vibratory tool to the structural elements of the equipment, but also to the attendant operator. Making it from elastomeric materials (such as fiber-reinforced elastomers) improves vibration damping, increasing operator comfort and extending the life of compaction technology equipment. The engine housing has the role of protecting it, but also other internal components from dust, dirt and impacts. The use of fiberglass or carbon fiber composites provides increased corrosion resistance in harsh working environments and has the benefit of reducing overall weight. The control lever and handles are slightly easier to handle and more comfortable for the operator if they are made of fiber-reinforced plastic composite materials, offering an ergonomic design, increased resistance to wear and harsh operating conditions. The joining parts and supports in the structure of the equipment that ensure the connection and support of the different components of the compactor can also be made of composite materials with carbon fiber or glass, thus offering increased resistance to traction and bending, being ideal for parts that must be light and durable at the same time. Also, rubber-fiber composites are used in drive belts due to their high durability and flexibility. The gallon tank is made from fiber-reinforced polymers (FRPs) because these materials offer high strength-to-weight ratios, corrosion resistance, and durability.

3. CASE STUDIES: ADVANCES OF COMPOSITE MATERIALS IN COMPACTION EQUIPMENTS FABRICATION

The choice of composite materials appropriate to the technical or constructive requirements of the compaction equipment is made following a rigorous selection according to their application role, such as: weight reduction (Table1), wear resistance, structural integrity, etc. Already major compactor manufacturers have replaced traditional materials with composite-based ones and have noted improvements in performance, durability and operator comfort, and implicitly more efficient operation. In the following, some case studies will be presented regarding the current situation regarding the introduction of advanced composite materials into the current manufacturing of compactor structural components.

Table1. Weight reduction vs. traditional material when using composite materials

Parts of compactor equipment	Manufacturer	Materials	Values
Drum roller, plate base (rammer, vibratory plate)	Bomag	CFRP	30%
	Volvo	CFRP + steel	40%
	Caterpillar	CFRP + aramid fibers	35%
	Ammann	CFRP + aramid fibers	40%
	Wirtgen Group	CFRP	n.a.
Frame and chassis	Bomag	GFRP	20%
	Volvo	CFRP + Kevlar	30%
	Ammann	GFRP + carbon fibers	30%
Operator cab	Bomag	GFRP	20%
	Volvo	GFRP	25%
	Caterpillar	GFRP	30%
	Ammann	GFRP	30%
	Wirtgen Group	GFRP + carbon fibers	
Engine hood and side panels	Volvo	CFRP + Kevlar	30%
	Wirtgen Group	GFRP	n.a.

Vibration isolators are usually made from elastomeric materials like rubber, but with the advanced composite materials (ACMs), these damping systems are becoming more efficient and durable (Table2). Their applications in compactors equipments are used in several critical areas: engine mounts (isolating the engine from the rest of the compactor structure to reduce noise and vibration transmission), operator cabin mounts (ensuring a smoother and more comfortable ride by isolating the operator's cabin from the vibrations of the compactor's frame) and component isolation (protecting sensitive components like hydraulic systems and electronics from excessive vibrations, which could lead to premature failure).

Table2. Incorporate isolation mounts made from ACMs

Manufacturer	Materials	Model
Bomag	CFRP + rubber	BT 60/4, BT 65, BT 120
Volvo	CFRP + rubber	SD160B
	GFRP + rubber	DD120C
	Kevlar + rubber	SD75B
	Thermoplastic composites reinforced + carbon nanofibers	CR30B
Ammann	GFRP + rubber	ARX 91
	CFRP + rubber	ASC 110, APR 5920
	Kevlar + rubber	ARS 122
	Thermoplastic composites reinforced + carbon nanofibers	ARX 26-2
Caterpillar	CFRP + rubber	CS56B, CP74B
	Kevlar + rubber	CB10
	GFRP + rubber	826K
Hamm	CFRP + rubber	HD+ 120i VO, GRW 280i
	Kevlar + rubber	H 13i
	GFRP + rubber	3410 VIO
	Thermoplastic composites reinforced + carbon nanofibers	HD 14i VV

The use of advanced composites in compactor vibration isolators results in increased operational performance characteristics, providing further improvements in vibration isolation, durability and cost effectiveness.

All manufacturers estimated the increasing of the service life of the compactor's parts fabricated with composites materials compared to traditional materials (e.g. Bomag: 25 %, Volvo CE: 30 %, Caterpillar: 20 – 25 %, Ammann: 25 - 30 %, Wirtgen Group: 30 %).

Also, reducing of the fuel consumption of these machines represents another strength point that require implementation of these kinds of materials in the current fabrication (e.g. Bomag: 15 %, Volvo CE: 20 %, Caterpillar: 15 %, Ammann: 15 - 20 %, Wirtgen Group: 15 %).

4. CONCLUSIONS

The use of composite materials by major compaction equipment manufacturers is currently increasing due to their multiple benefits, the most significant of which are: weight reduction, increased strength and durability, and improved operator efficiency and comfort. In this direction, as production technologies evolve, the use of composite materials is expected to become even more widespread in the construction equipment industry.

BIBLIOGRAFIE

[1] Fardin Khan, Nayem Hossain, Juhi Jannat Mim, SM Maksudur Rahman, Md. Jayed Iqbal, Mostakim Billah, Mohammad Asaduzzaman Chowdhury, Advances of composite materials in automobile applications – A review, Journal of Engineering Research, 2024

[2] Hariz H.M., Sapuan M., Sapuan M., Ilyas R.A., Muhammad Hariz Bin Hassim, Advanced composite in aerospace application: A review on future aspect of fiber-reinforced polymer (frp) in aerospace industry, Seminar on Advanced Bio- and Mineral based Natural Fibre Composites (SBMC2021), 2001

[3] Todd Griffith D., Dongyang Cao, Hongbing Lu and Dong Qian, Composite materials in wind energy: design, manufacturing, operation, and end-of-life, 43rd Risoe International Symposium on Materials Science, 1293, 012002, 2023

[4] Debeleac C.-N., Nechita P., Nastac S.-M., Computational investigations on soundproof applications of foam-formed cellulose materials, Polymers, 11(7), 1224, 2019

[5] Nastac S.-M., Nechita P., Debeleac C.-N., Simionescu C., Seciureanu M., The acoustic performance of expanded perlite composites reinforced with rapeseed waste and natural polymers, Sustainability, 14(1), 103, 2021

[6] Rajak D.-K., Pagar D.-D., Menezes P.-L., Linul E., Fiber-reinforced polymer composites: manufacturing, properties, and applications, Polymers, 11(10):1667, 2019 https://doi.org/10.3390/polym11101667

[7] Dickson A.-N., Barry J.-N., McDonnell K.-A., Dowling D.-P., Fabrication of continuous carbon, glass and Kevlar fibre reinforced polymer composites using additive manufacturing, Additive Manufacturing, Volume 16, 2017, pp. 146-152, ISSN 2214-8604, https://doi.org/10.1016/j.addma.2017.06.004

[8] Muhammad Yasir Khalid, Ans Al Rashid, Zia Ullah Arif, Waqas Ahmed, Hassan Arshad, Asad Ali Zaidi, Natural fiber reinforced composites: Sustainable materials for emerging applications, Results in Engineering, Volume 11, 2021, 100263, ISSN 2590-1230, https://doi.org/10.1016/j.rineng.2021.100263

[9] Seciureanu M., Guiman M.-V., Nastac S.-M., Nechita P., Debeleac C.-N., Capatana G.-F., On Experimental Evaluation of Tortuosity for Cellulose-Based Highly Porous Composites Used Within Noise Insulation Applications, Materials & Design, 28(4), 2007, pp. 1288-1297, ISSN 0261-3069, https://doi.org/10.1016/j.matdes.2005.12.009

[10] Dobrescu C., The dynamic response of the vibrating compactor roller, depending on the viscoelastic properties of the soil, Applied System Innovation, 3(2):25, 2020. https://doi.org/10.3390/asi3020025

[11] Chendi Zhu, Jian Yang, Chris Rudd, Vibration transmission and power flow of laminated composite plates with inerter-based suppression configurations, International Journal of Mechanical Sciences, Volume 190, 2021, 106012, ISSN 0020-7403, https://doi.org/10.1016/j.ijmecsci.2020.10601

[12] Li H, Wang Z, Chang Y, Xu Z, Mou C., Characterization test on nonlinear vibration of the fibre-reinforced composite thin plate, Measurement and Control, 2020, 53(7-8):1318-1330. doi:10.1177/0020294019842608

[13] Xue K., Huang W., Li Q., Three-Dimensional Vibration Analysis of Laminated Composite Rectangular Plate with Cutouts, Materials, 2020, 13(14):3113. https://doi.org/10.3390/ma13143113

[14] Rutger Kok, Marco Peroni, Francisca Martinez-Hergueta, Antonio Pellegrino, Dynamic response of Advanced Placed Ply composites, Composites Part B: Engineering, Volume 248, 2023, 110347, ISSN 1359-8368, https://doi.org/10.1016/j.compositesb.2022.110347

[15] Nur Izzah Nabilah Haris, Mohamad Zaki Hassan, R.A. Ilyas, Mohamed Azlan Suhot, S.M. Sapuan, Rozzeta Dolah, Roslina Mohammad, M.R.M. Asyraf, Dynamic mechanical properties of natural fiber reinforced hybrid polymer composites: a review, Journal of Materials Research and Technology, Volume 19, 2022, pp. 167-182, ISSN 2238-7854, https://doi.org/10.1016/j.jmrt.2022.04.155

[16] Rooney M., Roberts J.-C., Murray G.-M., and Romenesko B.-M., Advanced Materials: Challenges and Opportunities, Johns Hopkins APL Technical Digest, Volume 21, Number 4 (2000), pp. 516 – 527

[17] Yong Li, Yao Xiao, Long Yu, Kang Ji, Dongsheng Li, A review on the tooling technologies for composites manufacturing of aerospace structures: materials, structures and processes, Composites Part A: Applied Science and Manufacturing, Volume 154, 2022, 106762, ISSN 1359-835X, https://doi.org/10.1016/j.compositesa.2021.106762

[18] Nwakamma Ninduwezuor-Ehiobu, Olawe Alaba Tula, Chibuike Daraojimba, Kelechi Anthony Ofonagoro, Oluwaseun Ayo Ogunjobi, Joachim Osheyor Gidiagba, Blessed Afeyokalo Egbokhaebho, & Adeyinka Alex Banso, Exploring innovative material integration in modern manufacturing for advancing U.S. competitiveness in sustainable global economy, Engineering Science & Technology Journal, 4(3), pp. 140-168, 2023, https://doi.org/10.51594/estj.v4i3.558

[19] Mamta Saiyad, Devashrayee N.M., Lifetime estimation of epoxy based composite materials on irradiating with gamma radiation for shielding applications, Polymer Testing, Volume 93, 2021, 106929, ISSN 0142-9418, https://doi.org/10.1016/j.polymertesting.2020.106929

[20] Gong Cheng, Xinzhi Wang, Zhangzhou Wang, Yurong He, Heat transfer and storage characteristics of composite phase change materials with high oriented thermal conductivity based on polymer/graphite nanosheets networks, International Journal of Heat and Mass Transfer, Volume 183, Part B, 2022, 122127, ISSN 0017-9310, https://doi.org/10.1016/j.ijheatmasstransfer.2021.122127

[21] Tridech C., Maples H.-A., Robinson P., Bismarck A., High Performance Composites with Active Stiffness, ACS Applied Materials & Interfaces, 5(18), 2013, https://doi.org/10.1021/am402495n

[22] Hongjuan Yang, Lei Yang, Zhengyan Yang, Yinan Shan, Haosen Gu, Jitong Ma, Xu Zeng, Tong Tian, Shuyi Ma, Zhanjun Wu, Ultrasonic detection methods for mechanical characterization and damage diagnosis of advanced composite materials: A review, Composite Structures, Volume 324, 2023, 117554, ISSN 0263-8223, https://doi.org/10.1016/j.compstruct.2023.117554

[23] Duchene, P., Chaki, S., Ayadi, A. et al. A review of non-destructive techniques used for mechanical damage assessment in polymer composites, Journal of Materials Science, vol. 53, pp. 7915–7938, 2018, https://doi.org/10.1007/s10853-018-2045-6

COMAT

The 10th International Conference on ADVANCED COMPOSITE MATERIALS ENGINEERING

Transilvania University of Brasov
FACULTY OF MECHANICAL ENGINEERING

30-31 October 2024

ABOUT SIMULATION OF VIBRATORY COMPACTION EQUIPMENT WITH COMPOSITE MATERIALS INCORPORATED

Miron D.S., Debeleac C.N.*

"Dunarea de Jos" University of Galati, Engineering and Agronomy Faculty in Braila, Research Center for Mechanics of Machines and Technological Equipments, Braila, Romania, carmen.debeleac@ugal.ro
*Corresponding author: carmen.debeleac@ugal.ro

Abstract: *In this paper, the authors addressed the topic of computational simulation of composite materials from the constructive structure of vibratory compaction equipment (roller, rammer, vibratory plate). The aspects that must be considered for the development of dynamic models that accurately simulate the engineering phenomenon have been identified. In the current context of the digitization of industry 4.0, the estimation based on such models of the efficiency of the compaction process is of great relevance.*

Keywords: *compactors, advanced composite materials, challenges, computational simulation*

1. INTRODUCTION

Some compaction quality control techniques to improve the efficiency of construction work are based on monitoring the response parameters of a dynamic model subjected to computer simulation [1,2]. The adoption of the dynamic vibration model for its integration into AI, BIM, data mining or intelligent control must consider the dynamic behavior of each part embedded in the analyzed machine-land system. Changing the materials from which component parts of the compactor structure are made leads to the modification of some parameters that have a significant influence on the efficiency of the vibration compaction process, such as: mass, stiffness, rigidities etc. Vibratory compaction involves a technological process where a vibrating tool applies oscillating forces transmitted into terrain or construction materials. Currently, the incorporation of composite materials in the construction of compaction equipment brings significant benefits, such as weight reduction, increased corrosion resistance, increased service life etc. The manufacture of these

materials involves the use of several principles and methods aimed at ensuring optimal fiber alignment, resin distribution and void elimination [3-5].

2. APPLICABILITY OF COMPOSITE MATERIALS IN COMPACTOR EQUIPMENTS FABRICATION

In the last decade, composite materials are increasingly used in the manufacturing of compaction equipment due to their outstanding features, such as high strength-to-weight ratio, durability, and resistance to corrosion and wear. In Table 1 are shown the composite materials commonly used in equipment for vibratory compaction.

Table 1. Examples of the compactor parts fabricated with composite materials

Composite materials	Products	Benefits
Glass Fiber-Reinforced Polymer (GFRP)	• Covers and housings • Handlebars and frames	GFRP offers a good balance of strength, flexibility, and cost-effectiveness. It is lightweight and resistant to corrosion, making it suitable for components that require both strength and durability.
Carbon Fiber-Reinforced Polymer (CFRP)	• Structural components • Vibration damping	CFRP is known for its high strength-to-weight ratio, excellent stiffness, and fatigue resistance. It is more expensive than GFRP but offers superior performance, especially in high-stress applications.
Aramid Fiber-Reinforced Polymer	• Drive Belts • Protective layers	Aramid fibers offer excellent tensile strength, impact resistance, and abrasion resistance, making them ideal for applications that require high durability under dynamic loads.
Metal Matrix Composites (MMCs)	• Feet of the rammer • Drum of the roller	MMCs offer enhanced mechanical properties, such as higher strength, stiffness, and wear resistance compared to the base metal. They also maintain good thermal conductivity and are more resistant to thermal degradation.
Polyurethane Composites	• Bellows and seals • Vibration pads	Polyurethane composites are flexible, durable, and resistant to abrasion and impact. They also have good vibration damping properties.
Rubber-Fiber Composites	• Shock absorbers • Drive belts and pads	These composites offer excellent elasticity, impact resistance, and wear resistance. They are particularly useful for applications requiring significant flexibility and durability.
Ceramic Matrix Composites (CMCs)	High-temperature components	CMCs are known for their excellent thermal stability, high strength at elevated temperatures, and resistance to wear and corrosion
Hybrid Composites	Custom components	Hybrid composites allow for the optimization of specific properties, such as balancing strength, stiffness, and cost.

Currently, the chassis or the main frame of the technological equipment, as well as the working organs (drum or base plate at vibratory plate and rammer) are made of materials based on composites with glass fiber or carbon fiber giving high resistance to abrasion compared to traditional materials (such as steel or its alloys) and reducing the transmission of unwanted vibrations to the user operator [6]. The realization of anti-vibration elements from elastomeric materials (such as fiber-reinforced elastomers) leads to an increase in the level of vibration damping in the structural elements of the equipment (extending the

life of the technological compaction equipment), as well as the comfort of the attendant operator. The use of fiberglass or carbon fiber composite materials in the engine housing provides greater corrosion resistance in harsh working environments and helps reduce overall weight. Also, the control lever and handles are easier to handle and more comfortable for the operator, if they are made of fiber-reinforced plastic composite materials, offering an ergonomic design, increased resistance to wear and tough working conditions. The joining parts and supports in the structure of the equipment that ensure the connection and support of the various components of the vibratory compaction equipment are also made of composite materials with carbon fiber or glass, thus offering increased resistance to traction and bending, being ideal for parts that must be at the same time light and durable. Thus, the engine impact protection housing is made of a single piece made of high strength composite material (Figure 1).

Figure 1: New material used to protective housing of the compactors equipment [13-15]

In addition, the drive belts are much more resistant to high tensions and more stable under the action of variable loads after the traditional rubber was replaced with aramid fiber composite (Figure 2).

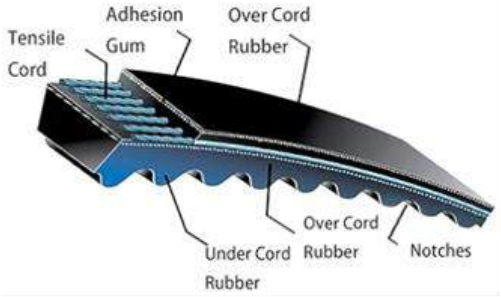

Figure 2: The structure of a belt drive with aramid fiber composite

The main advantages of aramid composite material are high tensile strength, durability, dimensional stability, heat resistance. A comparison between the two materials (rubber and aramid fiber composite) is given in Table 2.

Table 2. Summary of material properties: rubber belt vs aramid fiber composite belt

Properties / Material	Rubber	Aramid fiber composite
Density	1.1 - 1.5 g/cm³	around 1.44 g/cm³
Young's modulus	2 - 10 MPa	70 - 180 GPa
Poisson's ratio	0.45 – 0.50	0.35
Tensile strength	10 - 30 MPa	3600 MPa
Heat resistance	100°C	150 - 200°C
Elongation at break	500 %	less than 5%
Flexibility	Highly	Less (more rigid)

Although currently the working tools (e.g. drums or base plates) of vibratory compactors are made of metallic materials, there is a significant potential for the use of composite materials in the future, depending on technological progress and market requirements.

3. CHALLENGES TO SIMULATION OF THE DYNAMIC BEHAVIOR OF COMPACTION EQUIPMENTS

The simulation of the behavior of a transmission with an aramid material belt must highlight the efficient transmission of power (without significant energy losses at high speeds), the dynamic behavior under variable load conditions (without permanent deformations or stretches), the reduction of vibrations and noise in performance, flexibility and fatigue resistance (and implicitly extended life even under continuous or cyclical operating conditions). Dedicated software applications are available to simulate the dynamic behavior of the belt transmission system, such as: ANSYS, Abaqus, LS-DYNA, Matlab etc. The results of data processing that are of interest in this case refer to: stress and strain analysis (stress distributions, strain rates, and identify potential failure points in the composite), dynamic response (vibrational modes, resonance frequencies, and damping characteristics) and fatigue life under cyclic loading conditions.

Regarding the overall approach of a compaction equipment such as a roller, then the aspects targeted by the simulation of the technological process are oriented to the evaluation of the operational performance. In this regard, the linear elastic two-degree-of-freedom model is frequently used for the vibration compaction simulation process, which model is based on the linear elastic vibration theory and uses the mass-spring-damping system to describe roller-terrain vibratory system. As shown in Figure 3 (ks is the elastic stiffness of the terrain; cs is the damping of the soil; kf is the stiffness of the shock absorber; cf is the damping of the shock absorber; xf is the displacement of the upper frame; xd is the displacement of the vibratory drum), the model simplifies the vibratory roller into two main parts, namely, the upper frame and the vibratory drum. Both parts are connected by a damping system, the terrain is supposed to a preponderantly elastic body, and the Kelvin model is used to simulate the behavior of the terrain.

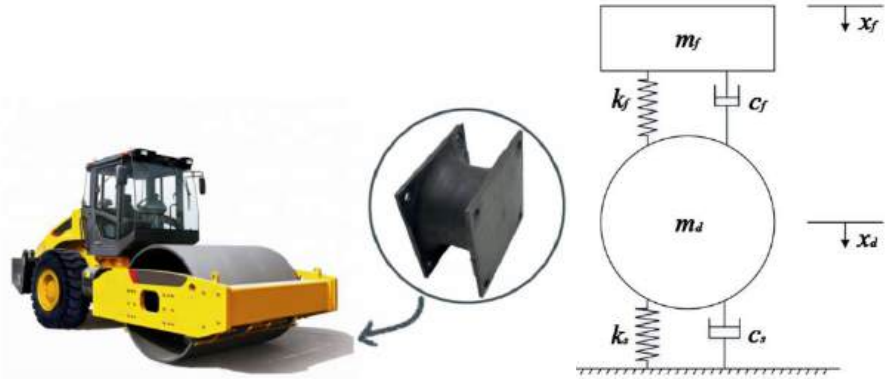

Figure 3: 2-DOF dynamic model for behavior simulation of the vibratory compaction process

The dynamic differential equation of the model is expressed as:

$$\begin{bmatrix} m_f & 0 \\ 0 & m_d \end{bmatrix} \begin{Bmatrix} \ddot{x}_f \\ \ddot{x}_d \end{Bmatrix} + \begin{bmatrix} c_f & -c_f \\ -c_f & c_f + c_d \end{bmatrix} \begin{Bmatrix} \dot{x}_f \\ \dot{x}_d \end{Bmatrix} + \begin{bmatrix} k_f & -k_f \\ -k_f & k_f + k_d \end{bmatrix} \begin{Bmatrix} x_f \\ x_d \end{Bmatrix} + \begin{bmatrix} m_f \\ m_d \end{bmatrix} = \begin{Bmatrix} 0 \\ F_0 sin\omega t \end{Bmatrix}, \quad (1)$$

where m_f is the mass of the upper frame; m_d is the mass of the vibratory drum; $\dot{x}_f$ and $\ddot{x}_f$ are the speed and acceleration of the upper frame, respectively; $\dot{x}_d$ and $\ddot{x}_d$ are the speed and acceleration of the vibratory drum, respectively; F_0 is the dynamic force; ω is the rotational speed of the eccentric mass; t is time.

By changing the traditional material with composite material, a reconsidered approach of the dynamic model of compactor-terrain interaction are needed. This implies detailed knowledge of the inertial characteristics as an effect of reducing the mass of the component elements (m_d and m_f), the stiffness and damping characteristics of the anti-vibration elements (k_f and c_f), the range of values of the natural vibrations of the replaced parts for avoided resonance under working conditions, etc. The basic idea of a vibration compaction model is the accuracy with which it simulates the vibration compaction process, by evaluating the dynamic response of the soil-working tool interaction, the deformation of the filling materials and the influence of different parameters on the compaction effect [7,8] etc. In the specialized literature [9], the study of this interaction was carried out based on many vibration compaction models (linear and nonlinear elastic, viscoelastic, viscoelastic plastic, etc.) with the aim of analyzing the influence of different compaction parameters on the dynamic characteristics and compaction effects of system, to provide a theoretical evaluation. In this way, by adopting an adequate model for simulation, the influence of the structural parameters (the distribution of the quality of the upper and lower parts, the stiffness and rigidity of the damper), the operating parameters (amplitude and frequency of vibration, dynamic force), and the soil parameters (stiffness and rigidity) on the dynamic response of the vibratory roller–terrain system can be analyzed.

At present, for vibrations isolations three types of damping materials that are widely used: damping alloy, viscoelastic damping and composites materials [10-12]. Simulation of vibration absorbers made of advanced composite materials involves consideration of the following aspects in order to obtain accurate and useful results:

a) composite material properties: modulus of elasticity, tensile strength, compressive strength, Poisson's ratio, density, damping, etc. Some composite materials have anisotropic mechanical properties, have different internal damping depending on the matrix used and fiber arrangement, and their density influences the dynamic behavior of the absorber.
b) the layered structure of the composite material: configuration of the layers by fiber orientation, the thickness of each layer, and the layering sequence can significantly influence the dynamic behavior, and the interlaminar interaction must be simulated to evaluate the fatigue resistance.

In working conditions with high-amplitude or high-frequency vibrations, vibration absorbers can have a non-linear behavior of the material which is important in choosing the appropriate damping model (viscoelastic, hysteretic, etc.) to correctly simulate the vibration damping generated by the tool active work of the compactor. The natural frequencies depend on the geometry, support conditions, material properties and layered configuration of the composite. Thus, the knowledge of the natural frequencies and natural modes

of vibration of the absorber through a modal analysis (using the Finite Element Method) is necessary to evaluate its performance under resonant conditions.

4. CONCLUSIONS

The use of composite materials by major compactors manufacturers expected to become a very common practice in the fields of construction equipment industry, based on the multiple benefits, as: weight reduction, increased strength and durability, and improved operator efficiency and comfort. Simulating mechanical systems based on composite materials is a complex goal that requires advanced modeling methods, significant computational resources, and a deep understanding of the behavior of these materials under different working conditions. The simulation of composite materials requires the development of complex multi-scale models that highlight the behavior at different scales, from the macro level (general structural behavior) to the micro level (fiber and matrix structure). The computational cost can be extremely high requiring the development of efficient algorithms to reduce the computation time. As composite materials are in continuous development, new combinations of fibers and matrices will be created frequently, making simulation models flexible and able to adapt to new materials. The correlation of simulation results with experimental data is what leads to the validation of the dynamic model, thus ensuring the accuracy of the simulation process of the real phenomenon.

BIBLIOGRAFIE

[1] Zhang Q., An Z., Huangfu Z., Li Q., A review on roller compaction quality control and assurance methods for earthwork in five application scenarios, Materials, 15(7):2610, 2022

[2] Buraga A., Debeleac C., A state-of-the-art review of compaction control tests methods, Magazine of hydraulics, pneumatics, tribology, ecology, sensorics, mechatronics, ,,Hidraulica", No.4, pp. 42 – 51, 2022

[3] Mehdikhani M, Gorbatikh L, Verpoest I, Lomov S.-V., Voids in fiber-reinforced polymer composites: A review on their formation, characteristics, and effects on mechanical performance, Journal of Composite Materials, 53(12):1579-1669, 2019

[4] Bannister M., Challenges for composites into the next millennium - a reinforcement perspective, Composites Part A: Applied Science and Manufacturing, 32(7):901-910, 2001

[5] Meegan J., Some of the challenges faced by the Composites Industry in its bid to become more sustainable, RSC Sustainability, Volume 1, pp. 1737 – 1742, 2023

[6] Debeleac C.-N., Nechita P., Nastac S.-M., Computational investigations on soundproof applications of foam-formed cellulose materials, Polymers, 11(7):1224, 2019

[7] Dobrescu C., The dynamic response of the vibrating compactor roller, depending on the viscoelastic properties of the soil, Applied System Innovation, 3(2):25, 2020

[8] Capatana G., Analytical and computational assessments in vibratory compaction process, Acta Technica Napocensis Series: Applied Mathematics and Mechanics, 56(4):823–828, 2013

[9] Le Van Quynh et al., Optimal design parameters of drum's isolation system for a double-drum vibratory roller, Vibroengineering Procedia, 31:74–79, 2020

[10] Duc F., Bourban P.E., Plummer C.J.G., Månson J.-A.E., Damping of thermoset and thermoplastic flax fibre composites, Composites Part A: Applied Science and Manufacturing, Volume 64, Pp. 115-123, 2014

[11] Treviso A., Van Genechten B., Mundo D., Tournour M., Damping in composite materials: Properties and models, Composites Part B: Engineering, Volume 78, Pp. 144-152, 2015

[12] Wu Jiejun, Li Chenggong, Wang Dianbin, Gui Manchang, Damping and sound absorption properties of particle reinforced Al matrix composite foams, Composites Science and Technology, Volume 63, Issues 3–4, Pp. 569-574, 2003

COMAT

The 10th International Conference on ADVANCED COMPOSITE MATERIALS ENGINEERING

Transilvania University of Brasov
FACULTY OF MECHANICAL ENGINEERING

22-23 October 2024

HEMP-BASED COMPOSITE MATERIALS AS A SUSTAINABLE SOLUTION FOR MODERN INDUSTRIES

Mitroi R.D.[1], Buican G.R.*[2], Bencze A. [3]

1. University Transilvania of Brașov, Brașov, Romania, razvan.mitroi@student.unitbv.ro
2. University Transilvania of Brașov, Brașov, Romania, buican.george@unitbv.ro
3. University Transilvania of Brașov, Brașov, Romania, andrei.bencze@unitbv.ro

*Corresponding author: buican.george@unitbv.ro

Abstract: *In the global effort to develop sustainable solutions, hemp-based composite materials have emerged as a viable, less toxic and environmentally friendly alternative to traditional materials. Due to its physical and mechanical properties, hemp is a renewable resource with significant potential in industries such as aerospace, construction, transportation, and energy. This article aims to investigate the manufacture and tensile strength of hemp roving, hemp coupled with fiber glass and fiber glass composites. Microscopic observations are also made to evaluate the failure of the test specimens.*

Keywords: *Composite materials, hemp, hemp roving, fiber glass, tensile strength*

1. INTRODUCTION

The increasing demand for sustainable and environmentally friendly materials has driven extensive research into natural fiber composites.[1] Among these, hemp fiber has emerged as a promising alternative due to its mechanical properties, low cost, biodegradability, and minimal environmental impact compared to synthetic fibers.[2] As industries such as automotive, construction, and aerospace explore the use of renewable resources, there is a growing interest in understanding the potential of hemp composites in various combinations.[3,4,5,6]

This paper investigates the mechanical properties and performance of different composite materials, specifically focusing on combinations of hemp, hemp fiber with fiberglass and fiberglass. By combining hemp with these synthetic fibers, the goal is to assess whether the natural fiber's benefits can be enhanced by the superior strength and durability offered by fiberglass. [5,6]

The research aims to evaluate properties such as tensile strength, bending strength and overall structural integrity. This study will contribute to a deeper understanding of how hemp-based composites perform in comparison to traditional composite materials and explore the potential for these hybrid composites in both structural and non-structural applications.

The findings of this study will help inform the future design and development of sustainable composite materials that can be applied across a range of industries, ultimately supporting a transition to more eco-friendly manufacturing practices.

2. Fabrication

To assess the mechanical properties, we prepared three types of composite materials. The first type consisted of hemp roving fibers, the second type combined hemp roving with fiberglass, and the third type utilized only fiberglass. An unsaturated polyester resin (ENYDYNE H 68372 TA) served as the matrix material, with BUTANOX M-50 as the hardener, applied at a ratio of 200 mL of resin to 4 mL of hardener. The working time of the resin is approximately 20 to 24 minutes, while the hardening time is determined experimental and for this case is 24 hours.

To eliminate air bubbles from the hemp roving woven fabric impregnated with resin, we employed a specialized roller to facilitate the impregnation of the material within the fabrication matrix, as illustrated in Figure 1.

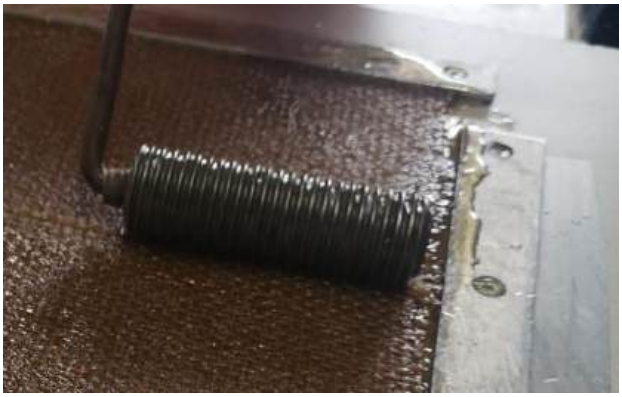

Figure 1: Hemp resin treated for air bubbles.

3. Method

In order to evaluate the hemp composite mixtures, we followed the guidelines of ISO-527-4:2021, issued by EASA, to define the geometry and dimensions of the test specimens. Based on this standard, we fabricated test samples for composites reinforced with continuous fibers, maintaining a uniform thickness of 2 mm. The thickness of compression-molded materials must be consistent at all points, with deviations not exceeding 2% of the mean value. Initially, we will employ the Type 2 test specimen, as depicted in Figure 2, for tensile strength testing, and the Type 1 test specimen for bending tests, as shown in Figure 3.

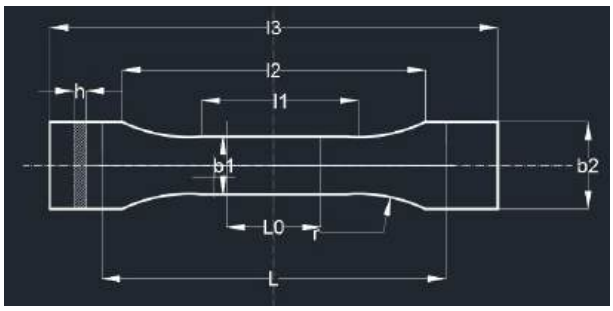

Figure 2: Type 2 test specimen.

Figure 3: Type 1 test specimen.

For the investigation of mechanical properties such as tensile and bending strength, and to determine the modulus of elasticity and Poisson's ratio, we utilized a Universal Testing Machine (WDW 150-S), as shown in Figure 4.a).

a) b) c)

Figure 4: a) General view of Universal Testing Machine WDW 150-S; b) Tensile strength configuration of WDW 150-S; c) Bending test configuration of WDW 150-S.

To characterize the mechanical properties of the three types of composites, five test specimens were manufactured for each fiber combination in accordance with ISO 527-4:2021. The first set consisted of hemp roving fibers, the second set combined hemp roving with fiberglass, and the third set utilized only fiberglass. These specimens were coded as shown in Table 1.

Table1. Specimen coding for tensile strength

Fiber glass	Fiber glass + Hemp	Hemp roving
S-1	SC-1	C1
S-2	SC-2	C2
S-3	SC-3	C3
S-4	SC-4	C4
S-5	SC-5	C5

In figure 5 we can see test specimens after tensile strength testing.

a)

b)

c)

Figure 5: a) Test specimen Fiber glass after testing; b) Test specimen Fiber glass + Hemp after testing; c) Test specimen Hemp roving after testing.

Table 2 and Figure 6 display the tensile strength values for each tested specimen. The mean values for each type of fiber are as follows: 48.8 MPa for fiberglass composites, 25 MPa for fiberglass with hemp composites, and 8.5 MPa for hemp composites.

Table2. Tensile strength values

Test specimen	Max tensile strength Fiber Glass [MPa]	Test specimen	Max tensile strength Fiber Glass Hemp[MPa]	Test specimen	Max tensile strength Fiber Glass Hemp roving[MPa]
S-1	42	SC-1	21	C-1	6
S-2	54	SC-2	20	C-2	10
S-3	43	SC-3	29	C-3	6
S-4	50	SC-4	32	C-4	6
S-5	55	SC-5	23	C-5	14

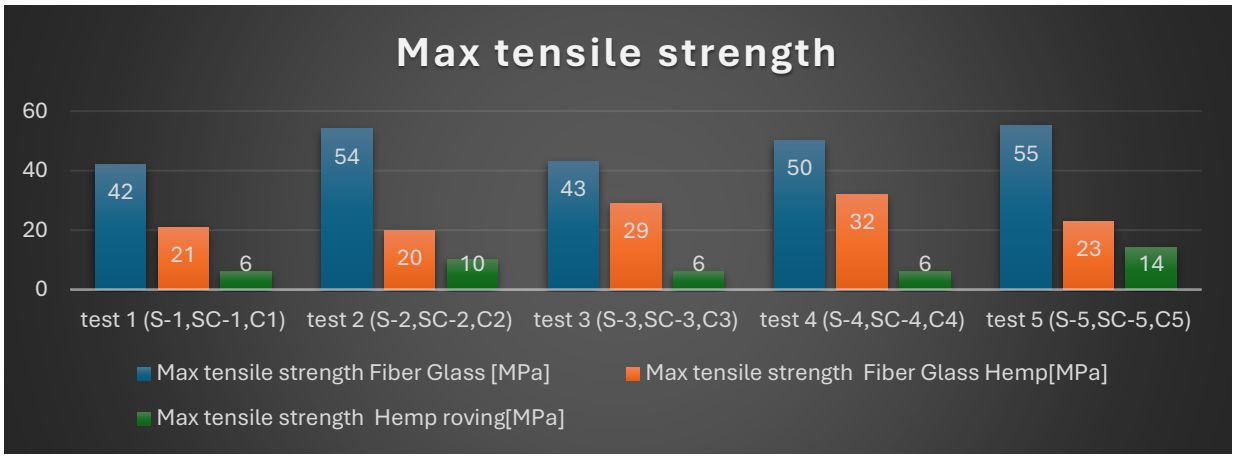

Figure 6: Tensile strength results for fiberglass fibers, fiber glass with hemp and hemp roving

The data presented in Table 2 and Figure 6 highlight the tensile strength values for each tested specimen, revealing important insights regarding hemp fiber. While fiberglass composites exhibit the highest tensile strength with a mean value of 48.8 MPa, the incorporation of hemp fibers into these composites results in a reduction of tensile strength to 25 MPa. Additionally, hemp composites alone demonstrate the lowest tensile strength at just 8.5 MPa.

Despite this decrease, the combination of hemp fibers with fiberglass offers notable benefits. By coupling hemp fibers with fiberglass, we enhance the overall performance of the composite, potentially improving its sustainability and environmental impact while still achieving substantial strength. This approach demonstrates that integrating hemp fibers into fiberglass composites can create a balanced material that leverages the advantages of both fibers.

Table3. Bending strength values

Test specimen	Max bending strenght Fiber glass [MPa]	Test specimen	Max bending strenght Fiber glass with Hemp [MPa]	Test specimen	Max bending strenght Hemp [MPa]
S-1	210	C-1	84	SC-1	181
S-2	240	C-2	84	SC-2	174
S-3	205	C-3	58	SC-3	147
S-4	225	C-4	58	SC-4	188
S-5	240	C-5	52	SC-5	100

For the bending test, we utilized a Type 1 geometry for the test specimens, as shown in Figure 3. The coding remained consistent with that used for the tensile strength tests, as indicated in Table 1.

Table 3 and Figure 7 display the bending strength values for each tested specimen. The mean values for each type of fiber are as follows: 224 MPa for fiberglass composites, 158 MPa for fiberglass with hemp composites, and 67,2 MPa for hemp composites.

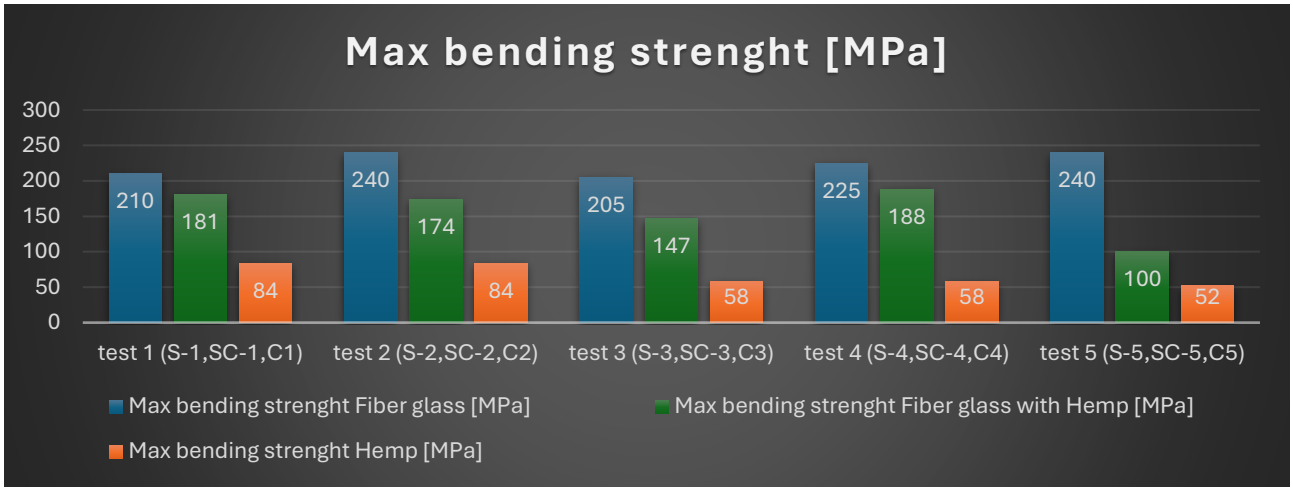

Figure 7: Bending strength results for fiberglass fibers, fiber glass with hemp and hemp roving

The data presented in Table 3 and Figure 7 highlight the bending strength values for each tested specimen, revealing important insights regarding hemp fiber. While fiberglass composites exhibit the highest tensile strength with a mean value of 224 MPa, the incorporation of hemp fibers into these composites results in a reduction of bending strength to 158 MPa. Additionally, hemp composites alone demonstrate the lowest bending strength at just 67,2 MPa. This highlights the advantages of combining hemp fibers with fiberglass; despite a decrease in

strength, the resulting fiberglass with hemp composites offers a balanced performance that capitalizes on the sustainability and environmental benefits of hemp. Thus, this composite provides a practical solution for applications that require both strength and eco-friendliness.

4. CONCLUSIONS

Based on this testing, we conclude that hemp composites alone, with a tensile strength of 8,5 MPa and bending strength of 67,2 MPa, are not suitable for structural parts. However, they can effectively be used for internal components such as chairs, chair arm inserts or floor and ceiling panels due to their good bending resistance. While these composites may sacrifice some strength, they excel in sustainability, as hemp fibers are less toxic to both the environment and human health. Future research could explore replacing the matrix with bio-resin and testing the composite for fire and smoke generation.

Additionally, when combining fiberglass with hemp roving weaving, we achieve a composite that retains roughly half the properties of pure fiberglass composites, which have a tensile strength of 48.8 MPa and bending strength of 224 MPa, while significantly reducing toxicity. This hybrid material, with a tensile strength of 25 MPa and bending strength of 158 MPa, could be viable for certain structural applications.

Further investigations should focus on using bio-resins and experimenting with various organic fibers, such as flax, silk, and hemp, both individually and in combination, to develop a fully organic and non-toxic composite material.

5. Acknowledgement

We also acknowledge PRO-DD Structural Founds Project (POS-CCE, O.2.2.1., ID 123, SMIS 2637, ctr. no 11/2009) for providing the infrastructure used in this work.

BIBLIOGRAFIE

[1] Vershinina A.V., Veselova O.V., Ivanova S.N., Investigation of the Characteristics of Bio-based Raw Materials: Technical Hemp Fibers, Nanotechnol Russia 18, 64–72 (2023)

[2] Dahal R.K., Acharya B., Dutta A., Mechanical response of the hemp biocarbon-filled hemp-reinforced biopolymer composites. J Polym Res 30, 267 (2023)

[3] Dahal R.K., Acharya B., Dony B., Dutta A., Biocarbon Filled Hemp-Epoxy Composite: Its Physical, Mechanical, and Thermal Properties. Appl Compos Mater 29, 2185–2202 (2022)

[4] Salpriyan P.M., Krishna K., Singh T., Recent developments in natural fibre polymer composite materials for interior design applications: an overview from acoustic perspective. Int J Interact Des Manuf (2024)

[5] Gangwar A., Kumar V., Yaylaci M., Panda S.K., Computational Modelling and Mechanical Characteristics of Polymeric Hybrid Composite Materials: An Extensive Review. Arch Computat Methods Eng 31, 3901–3921 (2024).

[6] AL-Oqla F.M., Hayajneh M.T., Nawafleh, N., Advanced synthetic and biobased composite materials in sustainable applications: a comprehensive review. emergent mater. 6, 809–826 (2023)

COMAT The 10th International Conference on ADVANCED COMPOSITE MATERIALS ENGINEERING

Transilvania University of Brasov
FACULTY OF MECHANICAL ENGINEERING

22-23 October 2024

STATIC ANALYSIS AND SIMULATION OF THE BEHAVIOR OF ALUMINUM COMPOSITE MATERIALS

Munteanu M.V. *[1], Scutaru M.L.[1], Cerneleac I.[1]

1.Transilvania University of Brașov, Romania, v.munteanu@unitbv.ro, lscutaru@unitbv.ro

Abstract: *The mechanical behavior of aluminum-based composites (MMC) under static stress is investigated, focusing on Aluminum 2024 and Aluminum 2024-T3 alloys. Through a series of mechanical tests, such as tensile and bending, the strength and stiffness properties of the materials were evaluated, with a significant improvement observed in the case of heat treatment. Numerical simulations using the finite element method (FEM) were also performed to validate the predicted behavior of these materials. The obtained results showed a strong correlation between experimental and simulated data, highlighting the potential of using aluminum-based composite materials in industrial applications, such as aeronautics and the automotive industry.*

Keywords*: Composite materials, Aluminum 2024, Static loads, Tensile and bending, MEF simulation*

1. INTRODUCTION

Aluminum-based composite materials, or metal matrix composites (MMCs), play a crucial role in industry due to their improved mechanical and physical properties, such as high strength-to-weight ratio, corrosion resistance and thermal conductivity[1-14]. These advantages make them ideal for applications in the aeronautical, automotive and construction industries [11-19]. The objective of this study is to analyze the static behavior of aluminum-based composite materials, focusing on Aluminum 2024 and Aluminum 2024-T3 alloys, with reference to manufacturing methods and experimental results.

Aluminum 2024 and Aluminum 2024-T3 alloys are widely recognized materials for their applicability in industries with high structural requirements[17-25]. Aluminum 2024 is a high-performance alloy with additions of copper, magnesium and manganese, being heat treated to enhance mechanical properties.

2. MATERIAL AND METHOD

Material Selection Aluminum 2024 and Aluminum 2024-T3 alloys were chosen for industrial applications due to their mechanical properties.

Mechanical tests were performed to evaluate the strength and stiffness of the materials under static load. In the case of tensile tests, Aluminum 2024 and Aluminum 2024-T3 showed significant differences in elongation and maximum stress. These tests highlighted that the T3 heat treatment significantly improves the mechanical properties of the material, with a notable increase in tensile strength.

2.1 Optical Spectral Analysis

To verify the chemical composition of the samples, optical spectral analysis was performed using an optical emission spectrometer, SPECTROMAXx M (Figure 1). The samples were prepared by polishing (Figure 2) to remove surface contaminants, and the analysis results (Figure 3 and 3) confirmed the chemical composition according to accepted standards for Aluminum 2024.

Figure 1. SPECTROMAXx M optical emission spectrometer

Figure 2. Presi-Minitech 233 Polishing Machine

Aluminum, Al	90.7 - 94.7 %	90.7 - 94.7 %
Chromium, Cr	<= 0.10 %	<= 0.10 %
Copper, Cu	3.8 - 4.9 %	3.8 - 4.9 %
Iron, Fe	<= 0.50 %	<= 0.50 %
Magnesium, Mg	1.2 - 1.8 %	1.2 - 1.8 %
Manganese, Mn	0.30 - 0.90 %	0.30 - 0.90 %
Other, each	<= 0.05 %	<= 0.05 %
Other, total	<= 0.15 %	<= 0.15 %
Silicon, Si	<= 0.50 %	<= 0.50 %
Titanium, Ti	<= 0.15 %	<= 0.15 %
Zinc, Zn	<= 0.25 %	<= 0.25 %

Figure 3. Chemical composition of Aluminum 2024 - minimum and maximum limits

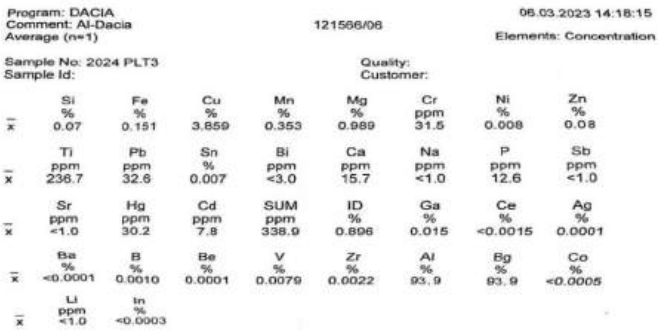
Program: DACIA
Comment: Al-Dacia
Average (n=1)
121566/06
06.03.2023 14:18:15
Elements: Concentration
Sample No: 2024 PLT3
Sample Id:
Quality:
Customer:

x̄	Si % 0.07	Fe % 0.151	Cu % 3.859	Mn % 0.353	Mg % 0.989	Cr ppm 31.5	Ni % 0.008	Zn % 0.08
x̄	Ti ppm 236.7	Pb ppm 32.6	Sn % 0.007	Bi ppm <3.0	Ca ppm 15.7	Na ppm <1.0	P ppm 12.6	Sb ppm <1.0
x̄	Sr ppm <1.0	Hg ppm 30.2	Cd ppm 7.8	SUM ppm 338.9	ID % 0.896	Ga % 0.015	Ce % <0.0015	Ag % 0.0001
x̄	Ba % <0.0001	B % 0.0010	Be % 0.0001	V % 0.0079	Zr % 0.0022	Al % 93.9	Bg % 93.9	Co % <0.0005
x̄	Li ppm <1.0	In % <0.0003						

Figure 4. The result of the spectral analysis

2.2 Optical Micrography

The internal structure of the samples was examined by optical micrography using a Zeiss Axio microscope, equipped with an AxioCam Erc5s digital camera. The samples were prepared by polishing, using abrasive cloths with variable grain sizes to obtain a smooth and imperfect surface. This analysis method provided a detailed assessment of the microstructure of the materials, verifying compliance with the ASRO standards for Aluminum 2024.

2.3 Mechanical Tensile and Bending Tests

For the tensile test, the tests were performed on the LLOYD Instruments LS100 Plus machine. The resulting mechanical properties are summarized in Table 1.

Table 1. Properties of the samples after tensile loading.

Aluminum alloy type	Sample number	Maximum force at maximum load	Maximum voltage at full load	Elongation at break	Young's modulus	Stiffness
		[kN]	[MPa]	[mm]	[MPa]	[N/m]
Al 2024	Sample 1	2.336645729	389.4409549	7.676661398	61795.02271	7415402.725
	Sample 2	2.546943845	424.4906408	7.753428012	61177.07248	7341248.698
	Sample 3	2.327299147	387.8831912	8.060494468	67974.52498	8156942.998
	Sample 4	2.383378644	397.229774	7.446361557	62721.94805	7526633.766
	Sample 5	2.430111559	405.0185932	7.90696124	66120.6743	7934480.916
ε	**Average values**	**2.404875785**	**400.8126308**	**7.768781335**	**63957.8485**	**7674941.82**
Al 2024 T3	Sample 1	2.407104824	401.1841374	6.529193232	66939.30789	8032716.947
	Sample 2	2.567459975	427.9099958	5.219486094	71313.692	8557643.04
	Sample 3	2.406676443	401.1127405	2.072679759	70189.23021	8422707.625
	Sample 4	2.493541506	415.590251	4.736249309	57658.21122	6918985.346
	Sample 5	2.493541506	409.0690923	4.746554598	66673.42067	8000810.48

ε	**Average values**	**2.46583946**	**410.9732434**	**4.660832599**	**66554.7724**	**7986572.688**

The results of the tensile tests were presented by the Force-Displacement and Stress-Deformation characteristic curves (Figures 5 - 10), which provide a clear picture of the behavior of composite materials under static loading.

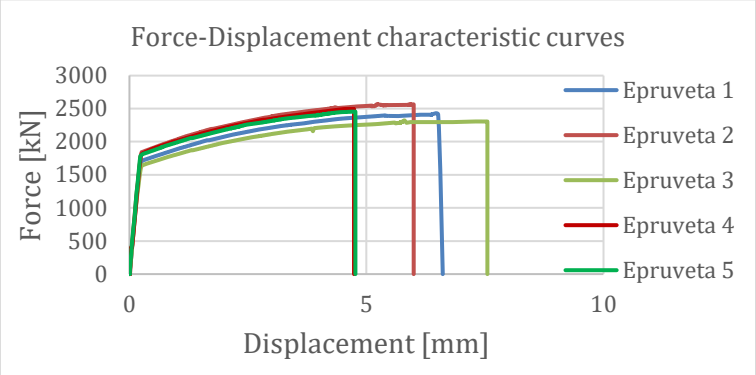

Figure 5. Force-Displacement characteristic curves for 2024 T3 aluminum samples subjected to tensile testing

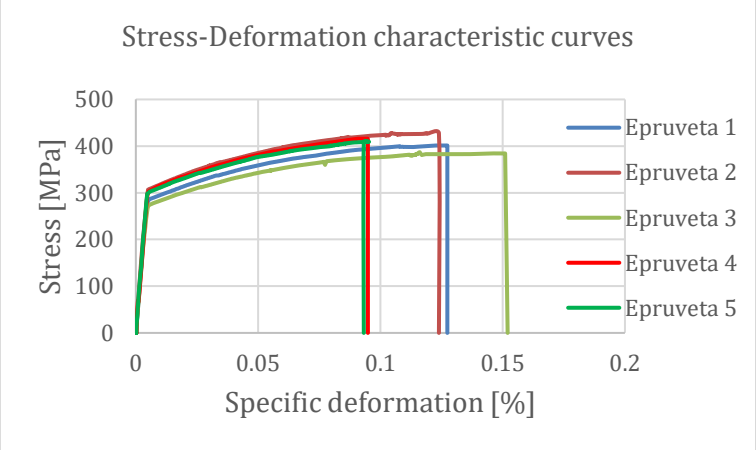

Figure 6. Stress-Deformation characteristic curves for 2024 T3 aluminum samples subjected to tensile testing

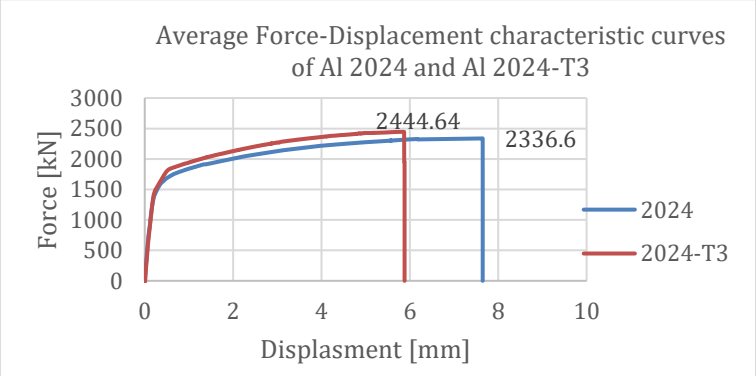

Figure 7. Average Force-Displacement characteristic curves of Al 2024 and Al 2024-T3 subjected to tensile testing

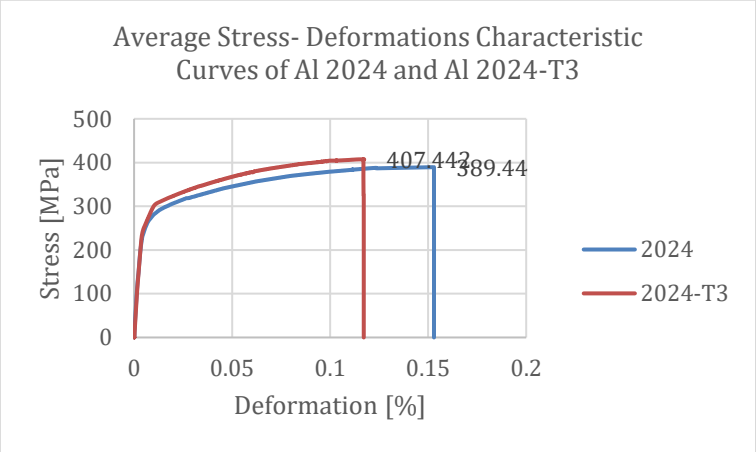

Figure 8. Average Stress- Deformations Characteristic Curves of Al 2024 and Al 2024-T3 Subjected to Tensile Testing

For the bending tests, the LLOYD LR5K Plus bending testing machine was used. The mechanical properties resulting from the bending tests are presented in Table 2, and the force-displacement and stress-deformations characteristics are represented in Figures 9 - 13.

Table 2. Properties of the samples after bending stress

Aluminum alloy type	Sample number	Maximum force at maximum load	Maximum voltage at full load	Maximum Deformation at Maximum Bending	Young's modulus	Bending Stiffness
		[kN]	[MPa]	[mm]	[MPa]	[N/m]
Al 2024	Sample 1	0.023000439	408.8967012	0.044810153	32501.10341	0.008775298
	Sample 2	0.023028919	409.4029956	0.043954701	29969.78275	0.008091841
	Sample 3	0.023685193	421.0701038	0.043954205	30863.1349	0.008333046
	Sample 4	0.023892215	424.7504948	0.04395591	29862.28915	0.008062818
	Sample 5	0.023382113	415.6820023	0.043955451	28199.55946	0.007613881
ε	**Average values**	**0.023397776**	**415.9604596**	**0.044126084**	**30279.17393**	**0.008175377**
Al 2024 T3	Sample 1	0.028079	499.1751	0.035727575	34840.17959	0.009406848
	Sample 2	0.027543	489.6579	0.029746724	34727.4783	0.009376419
	Sample 3	0.0293	520.8926	0.026504176	34669.54903	0.009360778
	Sample 4	0.02871	510.4089	0.02897787	35292.79996	0.009529056
	Sample 5	0.027841	494.9553	0.057730432	34510.27769	0.009317775
ε	**Average values**	**0.028294759**	**503.0179455**	**0.035737356**	**34808.05692**	**0.009398175**

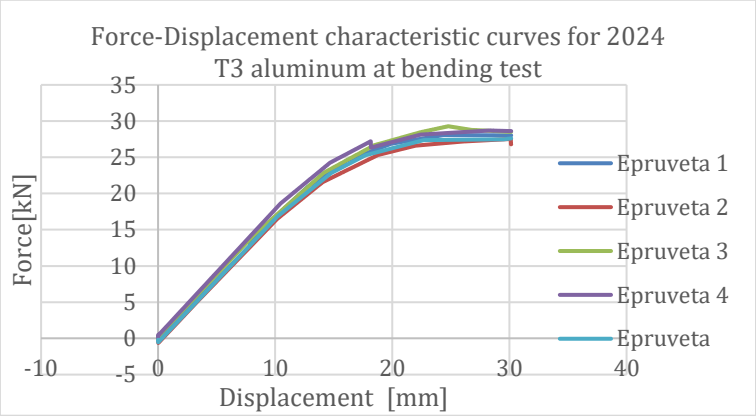

Figure 9. Force-Displacement characteristic curves for 2024 T3 aluminum samples subjected to bending test

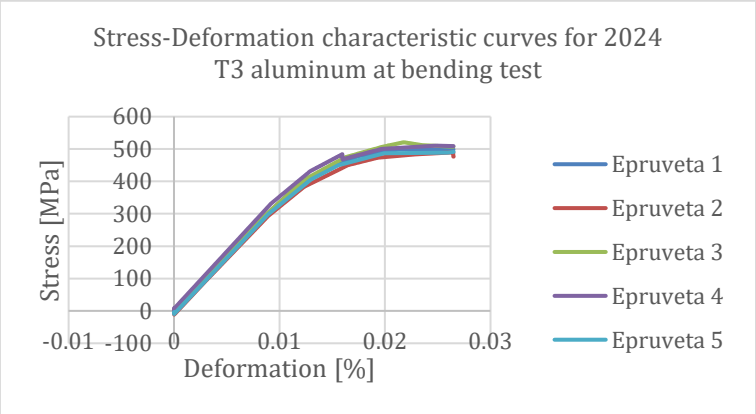

Figure 10. Stress-Deformation characteristic curves for 2024 T3 aluminum samples subjected to bending test

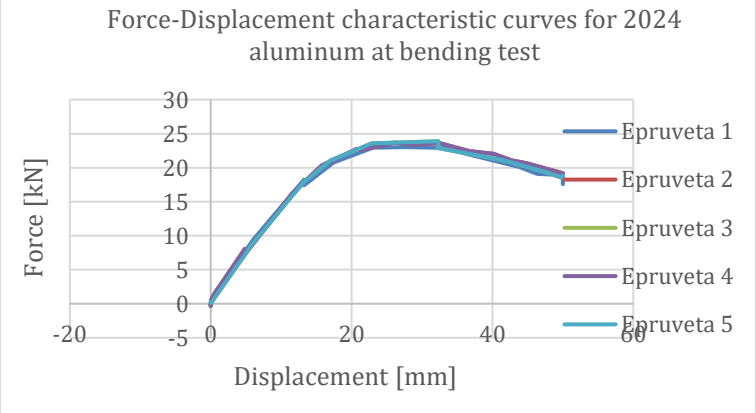

Figure 11. Force-Displacement characteristic curves for 2024 aluminum specimens subjected to bending test

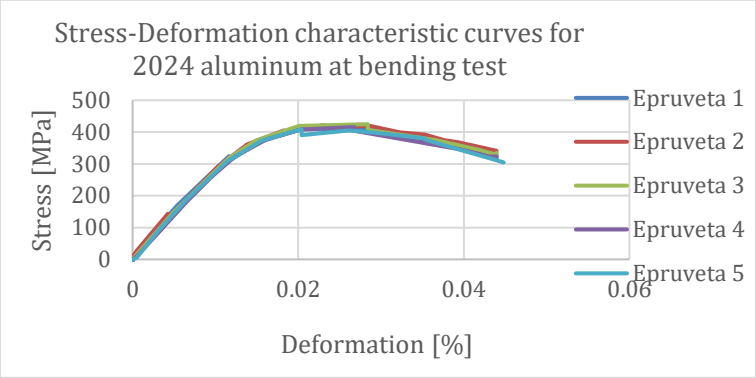

Figura 12. Stress-Deformations characteristic curves for 2024 aluminum specimens subjected to bending test

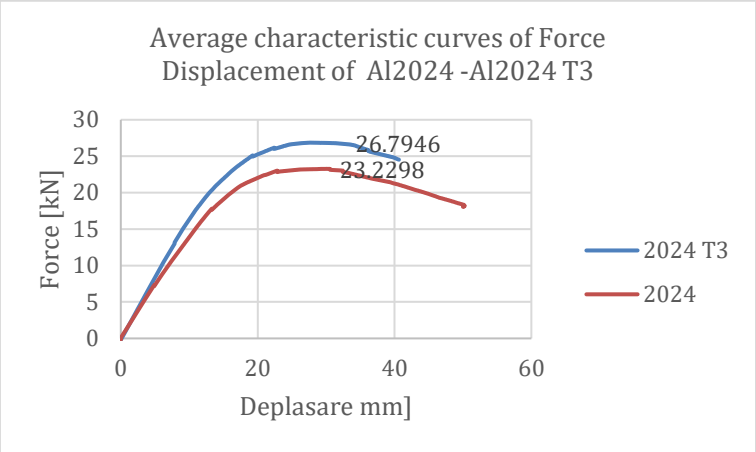

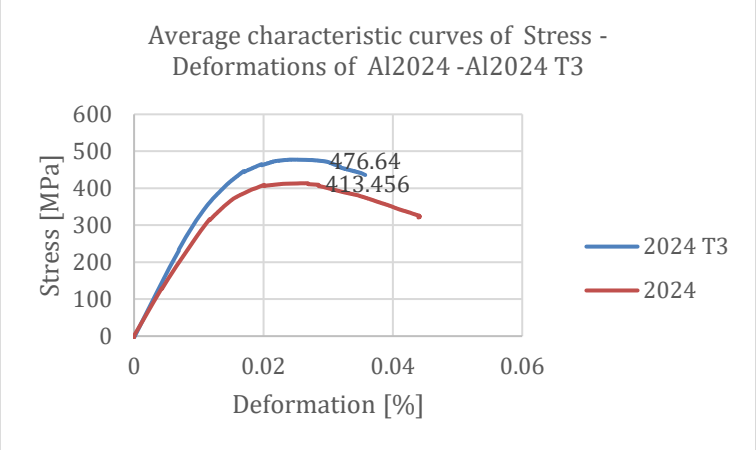

Figure 13. Average characteristic curves a) Force - Displacement and b) Stress - Deformations of Al 2024 and Al 2024-T3 subjected to bending test

2.4 Finite Element Method (FEM) Simulation

In order to better understand the behavior of composite materials under static conditions, the finite element method (FEM) was used, simulating tensile tests through Abaqus software, using 3D modeling for deformable bodies, see figure 14. The geometry of the part was entered according to the experimental dimensions. The analysis revealed that the FEM predictions are consistent with the experimental results, confirming the accuracy of the simulations in

describing the behavior of Aluminum 2024 composite materials subjected to tensile stress.

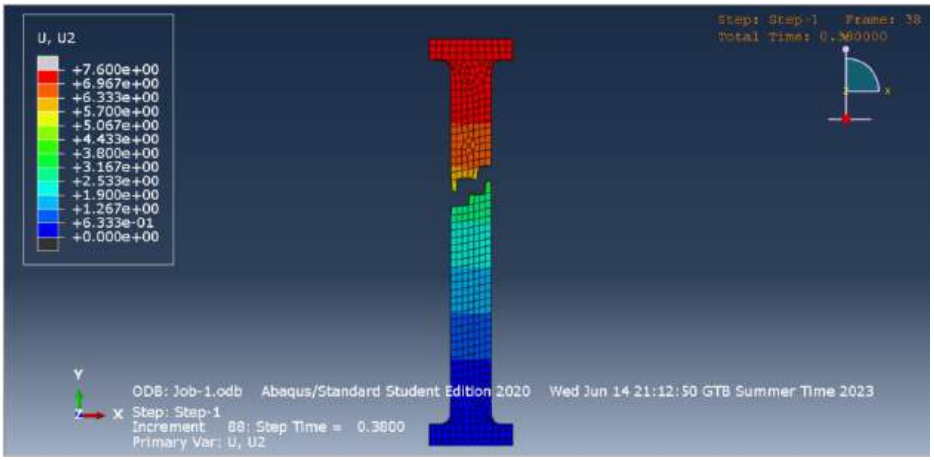

Figure 14. Finite element analysis

3. EXPERIMENTAL RESULT AND DISCUSSION

The experimental test results and FEM simulations showed a good correlation between the real and simulated behavior of the 2024 Aluminum composite materials. A significant improvement in mechanical properties was observed for the heat-treated materials (2024-T3 Aluminum) compared to the untreated materials (2024 Aluminum). The applied heat treatments increased the tensile and bending strength, and the use of Abaqus simulation allowed an accurate prediction of the mechanical behavior under static conditions.

The main factors influencing the static behavior of composite materials are the type and volume fraction of the reinforcement, the matrix-reinforcement interface, and the material microstructure. Also, the correct choice of heat treatment is essential for obtaining optimal mechanical properties.

4. CONCLUSION

Aluminum-based composite materials have shown improved performance under static loads when subjected to heat treatment. Tensile and flexural tests have demonstrated increased stiffness and mechanical strength of heat-treated aluminum, making them suitable for critical applications in the aerospace and automotive industries. Finite element simulations have provided accurate predictions and can be used to optimize the design of these materials.

REFERENCES

[1] K. Wang, "Investigation of dynamic stresses in aluminium-based composite materials," Ph.D. thesis, University of XYZ, 2016.
[2] J. Smith, "Mechanics of composite materials," 2nd ed., John Wiley & Sons, New York, NY, USA, 2008.
[3] T. Johnson, "Advanced composite materials: properties, testing, and design," Springer, New York, NY, USA, 2012.
[4] Y. Zhang, "Dynamic behavior of composite materials under impact loading," Journal of Composite Materials, vol. 45, no. 3, pp. 305-318, 2011.
[5] J. Davis, "Finite element analysis of composite materials," 2nd ed., John Wiley & Sons, New York, NY, USA, 2009.

[6] A. Patel, "Composite materials in aerospace engineering," Springer, New York, NY, USA, 2016.
[7] D. Chen, "Experimental investigation of dynamic stresses in aluminium-based composite materials," Journal of Materials Science, vol. 52, no. 4, pp. 2131-2139, 2017.
[8] M. Lee, "Fracture mechanics of composite materials," Cambridge University Press, Cambridge, UK, 2018.
[9] J. Brown, "Dynamic behavior of composite materials under high-strain-rate loading," Journal of Applied Mechanics, vol. 84, no. 1, pp. 011011-1-011011-11, 2017.
[10] R. Patel, "Damage assessment in composite materials using digital image correlation," Journal of Composite Materials, vol. 53, no. 12, pp. 1465-1479, 2019.
[11] A. Taylor, "Fatigue and fracture of composite materials," Elsevier, Amsterdam, Netherlands, 2010.
[12] S. Kim, "Experimental investigation of dynamic behavior of aluminium-based composite materials under impact loading," Journal of Materials Science and Engineering A, vol. 699, pp. 1-9, 2017.
[13] J. Kim, "Development of advanced composite materials for aerospace applications," Journal of Aerospace Engineering, vol. 29, no. 5, pp. 1-10, 2016.
[14] A. Kalkanli, S. Yilmaz , "Synthesis and characterization of aluminum alloy 7075 reinforced with silicon carbide particulates" Mater Des, 29 (4) (2008), pp. 775-780
[15] H.B. Zhang, B. Wang, Y.T. Zhang, Y. Li, J.L. He, Y.F. Zhang, "Influence of aging treatment on the microstructure and mechanical properties of CNTs/7075 Al composites" Alloys Compd, 814 (2020), Article 152357
[16] https://theconstructor.org/composite/composites-construction-uses/1570/
[17] Orbulov, Imre & Kientzl, Imre & Blücher, J. & Ginsztler, János & Németh, Á & Dobranszky, Janos. (2010). "Production and investigation of a metal matrix composite pipe. " Proceedings of 14th European conference on composite materials. 1-8.
[18] https://www.matweb.com/search/DataSheet.aspx?MatGUID=0cd1edf33ac145ee93a0aa6fc666c0e0
[19] https://esab.com/ro/eur_ro/esab-university/articles/how-and-why-alloying-elements-are-added-to-aluminum/
[20] Lakshmikanthan, A.; Angadi, S.; Malik, V.; Saxena, K.K.; Prakash, C.; Dixit, S.; Mohammed, K.A. ”Mechanical and Tribological Properties of Aluminum-Based Metal-Matrix Composites.” Materials 2022, 15, 6111. https://doi.org/10.3390/ma15176111
[21] Long-Jiang Zhang, Feng Qiu, Jin-Guo Wang, Hui-Yuan Wang, Qi-Chuan Jiang,
[22] ”Microstructures and mechanical properties of the Al2014 composites reinforced with bimodal sized SiC particles.” Materials Science and Engineering: A, Volume 637, 2015, Pages 70-74, https://doi.org/10.1016/j.msea.2015.04.012.
[23] Lakshmikanthan, Avinash, Santosh Angadi, Vinayak Malik, Kuldeep K. Saxena, Chandar Prakash, Saurav Dixit, and Kahtan A. Mohammed. 2022. "Mechanical and Tribological Properties of Aluminum-Based Metal-Matrix Composites" Materials 15, no. 17: 6111. https://doi.org/10.3390/ma15176111
[24] Carcea I, ”Materiale compozite - Fenomene la interfața” Editura Politehnium ,2008
[25] Cerbu C, Burlacu A, ” SIMULAREA SOLICITĂRII DE FORFECARE PRIN METODA IOSIPESCU A EPRUVETELOR DIN ALUMINIU”, Buletinul AGIR ,nr. 2, 2018 ,aprilie-iunie

COMAT The 10th International Conference on ADVANCED COMPOSITE MATERIALS ENGINEERING

Transilvania University of Brasov
FACULTY OF MECHANICAL ENGINEERING

22-23 October 2024

GLASS FIBER COMPOSITE MATERIALS: STUDIES AND EXPERIMENTAL TESTS

Munteanu M.V. *[1], Scutaru M.L.[1], Istrate S.[1]

1.Transilvania University of Brașov, Romania, v.munteanu@unitbv.ro, lscutaru@unitbv.ro

Abstract: *Glass-based composite materials have become increasingly important due to their exceptional mechanical and chemical properties. This article reviews the current state of research, describes the experimental methodology for testing the mechanical properties of glass fiber reinforced composites, and presents the results of tensile, compressive, and bending tests. The findings highlight the high potential of these materials in various industries, from construction to aviation*.

Keywords*: composite materials, glass fibers, mechanical tests, mechanical properties, reinforced materials.*

1. INTRODUCTION

Glass fibers are obtained by drawing molten glass at high temperatures and can be integrated into various types of matrices such as polymers, metals or ceramics to create versatile composite materials. These fibers are particularly valued for their high tensile strength and for the fact that they do not degrade in corrosive environments, making them ideal for applications in harsh industrial environments [1-7].

Another major advantage of fiberglass is its excellent weight-to-strength ratio. This makes glass fiber reinforced composite materials preferred in fields such as aeronautics, shipbuilding, civil infrastructure and the automotive industry. Glass fibers, as a reinforcing element, give composite materials increased tensile strength, corrosion resistance and high thermal stability [3, 7-10].

Although there are other reinforcing materials such as carbon and aramid fibers, fiberglass remains one of the most popular choices due to its cost-performance ratio. Despite the superior performance of carbon fibers, they are much more expensive to produce and their processing is more complicated, making fiberglass a more affordable and cost-effective alternative [10-16].

The objective of this study is to present a synthesis of the current state of glass-based composite materials, also presenting their experimental testing methodology and the results obtained, especially in tensile tests, bending tests

and compression tests, thus providing a basis for future research and applications in modern engineering.

2. THE CURRENT STATE OF GLASS-BASED COMPOSITE MATERIALS

Glass-based composite materials occupy an important place in the field of advanced materials, being widely used due to their outstanding properties, such as high mechanical strength, light weight, and durability under thermal and chemical stress conditions [6-8]. Glass fibers, as a reinforcing material, are the most used in the production of composites due to their relatively low cost, excellent mechanical properties and the ease with which they can be produced on an industrial scale [17-20].

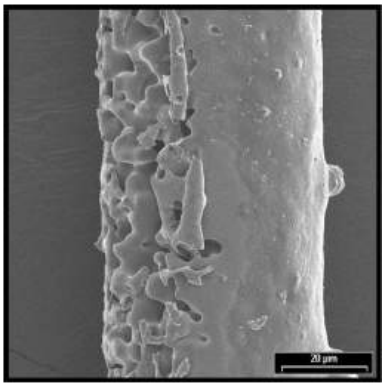

Figure 1: Fiberglass [8]

The industrial process of obtaining the fibers involves melting the glass at high temperatures and drawing the fibers through specially designed nozzles, which allow the formation of extremely fine filaments, usually between 5 and 20 µm in diameter [21-23]. After forming, these filaments are chemically treated to increase adhesion with the polymer matrix, especially in composites used in construction and the automotive industry [14, 24]. Figure 1 illustrates the structure of the glass fiber obtained by this process.

The properties of glass fibers make them ideal for use in aggressive environments, such as infrastructure exposed to corrosion or structures subject to high thermal stresses. These fibers are known for their chemical and thermal stability, as well as the fact that they do not absorb moisture, which makes them ideal in applications where water and moisture resistance is essential [25-26].

In the automotive industry, glass fiber reinforced composites are used for body parts, panels and internal components due to their ability to reduce the overall weight of the vehicle, resulting in lower fuel consumption. In construction, these composites are preferred for reinforcing concrete structures or for facade elements due to their resistance to corrosion [18, 21].

Another field with a significant increase in the use of glass-based composites is that of the wind turbine [19, 20]. Wind turbine blades are frequently made of glass fiber reinforced composites due to their excellent weight-to-strength ratio,

which allows them to rotate efficiently at high speeds while ensuring high durability against external factors.

Although glass fiber composites perform well in many applications, there are also certain limitations. Disadvantages include low strength at very high temperatures compared to other types of fibers, such as carbon, and some brittleness [21]. In addition, the recycling of these materials remains a challenge because thermoset composites cannot be reused in the same form [22, 23].

3. EXPERIMENTAL METHODOLOGY FOR TESTING COMPOSITE MATERIALS BASED ON GLASS FIBERS BENDING STRESS

The testing methodology of composite materials includes mechanical tensile testing, bending and compression tests of glass fiber reinforced composite samples [24, 25]. The samples are processed according to international standards, involve the use of samples specially processed for each type of test and subjected to mechanical stress to determine the resistance of the materials to various types of stress (Figure 2). The samples of composite materials were made using the Romanian standard SR EN ISO 14125 from 1998, Fiber-reinforced plastic composites, Determination of bending properties. This part of ISO 14125 is based on ISO 178 and deals with fiber-reinforced plastics. The testing process includes measuring the maximum force sustained and microscopic analysis of the fracture surface. The method is used to determine the bending behavior of the samples but also to determine the bending resistance, the bending modulus and other aspects related to the stress/deformation relationship under the given conditions. It applies to a simply supported lever, loaded at three or four bending points. The method of placing and testing the specimen is chosen in such a way as to limit shear deformation and avoid interlaminar shear breakage.

Figure 2. Composite material sample after bending stress

The equipment used is a constant speed testing machine. The testing machine for the three-point bending test used is the LR5K Plus, produced by Lloyd's Instruments, which provides a maximum force of Fmax = 5 kN. Two supports and a hemispherical load punch are arranged according to the scheme in Figure 3. The bending test machine allows the experimental results to be downloaded in electronic format, through the NEXYGEN Plus software.

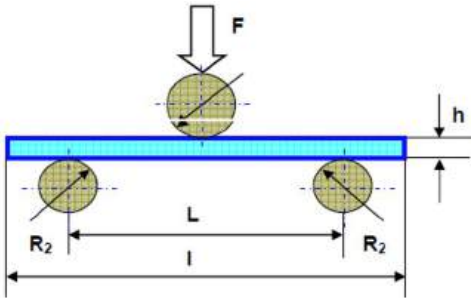

Figure 3: Schematic of the 3-point bending test

3.1 Testing the samples

The experimental research considered the study of the influence of Al2O3 inserts in glass-based composite materials. The specimens were tested in the mechanical testing laboratory of the Department of Mechanical Engineering. The tests were performed on three types of composites:

• 5 samples of composite material based on matte glass

• 5 glass-based composite material samples with 5% Al2O3 inserts

• respectively 5 glass-based composite material samples with 10% Al2O3 inserts.

All 3 sets of specimens were cut on a numerical control machine, to the dimensions indicated according to STAS. Each set of specimens was tested to see how the Al_2O_3 inserts influence the mechanical behavior. The specimens were subjected to a bending test and the results were analyzed to identify variations in strength and stiffness.

4. RESULTS AND DISCUSSION

4. 1. Bending test and the influence of Al_2O_3 inserts on the mechanical properties

The plain frosted glass specimens showed basic flexural strength with moderate breaking strength and elongation values. The insertion of 5% Al_2O_3 caused an increase in the fracture strength and stiffness of the specimens, with a general improvement in the mechanical properties being observed. However, when the proportion of Al_2O_3 was increased to 10%, the results indicated a slight decrease in the mechanical properties, which suggests that an excessive content of inserts may lead to an alteration of the structural homogeneity of the composite.

Due to some errors in testing the samples, the values for only 4 samples were considered in the case of the matte glass-based composite material.

The data generated by the test machine software were centralized in tables 1, 2 and 3, below, so that they can be interpreted through graphical representations.

Table 1. Characteristics of the test samples based on mat glass

NO. SAMPLES	BREAKING STRENGTH	ELONGATION	ADMISSIBLE TENSION	MODULE OF ELASTICITY	STIFFNESS

(MATT GLASS)	F [N]	ΔL [mm]	σ [Mpa]	E [Mpa]	k [N/mm]
SAMPLES 1	499	10.31	199	3365	49278
SAMPLES 2	711	8.25	285	975	14275
SAMPLES 3	541	9.83	217	4564	66849
SAMPLES 4	611	7.84	244	5759	84375

Table 2. Characteristics of the test samples based on mat glass with 5% Al2O3 inserts

NO. SAMPLES (GLASS WITH 5% AL2O3 INSERTS)	BREAKING STRENGTH F [N]	ELONGATION ΔL [mm]	ADMISSIBLE TENSION σ [Mpa]	MODULE OF ELASTICITY E [Mpa]	STIFFNESS k [N/mm]
SAMPLES 1	684	8.42	274	6519	95499
SAMPLES 2	754	8.74	302	7448	109102
SAMPLES 3	719	8.25	288	7302	106954
SAMPLES 4	660	8.90	265	6058	88746
SAMPLES 5	606	9.37	2422	5584	81788

Table 3. Characteristics of the test samples based on mat glass with 10% Al2O3 inserts

NO. SAMPLES (GLASS WITH 10% AL2O3 INSERTS)	BREAKING STRENGTH F [N]	ELONGATION ΔL [mm]	ADMISSIBLE TENSION σ [Mpa]	MODULE OF ELASTICITY E [Mpa]	STIFFNESS k [N/mm]
SAMPLES 1	826	7.51	199	4882	148983
SAMPLES 2	885	8.20	212	3543	108116
SAMPLES 3	703	9.05	169	2524	77006
SAMPLES 4	757	9.69	182	2307	70399
SAMPLES 5	783	7.82	188	4104	125243

4.2. Comparative analysis of flexural strength between specimens

Figures 4, 5 and 6 show the load (F-displacement) graphs made for each set of specimens showing a different stress and stiffness distribution depending on the material composition.

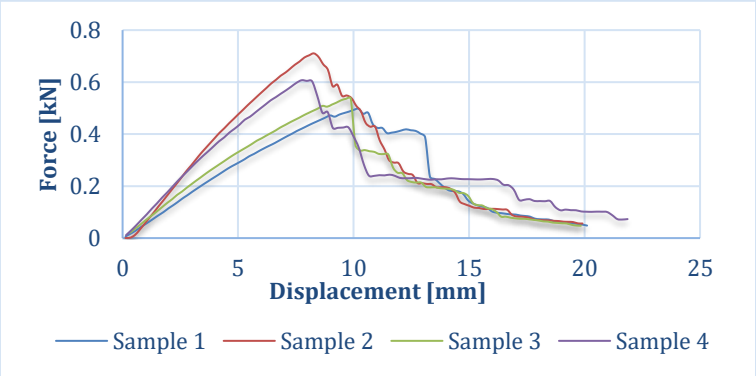

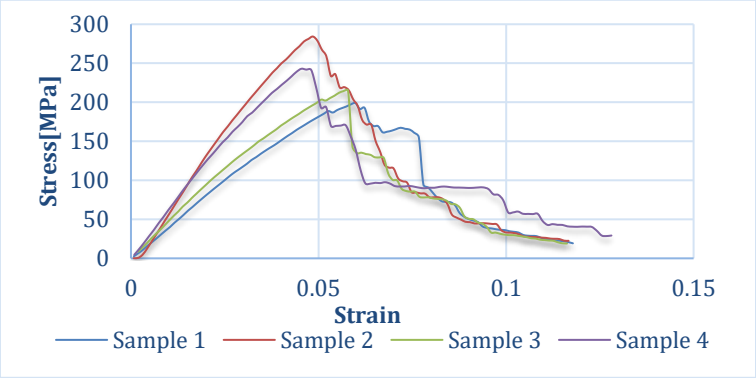

Figura 4. Load curves for the samples made of composite material based on mat glass

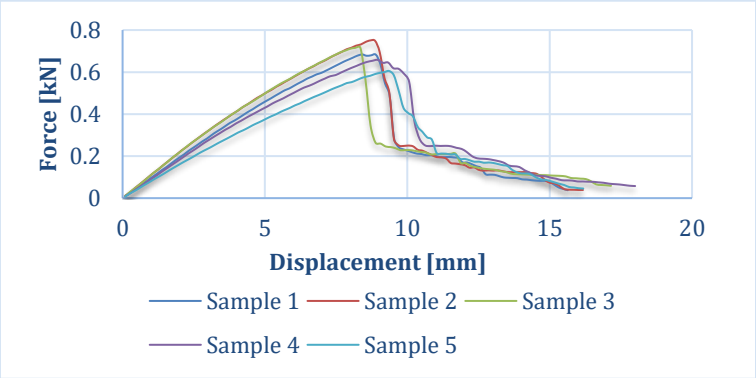

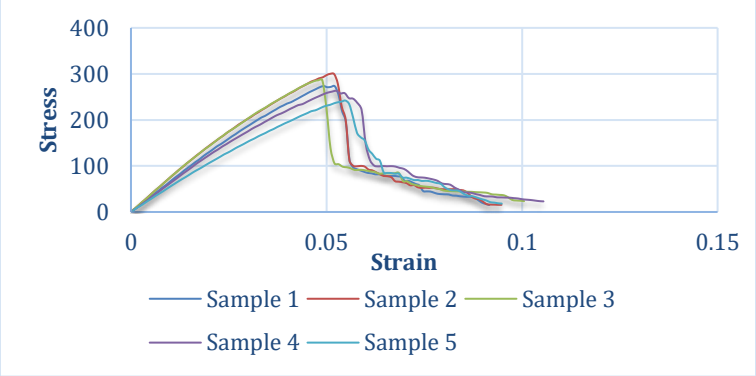

Figure 5. Load curves for the samples made of composite material based on mat glass with 5% Al_2O_3 inserts

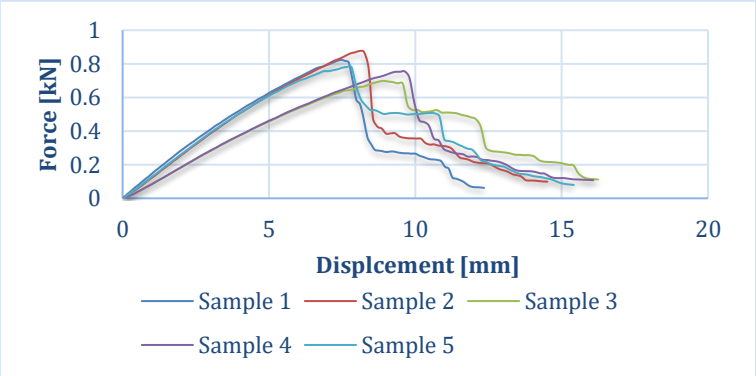

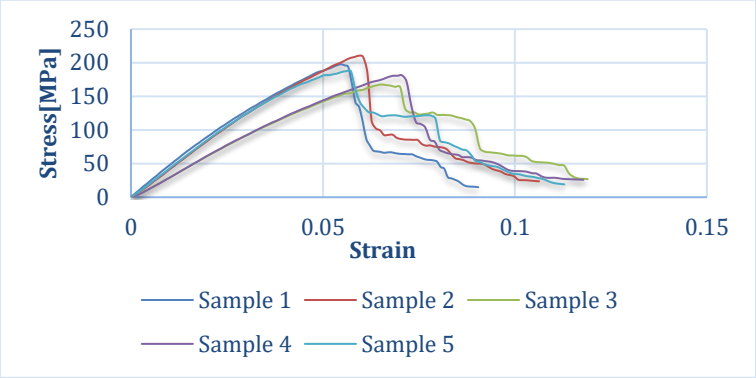

Figure 6. Load curves for the samples made of composite material based on mat glass with 10% Al_2O_3 inserts

Specimens with 5% Al_2O_3 showed an improvement in flexural strength, while specimens with 10% Al_2O_3 showed a slight decrease in strength, probably due to the formation of interlaminar defects or a non-uniform distribution of Al_2O_3 particles.

This can also be highlighted in the graphs in Figures 7 and 8, when on 2 representative specimens from each sample (frosted glass, frosted glass with 5% Al2O3, frosted glass with 10% Al2O3) the representative graphs were represented

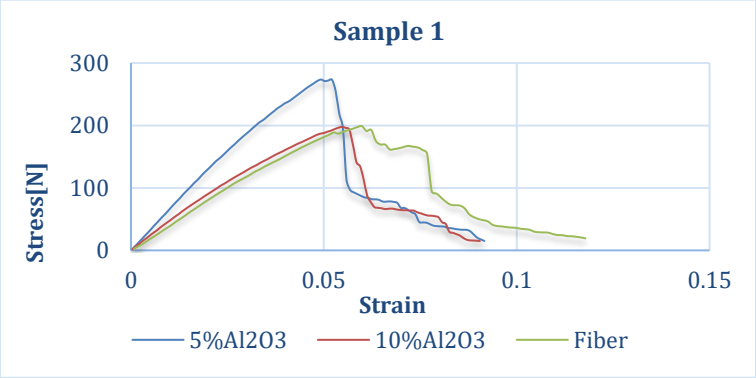

Figure 7. Comparative analysis on the influence of Al_2O_3 powders in glass fiber composites (sample 1 of 3 sets of samples)

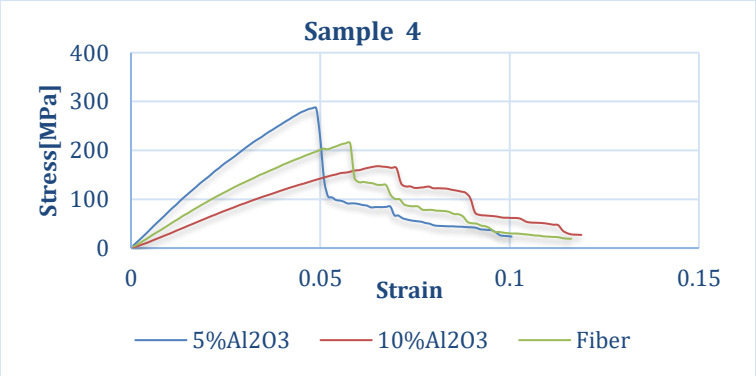

Figura 8. Comparative analysis on the influence of Al_2O_3 powders in glass fiber composites (sample 4 of 3 sets of samples)

4.3. Microscopic analysis of composites

The detailed visualization was made with a high-performance microscope, located within the ICDT-UNITBv. This microscope can magnify the studied surface 500 times, up to 2000 times, and the images were made as clearly as possible and even down to the depth of the material. The results obtained with the microscope were both 2D and 3D, observing at the same time how the entire structure of these materials changed.

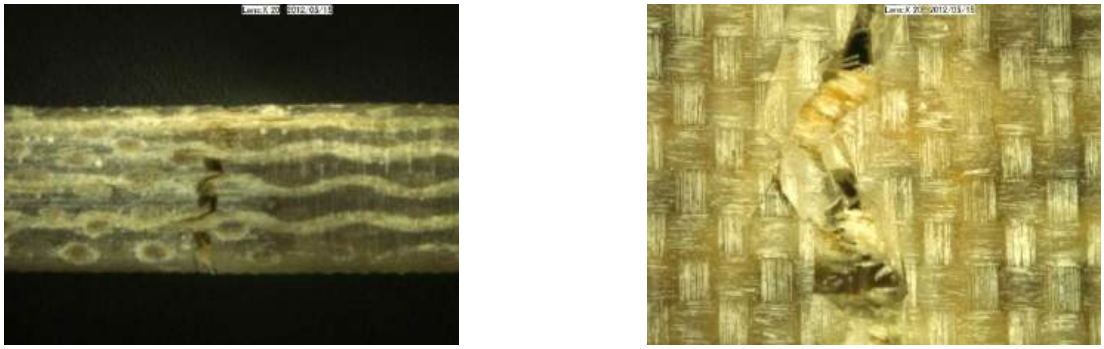

Figure 9. Side and front view of mat glass sample

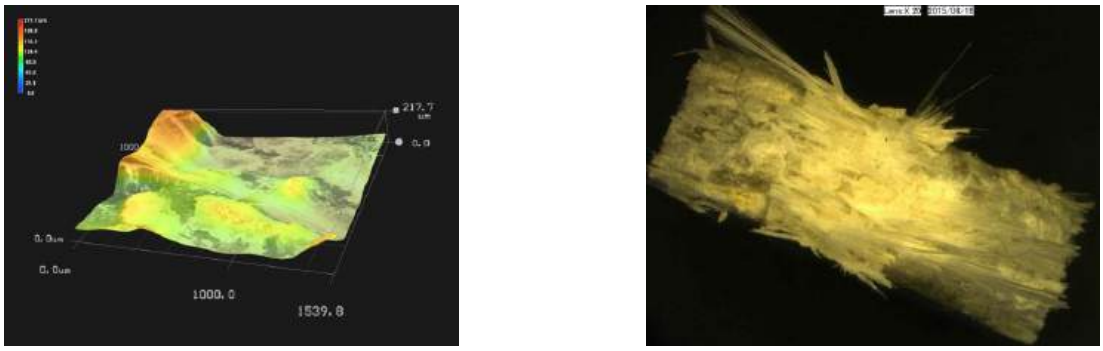

Figure 10. Sectional view for mat glass with 5% Al_2O_3 inserts

Figure 11. Sectional view for mat glass with 10% Al_2O_3 inserts

Microscopic images taken on the tested specimens revealed the layered structure and distribution of glass fibers and Al_2O_3 inserts. In the case of specimens with 5% Al_2O_3 inserts, the structure showed a relatively homogeneous distribution without major defects, which explains the improved mechanical performance. In the 10% Al_2O_3 specimens, microscopic analysis revealed small inclusions and defects in the composite matrix, which may contribute to a slight decrease in stiffness and flexural strength.

5. CONCLUSIONS

The study of glass-based composites with and without Al_2O_3 inserts showed that the addition of Al_2O_3 particles can have a significant impact on the mechanical properties of the material. Experimental results indicate that:

1. Insertions of 5% Al_2O_3 significantly improved the stiffness and flexural strength of the composites, demonstrating that an optimal concentration of Al_2O_3 can contribute positively to the mechanical performance of the material.

2. Increasing the proportion of Al_2O_3 to 10% did not generate a proportional improvement in mechanical properties, but even led to a slight decrease in bending strength, suggesting a limit to the optimal concentration of inserts to avoid structural inhomogeneities.

3. Microscopic analysis highlighted the impact of the composite structure on the mechanical performance, indicating that a uniform distribution of Al_2O_3 inserts can contribute to more durable and resistant materials.

In conclusion, glass-based composites with a low percentage of Al_2O_3 show potential for applications in fields such as aeronautics, construction and the automotive industry, which require materials with improved mechanical strength. The results of this study provide a basis for future research in optimizing the proportion of inserts in glass-based composites to maximize their mechanical performance and durability in industrial applications.

REFERENCES

[1] Burada, C. O., Mirițoiu, C. M., Bolcu, D., Stănescu, M. M. (2014). Determinari experimentale ale factorului de amortizare si rigiditatii pentru benzi sandwich noi cu armatura si miez diferit, 44 (4), pp. 405-413

[2] Burada, C. O., Mirițoiu, C. M., Bolcu, D., Stănescu, M. M. (2014). Determinari experimentale ale factorului de amortizare si rigiditatii pentru benzi sandwich noi cu armatura si miez diferit, 44 (4), pp. 405-413

[3] Malcom, A.J., Aronson, M.T., Deshpande V.S. et al. (2013). Răspuns compresiv al structurilor sandwich compozite din fibră de sticlă, Compozite: Part A, 54,88-97

[4] T.L. Anderson – Mecanica fracturilor-fundamente și aplicații – CRC Press LLC 1995 – ISBN 0-8493-4260-0

[5] ANSYS Release 16 January – ANSYS explicită Ghidul de analiză dinamică

[6] Ito, K., Evaluation of Glass Fiber Surface Treatment in Fabric-Reinforced Plastics, J. Polymer Sci., 45, 155 (1960)

[7] Jen, M.-H.R., Kan, Y.S., Hsu, J.M., Initiation and propagation of delamination in a centrally notched composite laminate, Journal of Composite Materials, Vol.27, No.3, 1993, p. 272-302

[8] Jones, R. M., Mechanics of Composite Materials, Mc Graw-Hill, Koga Kusha, Ltd., 1975

[9] Kelly, A., Fibrous Composite Materials. Material Science and Technology. A comprehensive Treatment. Vol.13, Structures and Properties of Composites, Ed. By R.W. Cahn, P. Haasen, E.J. Kramer, Ed. Weinheim, 1998, pp.1-25

[10] Laird, J.A., Glass Surface Chemistry Relating to the Glass Finish Resin Interface, 19th Conf. SPI Reinforced Plastic Division, 1964

[11] Opran C., Marinescu A., Iliescu M., Spanu P., Studies on modeling polymeric composites sandwich structures with polyurethane core, International Conference "Advanced Composite Materials Engineering ", 2006, pp.30-36.

[12] P.Morgan, Carbon Fibers and Their Composites, CRC Press, Boca Reton, 2005

[13] Petre, A. Mecanica materialelor compozite. Note de curs, Institutul Politehnic Bucureşti, 1988

[14] Preda, G.M., Influenţa factorilor tehnologici asupra calităţii pieselor din materiale composite poliester-fibre de sticlă, utilizate în construcţia automobilelor, teză de doctorat, Craiova 2000
[15] Pleuddemann, E.P., Evaluation of New Silane Coupling Agents for Glass Fiber Reinforced Plastics, 17th Conf. SPI Reinforced Plastic Division, 1962
[16] Popescu, M.: The advanced materials joining: composite materials. Eurostampa Ed., Timişoara, Romania, 2002, ISBN 973-8244-76-5.
[17] Puck, A., Grundlagen der Faserverbund-Konstruktion, Vorlesungs-skript, Gesamthochschule Kassel, 1988 Chirică, E. F. Beznea și I. Gavrilescu, Metode moderne de calcul al structurilor compozite, Ed. Cermi, Iasi, ISBN 978-973-667-283-5, 2007.
[18] E. F. Beznea și I. Chirica, Structuri compozite, Editura Galați University Press, ISBN 978-606-8008-86-8,2010.
[19] G. Vasile, Teza: Structuri cu rigiditate ridicată, din material compozite, utilizate în construcția de autovehicule, Nr. 5981 din iulie 2013, Brașov, Romania
[20] P. T. Sarafin, Spacecraft Structures and Mechanisms: From Concept to Launch, Microcosm Press, Kluwer Academic Publishers, 2011.
[21] G. Bianchi, Thesis: Structural Performance of Spacecraft Honeycomb Panels, University of Southampton, April 2011.
[22] Zhao, Z.H., Weng, G.J., Effective Elastic Moduli of Ribbon-Reinforced Composites. Journal of Applied Mechanics, Vol. 57, March 1990, pp. 158-167.
[23] Walpole, L.J., On Bounds for the Overall Elastic Moduli of Inhomogeneous Systems-I. J. Mech. Phys. Solids, 1966, Vol. 14, pp. 151-162
[24] http://cter-referate-a-11-a-c.blogspot.ro/2011/06/v-behaviorurldefaultvmlo.html
[25] https://www.google.ro/search?q=recycle+carbon+fiber&source=Inma&tbm=isch&sa=X&ved=0ahUKEwiltYHv9cHUAhWHyRoKHep8DuEQ_AUIBigB&biw=1536&bih=736#imgdii=rEyx2f6N68IJ2M:&imgrc=jDTmyiE302WJrM
[26] https://www.quora.com/Where-are-composites-used-in-aerospace

COMAT The 10th International Conference on ADVANCED COMPOSITE MATERIALS ENGINEERING

Transilvania University of Brasov
FACULTY OF MECHANICAL ENGINEERING

22-23 October 2024

EXPERIMENTAL RESEARCH ON THE MECHANICAL PROPERTIES OF THE CARBON AND KEVLAR BASED COMPOSITES

Munteanu M.V. *[1], Scutaru M.L.[1], Savu R.L.[1]

1.Transilvania University of Brașov, Romania, v.munteanu@unitbv.ro, lscutaru@unitbv.ro
*Corresponding author, v.munteanu@unitbv.ro

Abstract: *Composite materials, increasingly used in high-end fields such as aerospace and automotive, offer major advantages due to their high strength-to-weight ratio. This paper investigates the mechanical properties of carbon fiber and kevlar reinforced composites through flexural testing. Experimental tests were performed using standardized methods, and the results highlighted the differences in performance between the two materials. Carbon fiber composites have higher stiffness, while Kevlar ones are more elastic and impact resistant. The findings highlight the importance of applying these materials in industries where light weight and mechanical performance are critical.*

Keywords*: Composite materials, Carbon fibers, Kevlar, Mechanical properties, Bending*

1. INTRODUCTION

Composite materials have evolved significantly over time, being used in various technological applications due to their ability to combine two or more components with superior properties. Carbon fibers and Kevlar are two of the most used types of reinforcements, offering advantages such as low weight, high mechanical strength and thermal stability [1].

Carbon fibers, originally introduced in the aerospace industry, became popular due to their outstanding tensile strength and low density. Kevlar, a polymer of the aramid class, is known for its impact resistance and ballistic properties [2], being widely used in protective equipment and structures that require reduced weight and increased durability [3].

This work focuses on investigating the mechanical behavior of these two types of composites through experimental bending tests, with the aim of evaluating their performance in industrial applications.

2. CURRENT STATE OF RESEARCH

Composite materials reinforced with carbon fibers and kevlar have experienced accelerated development due to their outstanding properties. They are used in areas such as the aerospace, automotive, construction and sports equipment industries. A worldwide use of Kevlar fiber is in the military community, where it is recognized as a high-performance material for protecting life (body armor and bulletproof vests are light, comfortable, offering superior protection against fragmentation and ballistic threats).

To obtain carbon fiber, the predominant material is polyacrylonitrile (PAN) fiber, which is obtained by polymerization, spinning and then the designation of the polymer [1,5].

The chemical composition of Kevlar fiber is poly-paraphenylene terephthamide, known as para-aramid [2,6]. Kevlar filaments are manufactured by extrusion through a die [3,7].

Modern composites consist of a matrix (polymers, metals, or ceramics) and a reinforcing agent (usually fibers). Their main characteristic is that the component materials retain their individual properties but, when combined, generate new superior mechanical characteristics [4, 8, 9].

3. EXPERIMENTAL METHODOLOGY

To test the mechanical properties of the composites reinforced with carbon fibers and Kevlar, standardized specimens were made [10, 11, 12], according to SR EN ISO 14125. The bending tests were performed on a Lloyd's type mechanical test stand Instruments [13], model LR5K Plus (Figure 1).

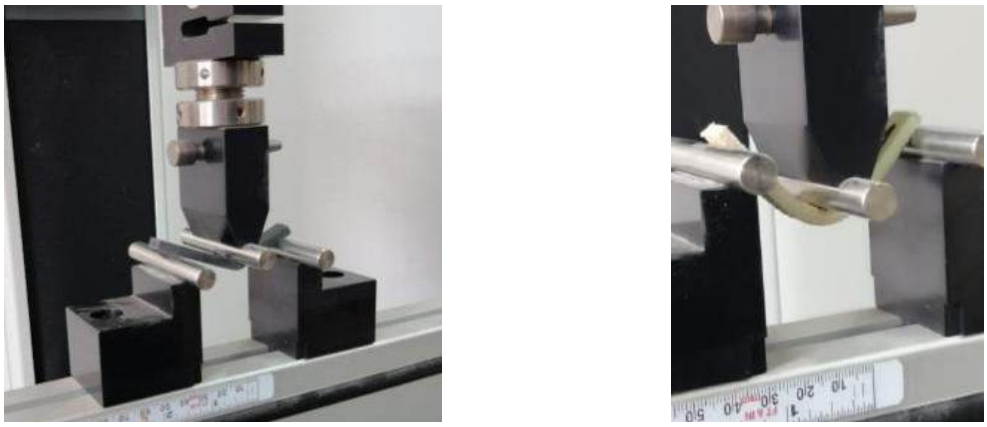

a b

Figure 1: Lloyd's Instruments LR5K Plus Test Machine [13]. a. Carbon fiber specimen during bending stress; b. Kevlar fiber specimen during bending stress

The specimens were subjected to a load applied perpendicular to the longitudinal axis, according to the three-point test method. They were made of composite reinforced with carbon fibers and Kevlar, and the results were recorded electronically by means of NEXYGEN Plus software [13].

The tests were carried out to determine the bending behavior of the samples, but also to determine the bending resistance, the bending modulus and other

aspects related to the stress/deformation relationship under the given conditions of the composites reinforced with carbon fibers and Kevlar.

The specimens were subjected to loads applied perpendicular to the longitudinal axis using the standard three-point test scheme, according to SR EN ISO 14125. The Lloyd's Instruments LR5K Plus [13] testing machine was used to perform the tests with a maximum force of 5 kN. The specimens were placed end-to-end on two supports and a central load was applied until the material failed (Figure 2).

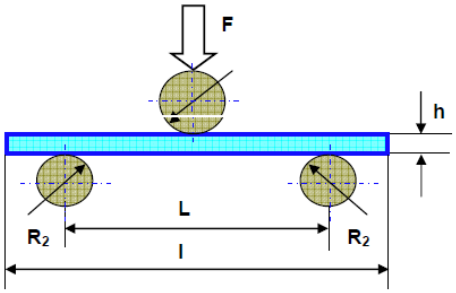

Figure 2: Scheme of the 3-point bending test

Tests were performed at different speeds to determine elasticity and breaking behavior. The exact dimensions of each specimen were also measured prior to testing to obtain accurate cross-sectional and length data. NEXYGEN Plus software [11] was used for experimental data recording and processing.

4. RESULTS AND DISCUSSION

Bending tests performed revealed significant differences between carbon fiber reinforced and kevlar reinforced composites.

determined following bending tests, for the carbon fiber and Kevlar samples: Carbon fibers were characterized by higher stiffness, with an average modulus of elasticity of approximately 14000 MPa, compared to Kevlar, which demonstrated higher elasticity but lower stiffness.

Test results showed that Kevlar-reinforced materials exhibit superior resistance to impact and dynamic stresses, while carbon fiber composites perform better in static stresses such as bending.

Table 1 below summarizes the main mechanical properties

Table 1. Mechanical properties of carbon fiber and Kevlar specimens, in bending

Material	Max. force [kN]	Max. tension [MPa]	Stiffness [N/mm]	Young's Modulus [MPa]
Carbon	0.68	267.77	1.423	14179
Kevlar	0.18	109.00	0.084	1281

The force-deformation graphs for both types of composites highlight the fact that carbon fiber reinforced materials exhibit a "brittle" behavior, while those with kevlar have a larger deformation before failure.

a. Composite materials reinforced with carbon fibers:

The results of the bending tests for the carbon fiber reinforced composite material are shown in Figure 3 and the representative data are shown in Table 2, from which it can be seen that the stiffness is directly related to the structure of the material

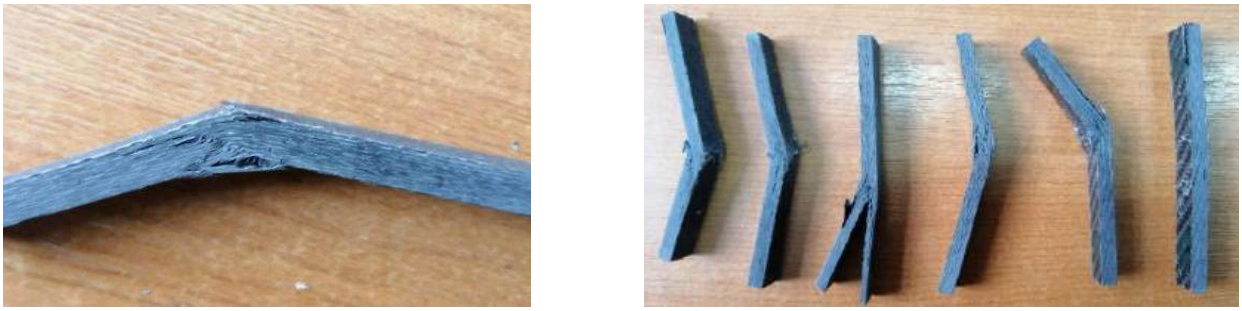

Figure 3: Carbon-based composite material specimen after bending stress

Table 2: Results of the carbon fiber specimens obtained from the stress in the bending tests

Sample No.	Force under max load.	Max. voltage on charg.	Bending stiffness	Young's Modulus
	[kN]	[MPa]	[Nm^2]	[MPa]
Sample 1	0,692731762	292,28289	1,288574414	14459,72227
Sample 2	0,602559878	241,0239511	1,267932452	1267,32452
Sample 3	0,67189371	274,4663849	1,361270153	14481,1044
Sample 4	0,750618108	282,5856408	1,454433116	13688,78227
Sample 5	0,69167873	250,5779724	1,530433504	13327,83489
Sample 6	0,59376362	242,5504984	1,440203032	15320,78729

During the test, the load borne by the specimen as well as its elongation are measured. At the same time, the dimensions of each sample were precisely measured: the cross section and the width of the sample. These dimensions were entered as input data in the computer connected to the test machine, having the NEXYGEN software [11], which takes the experimental data from the test machine and processes them statistically.

Thus, based on the results obtained from the bending tests for the carbon fiber samples, we represented the force-displacement characteristic curves (Figure 4), respectively the Stress-deformation characteristic curves (Figure 5).

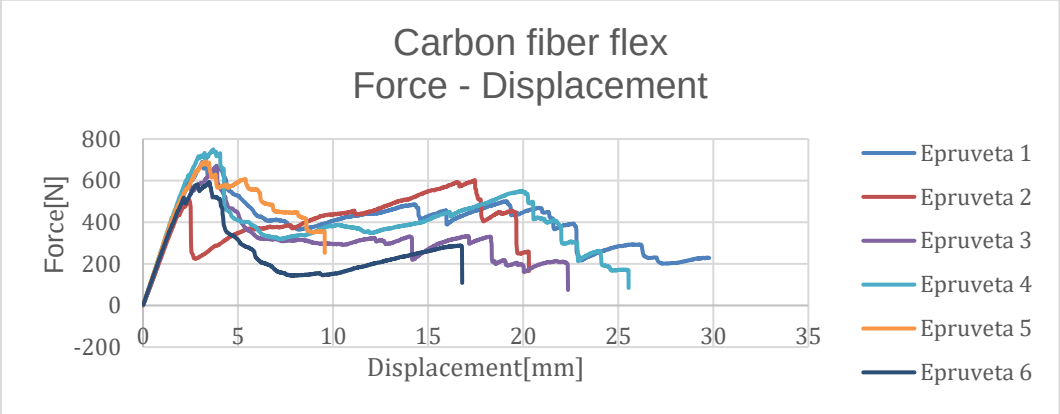

Figura 4: Force-Displacement Characteristics for Carbon Fiber Composite Specimens after Bending

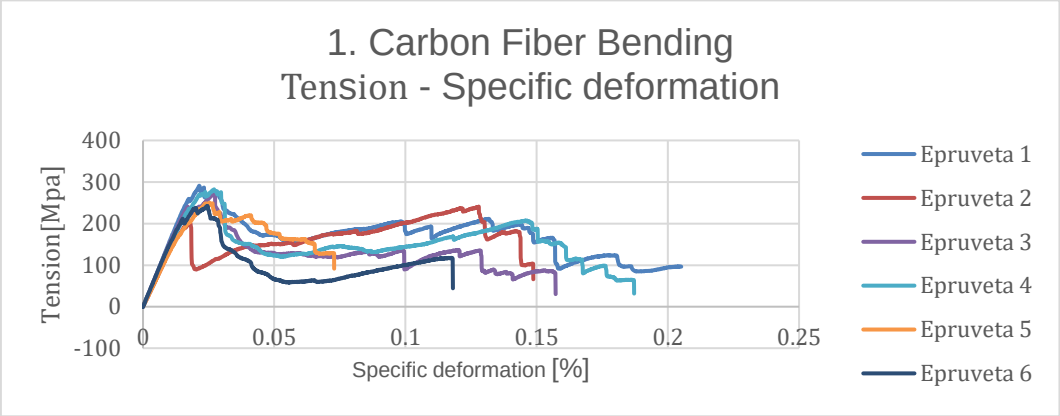

Figure 5: Carbon Fiber Samples - Characteristic Curves Tension – Displacement after bending stress

b. Composite materials reinforced with kevlar fibers:

Kevlar fiber composites were made at S.C COMPOZITE S.R.L., and following bending tests, they showed superior elasticity, but with a lower stiffness compared to carbon fibers (see table 1). The average modulus of elasticity recorded was approximately 1250 MPa.

During the test, both the load borne by the specimens and their elongation were measured. It can also be seen that the material deformed considerably before failure, confirming its ability to withstand impact and absorb energy. (Figure 1b).

The bending test results for the five-layer Kevlar fiber-reinforced composite material are shown in Table 3.

Table 3: The results of the Kevlar fiber specimens obtained from the bending test request

Sample No.	Force under load. max.	Max. voltage on charge.	Bending stiffness	Young's Modulus
	[kN]	[MPa]	[Nm²]	[MPa]
Sample 1	0,245589261	133,6267489	0,060201585	1049,874429
Sample 2	0,177125721	108,0336808	0,13880174	2784,831147

Sample 3	0,245617169	130,4161958	0,068463755	1136,013639
Sample 4	0,162779264	101,9177442	0,00300626	63,47020754
Sample 5	0,141966655	79,29575244	0,098083933	1755,928612
Sample 6	0,150300272	84,7006861	0,049589631	895,6952663

Based on the results obtained from the bending tests for the Kevlar fiber samples, we represented the force-displacement characteristic curves (Figure 6), respectively the Stress-Strain characteristic curves (Figure 7)

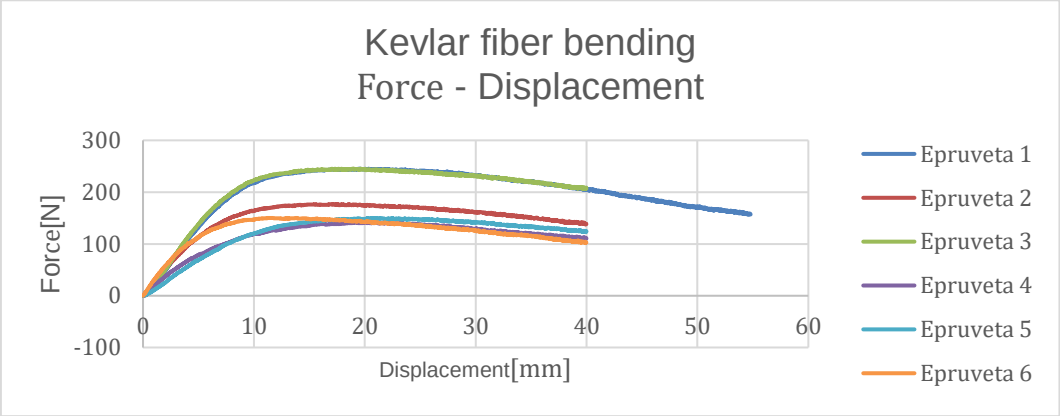

Figure 6: The Kevlar fiber samples - Characteristic curves Force – Displacement after bending stress

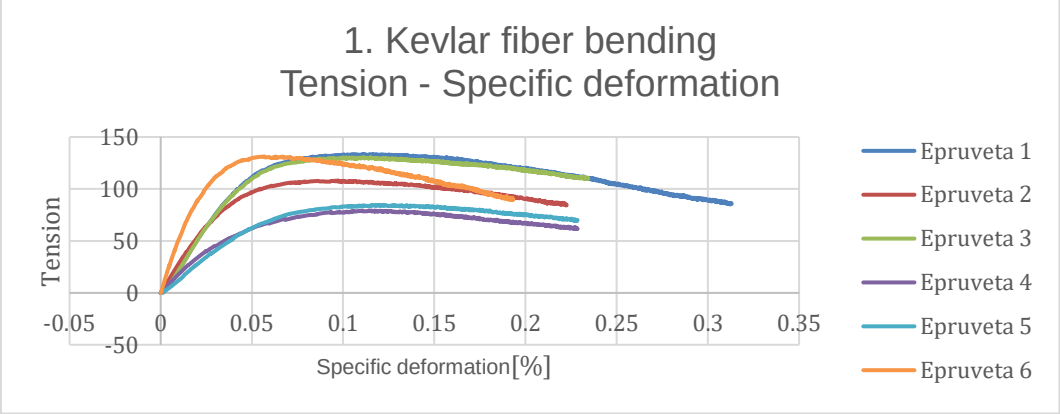

Figure 7: Kevlar fiber specimens - Characteristic curves Stress - Specific deformation after bending stress

These data highlight that Kevlar-reinforced composite materials are more suitable for applications that require resistance to dynamic stresses and large deformations, such as ballistic protection or energy-absorbing structures.

c. Comparative analysis:

From the comparison of the two types of materials, it can be seen that carbon fibers offer superior rigidity, but with a brittle behavior, while Kevlar has a much higher elasticity and better resists impact forces (see Figures 8 and 9)

a b

Figure 8: Visualization of cracks under the microscope, after bending stress: a. carbon fibers, b. kevlar fibers

The choice of material depends on the specific requirements of the application: carbon is ideal for static or structural applications, while Kevlar is preferred in areas where energy absorption and protection are priorities.

5. DESIGN AND SIMULATION OF MECHANICAL TESTS

Using HyperMesh 2021, we performed a bending stress simulation where we designed a carbon fiber reinforced specimen and simulated the bending stress, see Figure 9. Using arbitrary data and the material in the programming menu, I gradually acted with a bending strength, force that increases proportionally with time, to see the behavior of the composite material. The data being counted automatically by the program.

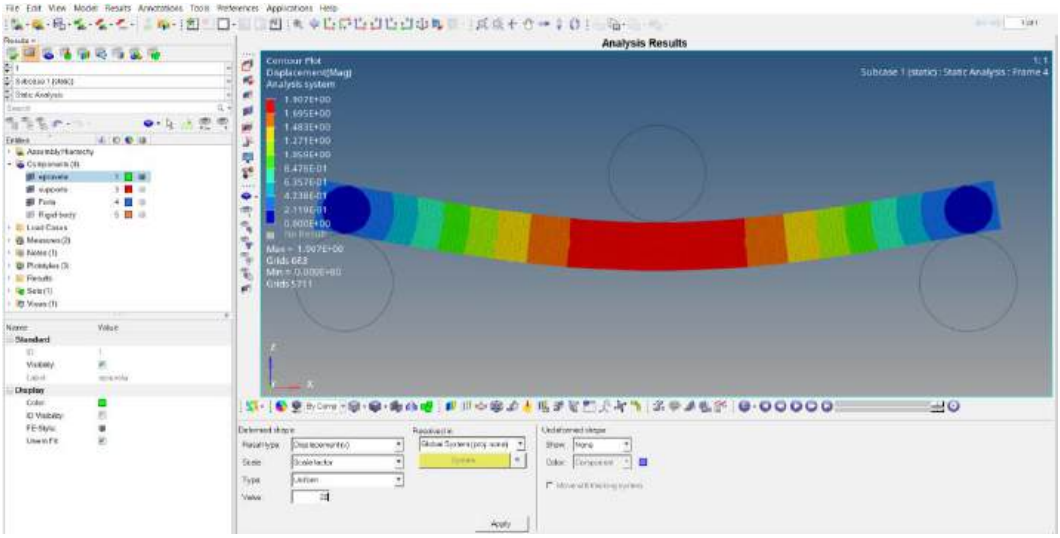

Figure 9: HyperMesh design Structural analysis - deformation of the carbon fiber specimen

Verification calculation for the carbon fiber composite material sample

F=500 N

L_0=64 mm

b=10 mm

h=5 mm

A= b* h= 50mm^2

E= 14 MP_a

$$I_Z = \frac{b * h^3}{12}$$

$I_Z = \frac{10*5^3}{12}$=104.166

The maximum arrow in the middle of the sample:

$$F = \frac{F*{L_0}^3}{48*E*I_Z}$$

$$F = \frac{500*(64)^3}{48*14000*104.16} = 1.872$$

Also, for the design of the bending stress of the composite material reinforced with Kevlar fiber, the same steps were followed as in the case of the composite material reinforced with carbon fiber (Figure 10).

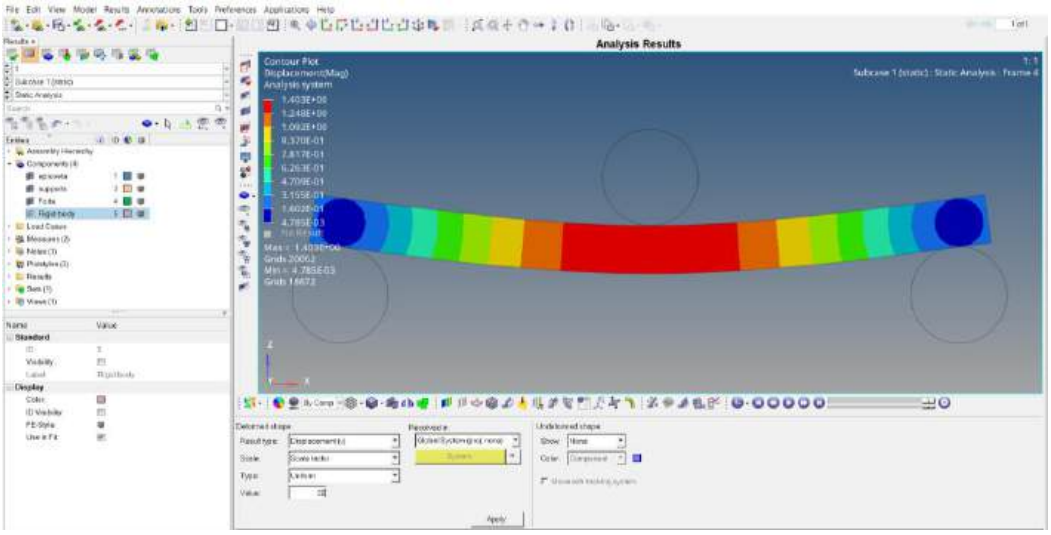

Figure 10: HyperMesh design Structural analysis - deformation of the Kevlar fiber specimen

The verification calculation for the modeling of the sample made of composite material reinforced with Kevlar fiber

F=500 N

L_0=64 mm

b=11 mm

h=5 mm

A= b* h= 51 mm^2

E= 19 MP_a

$$I_Z = \frac{b * h^3}{12}$$

$I_Z = \frac{11*5^3}{12}$=114.583

The maximum arrow in the middle of the sample:

$$F = \frac{F*{L_0}^3}{48*E*I_Z}$$

$$F = \frac{500*(64)^3}{48*14000*104.16} = 1.254$$

6. CONCLUSIONS

Based on the experimental tests, the following conclusions were drawn:

• Composites reinforced with carbon fibers offer superior rigidity and strength, but have a less elastic behavior, "brittle" under bending stress

• the composite material reinforced with Kevlar fibers presents better resistance properties, but lower permissible deformations than those of the composite material reinforced with carbon fibers.

• Kevlar fibers are more elastic and show better resistance to dynamic stress and impact. They offer a balance between elasticity and tear strength, making them ideal for applications such as ballistic protection and safety equipment.

• Increasing the number of layers in both composites improved the overall mechanical performance, increasing the allowable forces and increasing the specific stress (see Figures 4 and 6).

• Despite different mechanical properties, both carbon fiber and Kevlar are essential for high-end industrial applications, depending on the specifications of each project.

REFERENCES

[1] Curs Chimie - Curs 7 < Chimie Anorganică (regielive.ro)
[2] KEVLAR Technical Guide.pdf (pelicanrope.com)
[3] Kevlar | Military Wiki | Fandom
[4] Carbon fibers are manufactured by treating organic fibers (slidetodoc.com)
[5] Ştefănescu, F.- Materiale compozite, Editura Didactică şi Pedagogică, Buc. 1996
[6] Ioan Carcea, Materiale Compozite. Fenomene la interfață, Editura Politehnium 2008
[7] Aurel Crișan, Cercetări asupra sintezei, caracterizării și utilizării unor compozite cu matrice ceramică termorezistente, Școala Doctorală Interdisciplinară Facultatea Știința și Ingineria Materialelor 2019
[8] Jones, R. M., Mechanics of Composite Materials, Mc Graw-Hill, Koga Kusha, Ltd., 1975
[9] Gheorghe Vasile, Teza: Structuri cu rigiditate ridicată, din material compozite, utilizate în construcția de autovehicule, Nr. 5981 din iulie 2013, Brașov, Romania
[10] Elena Sima, Materiale compozite – necesitate și provocare în contextul dezvoltării durabile, Buletinul AGIR nr. 4/2017
[11] Reashad Bin Kabir, Nasrin Ferdous, Kevlar-The Super Tough Fiber, International Journal of Textile Science 2012
[12] Ibănescu Constanța, Curs universitar Ingineria materialelor compozite polimerice și procese de prelucrare a acestora, 2008
[13] https://www.tts-ltd.co.uk/lloyd-lr5k-tensile-machine

COMAT The 10th International Conference on ADVANCED COMPOSITE MATERIALS ENGINEERING

Transilvania University of Brasov
FACULTY OF MECHANICAL ENGINEERING

22-23 October 2024

STUDY ON THE MECHANICAL PROPRIETIES OF COMPOSITE PANELS BASED ON FIBER GLASS IMPREGNATED WITH DIFFERENT BINDING AGENTS

Ostrioglo M. [1], Chircan E.[2], Gheorghe V. [*3]

1. Transilvania University of Brasov, Brașov, Romania, maxim.ostrioglo@student.unitbv.ro
2. Transilvania University of Brasov, Brașov, Romania, chircan.eliza@unitbv.ro
3. Transilvania University of Brasov, Brașov, Romania, gheorghe.vasile@unitbv.ro

[*]Corresponding author: gheorghe.vasile@unitbv.ro

Abstract: *In the mechanical research of composite materials with fiber glass we explore the properties and behavior of these materials under varied conditions from static loads to dynamic ones. The composite materials for the tests are created by combining two or more components with different properties to achieve superior performance to individual components. A crucial aspect of the research is understanding the mechanical behavior of these materials under different loading conditions. Mechanical tests include tensile tests, compression, bending and bending to evaluate the strength and stiffness of the composite. In plus, impact tests can be performed to determine the material's ability to absorb energy during sudden charging. These tests provide essential data for optimization design and engineering of composite materials.*

Keywords: *composite panels, bending tests, hemp-based composites, fiber glass*

1. INTRODUCTION

In the mechanical research of composite materials with fiber glass we explore the properties and behavior of these materials under varied conditions from static loads to dynamic ones. The composite materials for the tests are created by combining two or more components with different properties to achieve superior performance to individual components. A crucial aspect of the research is understanding the mechanical behavior of these materials under

different loading conditions. Mechanical tests include tensile tests, compression, bending and bending to evaluate the strength and stiffness of the composite. In plus, impact tests can be performed to determine the material's ability to absorb energy during sudden charging. These tests provide essential data for optimization design and engineering of composite materials.

In the current context, the topic of mechanical research of composite materials with organic compounds remains extremely relevant and constantly evolving. Constant technological advancement and increasing demand for superior performance materials in various industrial and technological fields have generated significant interest and investment in this research area.

Mechanical tests are very important for performance evaluation and the behavior of materials under various types of loads. These tests provide information critical about material properties, such as strength, ductility, hardness, elasticity. These data are essential for engineers and researchers to select materials suitable for specific applications and to develop new materials with improved properties.

2. METHODS

For this paper we made three types of composite panels as follows:

- Plate 1 I made a cement board with dimensions of 25 x 25 x 3.5 cm, using a mix with balanced materials. The composition included cement, sand, water and layers of fiberglass, to ensure the durability and strength of the final product.
- Plate 2 I accurately measured 700 grams of cement and 700 grams of sand, 400 ml of water for the mix and the 4 layers of fiberglass
- Plate 3 For this plate a complex structure is described which is made up of several materials, the board is 25 by 25 cm with a total thickness of 3.8 cm. The central layer of the board is made up of a 3cm thick foam layer, over this layer comes a protection made up of 4 layers of glass fiber, a layer of hemp and finally 4 layers of fiberglass. The end result is an extremely strong and durable cement board with accurate dimensions of 25 x 25 cm, reinforced with layers of glass fiber for increased strength. This method ensures a high quality final product suitable for various structures.

All three plates were tested at bending in three points to find the mechanical proprieties as shown in the figure bellow.

a b c

Figure 1: Plate samples during testing (a- plaster, b- cement, c- hemp-based)

3. Results and conclusions

Following the tests and the results obtained, we generated Force-Displacement graphs for each individual board, as well as a comparative graph for all boards.

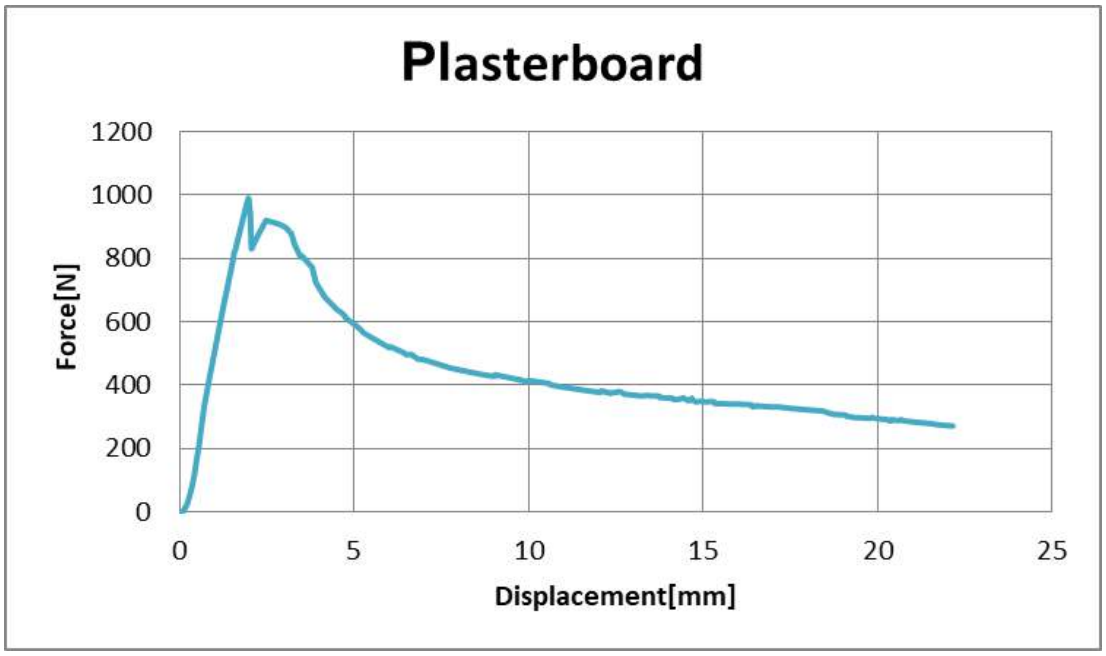

Figure 2: Force displacement chart for plasterboard

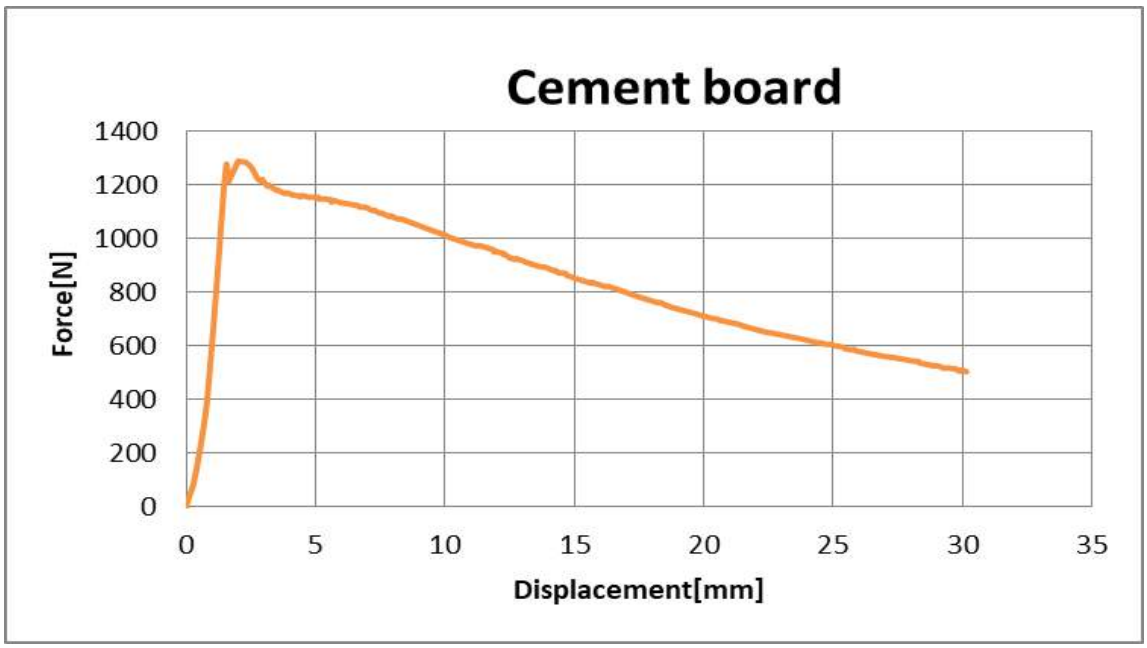

Figure 3: Force displacement chart for cement board

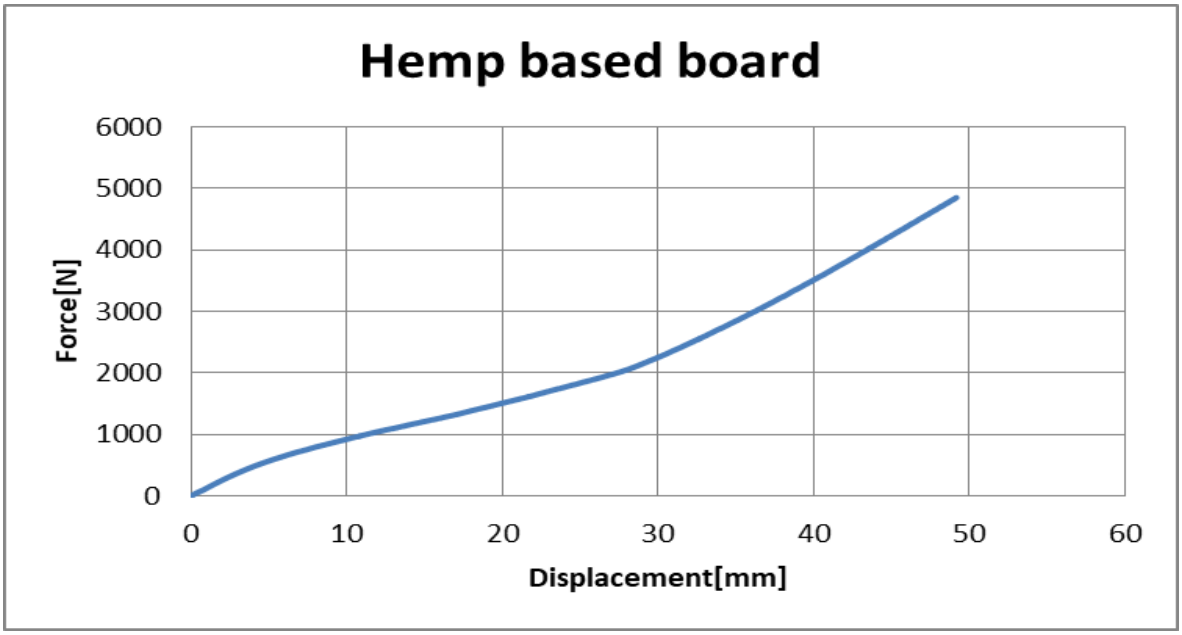

Figure 4: Force displacement chart for hem based board

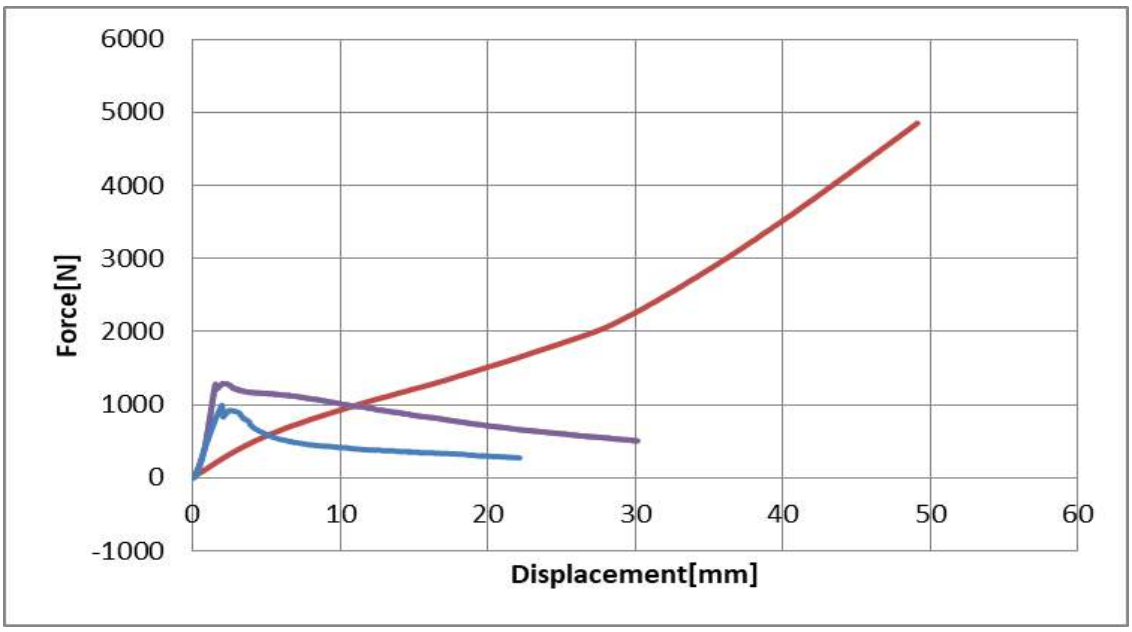

Figure 5: Force-Displacement comparison chart for all samples

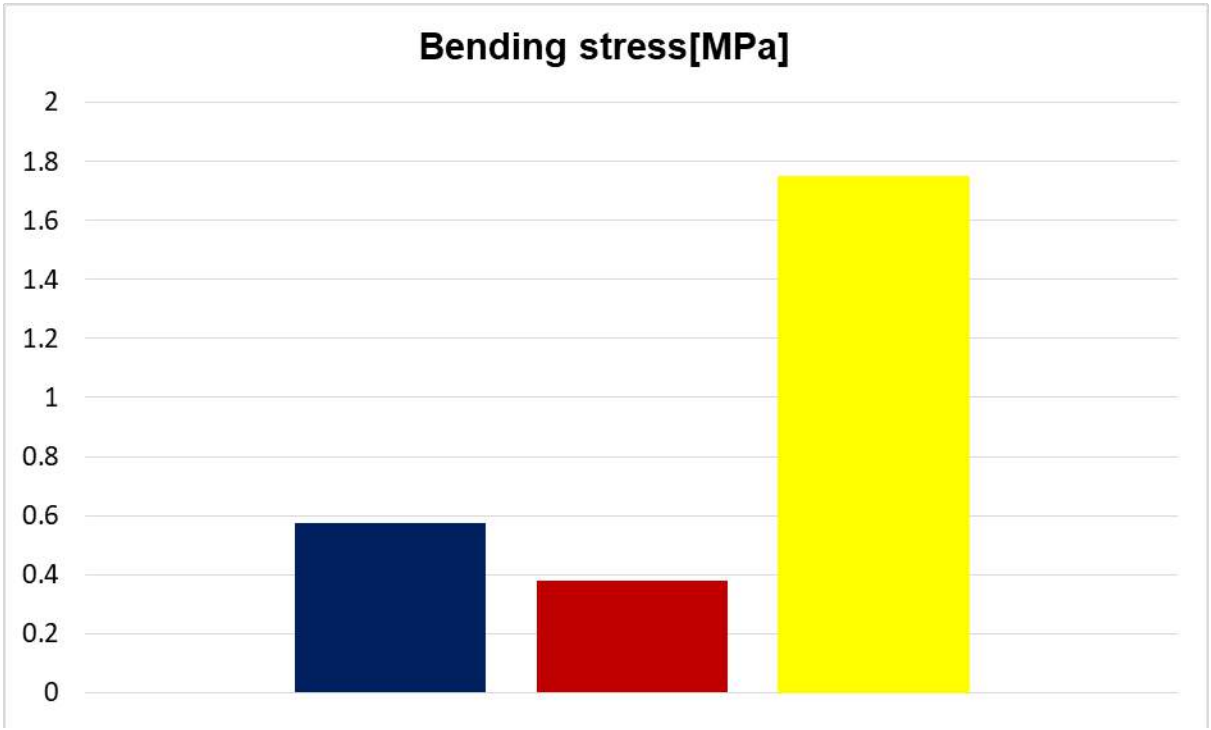

Figure 6: Bending stress resistance comparative chart.(Blue: cement, red: plasterboard, yellow: hemp based)

Table1. Maximum recorded values for all three plates

Plate	Maximum force [N]	Maximum displacement [mm]	Maximum stress [MPa]
Plaster	**991.17**	**22.172**	**0.37759**
Cement	**1289.9**	**30.167**	**0.57331**
Hemp-based	**4853.7**	**49.166**	**1.7491**

The study of mechanical tests of composite materials with organic compounds represents a crucial stage in the development and understanding of the performance of these advanced materials. Following the analysis of the

performed experiments, several significant conclusions can be drawn that contribute to the deepening of our knowledge on the behavior of these complex systems.

First, the results of the mechanical tests highlighted that the addition of organic compounds in composite materials can significantly improve their properties. For example, the tensile strength of these materials was significantly increased compared to composites without organic compounds. This suggests that the interactions between the polymer matrix and the organic compounds led to a homogeneous distribution of charges, thus contributing to the increase in strength.

On the other hand, studies have revealed that mechanical properties can vary depending on the type and concentration of organic compounds used. For example, certain organic compounds can contribute to better adhesion between the phases of composite materials, leading to an increase in shear strength. However, it is important to note that certain high concentrations can have a negative impact on performance, leading to decreased strength or ductility.

BIBLIOGRAFIE

[1] Brown, A. L., & Martinez, G. P. (2014). "Impact of Organic Additives on the Tensile Strength of Composite Materials." Polymer Composites, 28(4), 511-525.

[2] Evans, R. W., & Turner, H. A. (2016). "Improving Flexural Properties of Composite Materials Using Organic Fillers." Journal of Reinforced Plastics and Composites, 33(8), 712-726.

[3] Carter, S. H., & Johnson, D. L. (2011). "Analyzing the Effect of Organic Compounds on Composite Material Durability." Journal of Materials Science, 45(9), 2875-2890.

[4] Davis, K. L., & White, P. J. (2013). "Mechanical Characterization of Organic-Incorporated Composites under Dynamic Loading Conditions." Composites Science and Technology, 42(7), 931-945.

[5] Greene, N. L., & Murphy, R. E. (2019). "Enhanced Fatigue Life in Composite Materials with Organic Additives." Composites Part B: Engineering, 54(5), 321-335.

[6] Harrison, W. T., & Collins, A. S. (2017). "Influence of Organic Compounds on the Fracture Toughness of Composite Structures." International Journal of Fatigue, 25(11), 1435-1448.

[7] Foster, C. E., & Garcia, J. M. (2015). "Advanced Testing Methods for Assessing the Impact Resistance of Composites with Organic Compounds." Journal of Testing and Evaluation, 39(2), 187-201.

[8] Jackson, L. E., & Anderson, J. F. (2012). "Mechanical Behavior of Polymer Matrix Composites Reinforced with Organic Fibers." Journal of Composite Science, 18(4),489-504.

[9] Kim, Y. S., & Patel, A. B. (2014). "Effect of Organic Nanoparticles on the Shear Strength of Composite Materials." Composites Part C: Open Access, 21(8), 109-124.

[10] Adams, M. J., & Smith, R. K. (2012). "Enhancing Mechanical Performance of Composite Materials through the Incorporation of Organic Compounds." Journal of Composite Materials, 37(3), 215-228.

[11] Lawson, D. P., & Nguyen, Q. H. (2018). "Characterizing the Thermal Stability of Composites with Organic Inclusions." Journal of Thermal Analysis and Calorimetry, 36(12), 1785-1800.

[12] Inoue, T., & Yamamoto, S. (2013). "Organic-Inorganic Hybrid Composites: A Novel Approach to Tailoring Mechanical Properties." Composites Part A: Applied Science and Manufacturing, 30(6), 823-835.

COMAT The 10th International Conference on ADVANCED COMPOSITE MATERIALS ENGINEERING

Transilvania University of Brasov
FACULTY OF MECHANICAL ENGINEERING

22-23 October 2024

PROCESSING OF A COMPONENT USING A CNC MILLING MACHINE

Purcarea R.[1], Pufu G.*[1], Toth M.[1], Munteanu M.V.[2]

1. Kronstadt German Vocational School, Brașov, Romania, purcarea.ramona@sgk.ro, pufu.gabriela@sgk.ro, toth.mihaela@sgk.ro
2. Transilvania University of Brașov, Romania, v.munteanu@unitbv.ro,
*Corresponding author pufu.gabriela@sgk.ro

Abstract: *CNC (Computer Numerical Control) milling is an advanced technology essential in the manufacturing industry, providing solutions for manufacturing complex parts with a high degree of precision and repeatability. This paper reviews the fundamental processes of CNC milling, starting with CAD design and continuing with CAM programming, machine setup and execution of milling operations. Critical process parameters such as rotational speed, feed and depth of cut that influence product quality and efficiency are discussed. The machined part is made of annealed aluminum alloy Rm ≥ 300 N/mm^2. The machine tool used is Emco 840 CNC milling machine*

Keywords*: CNC milling, cutting velocity, rotation speed, clockwise circle interpolation*

1. INTRODUCTION

CNC milling is a machining process used to make parts of various shapes, sizes and complexities. Milling involves the use of tools called cutters to remove material from the blank to achieve the desired shape [1 ,2 ,3].

2. MECHANICAL TEST OF THE COMPONENT USING A CNC MILLING

The features of the Concept Mill 250 CNC milling machine (see Figure 1) are as follows:

- machine in three working axes, optional 4 and 5 axes,
- the operating interface is Sinumerik,
- the tool shed has 20 slots,
- changing the tools is done using the double gripper device for quick clamping of tools with cone type SK30 DIN 69871,
- axis speed = 0...10000 rpm,
- X-axis rapid advance speed; Y ; Z – 15 m/min,
- X-axis technological advance speed; Y ; Z – 0-10 m/min,
- air-based cooling

Figure 1: CNC Milling machine

To be able to determine the quality of the surface of the external contour [4 , 5, 6], a cylindrical - front cutter Ø20 mm - cutter with removable carbide pads and cylinder - front cutter Ø20 mm - monobloc HSS cutter was used. The material under processing is an aluminum alloy aged $R_m \geq 300$ N/mm^2.

To create the part, the execution drawing was used, after which we created the CAD program.

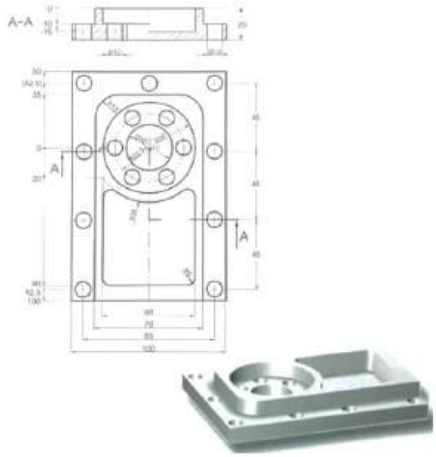

Figure 2: The execution drawing

External contour processing – cylindrical - front milling cutter - Ø20 mm - cutter with removable carbide pads

The parameters of the cutting regime were: v_c = 500mm/min (Figure 2):

- depth of cut of 10mm apmax = 10mm
- cutting speed vc = 500 mm/min
- feed on the cutter ft = 0,23mm
- the number of teeth z = 4 teeth
- speed n = 15.923 rot/min (n= vc *1000/ π*d)
- forward speed vf = 14.649 mm/min (vf = n * ft * z)

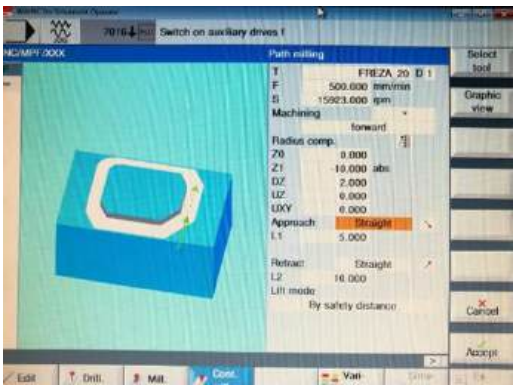

Figure 2: Machining at cutting speed of 500mm/min

The parameters of the cutting regime were: vc = 200mm/min (Figure 3):

- depth of cut of 5mm apmax = 5mm
- cutting speed vc = 200 mm/min
- feed on the cutter ft = 0,20 mm
- the number of teeth z = 4 teeth
- speed n = 3.184 rot/min
- forward speed vf = 2.547 mm/min (vf = n * ft * z)

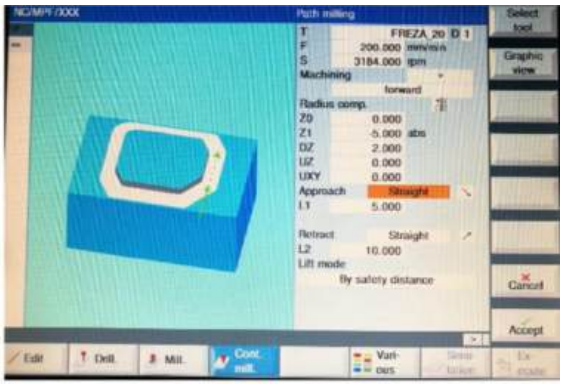

Figure 3: Machining at cutting speed of 500mm/min

The parameters are represented in Table 1.

Table 1. External contour processing – cylindrical - front milling cutter - Ø20 mm - milling cutter with removable carbide inserts

v_c	n	v_f	f_t	a_{pmax}
500	15.923	14.649	0,23	10
200	n = 3.184	2.547	0,20	5

External contour processing – cylindrical - front milling cutter - Ø20 mm – HSS monobloc milling cutter

The parameters of the cutting regime were vc = 150mm/min, (Figure 4):

- depth of cut of 10mm apmax = 0.5 mm
- cutting speed vc = 180 mm/min
- feed on the cutter ft = 0,055 mm

- the number of teeth z = 4 teeth
- speed n = 2.388 rot/min
- forward speed vf = 525 mm/min (vf = n * ft * z)

Figure 4: Machining at cutting speed of 150mm/min

The parameters are represented in Table 2.

Table 2. External contour processing – cylindrical - front milling cutter - Ø20 mm - HSS monobloc milling cutter

v_c	n	v_f	f_t	a_{pmax}
190	3025	665	0,055	1
150	2388	525	0,055	0.5

The programming language is sinumerik, see Figure 5. Linear and circular displacements are used to realize the contours. For the contour processing the software needs to define the direction of the cutter's movement in clockwise or trigonometric direction. After this setting the parameters of the trimming regime are set.

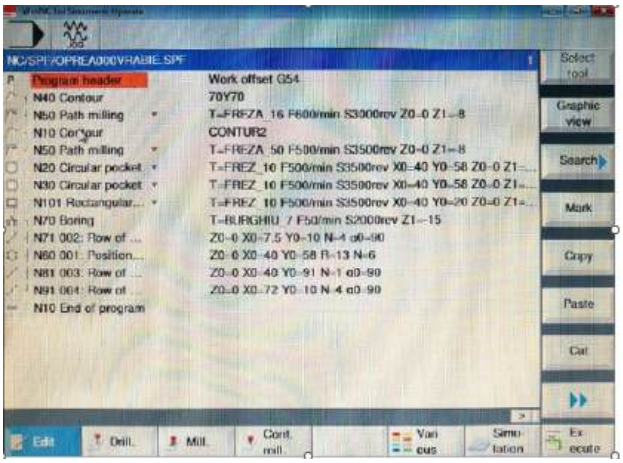

Figure 5: Programming in sinumerik language

3. **CONCLUSIONS**

The CNC milling machine tested does not use coolant during machining. The material being machined is cooled by compressed air only. This leads to

overheating of the tools increasing the friction between the tool and the material, and if the chipping regime is not appropriate the machined surface will also be non-conforming. For the machining to be carried out in accordance with the execution drawing, it is necessary to consider the cooling of the material and the tools when calculating the parameters of the cutting speed.

REFERENCES

[1] https://manualetehnice.ro/ingineria-metalelor
[2] Dziedzic K., Lis R., Montusiewicz J.: Bitmap graphics in teaching multimedia techniques. Postępy Nauki i Techniki, 2, 2008, 140–152.
[3] Józwik J., Włodarczyk M., Ścierka T.: Geometric and kinematics model of vertical CNC machine centre FV-580A. Postępy Nauki i Techniki, 5, 2010, 85–96.
[4] Zagórski I., Kuczmaszewski J.: The study of cutting forces and their amplitudes during high-speed dry milling magnesium alloys. Advances in Science and Technology Research Journal, 7(20), 2013, 61–66.
[5] Zagórski I., Pieśko P.: Comparative study of surface roughness of selected magnesium alloys after milling with carbide tool and PKD. Postępy Nauki i Techniki, 8, 2011, 53–58.
[6] Kocman, K. and Prokop, J. Machining technology (in Czech). Brno: CERM, s. r. o., 2005. ISBN 80- 214-3068-0

COMAT The 10th International Conference on ADVANCED COMPOSITE MATERIALS ENGINEERING

Transilvania University of Brasov
FACULTY OF MECHANICAL ENGINEERING

22-23 October 2024

OPTIMIZATION OF A SPATIAL SYSTEM OF BARS AT WHICH ONE ADDS AN EXTRA BAR

Răcășan V.[1], Stănescu N.D. *[1]

1. National University of Science and Technology Politehnica Bucharest, Pitești University Center, Pitești, Romania, racasan.valentin@yahoo.com
*Corresponding author: s_doru@yahoo.com

Abstract: *In a previous paper we have studied some conditions for optimizing a spatial system of spherical articulated bars at both ends and having a common end. Optimizations have been studied in the case of adding two bars. In this work, only one bar is added, the optimizations referring to the minimum displacement of the common point of the bars or the minimization of tension in a certain bar.*

Keywords: *spatial system of bars, numerical simulation, deformations, tensions*

1. INTRODUCTION

In our previous paper [1] we discuss the case of a spatial system of bars at which one adds two bars and wants to obtain a certain optimization based on a criterion. The bars were spherically jointed at their ends. In the present paper we add only one bar at the existent system of spatial bars and again we want to optimize some parameters.

The references [225-] were described in [1] and they will not be presented again here. The study is performed using the screw coordinates.

The working hypotheses are also presented in [1].

2. MATHEMATICAL MODEL

The mathematical model is captured in Fig. 1. Only one bar of the system is presented. The angles between the straight bar OB_i and the three axes of coordinates are α_i, β_i, and γ_i, respectively. The common point of the bars is point O and at this point the force $\mathbf{F}$ acts (the components of this force being F_x, F_y, and F_z on the three axes). Under the action of the force $\mathbf{F}$ the point O

suffers a spatial displacement of components Δx, Δy, and Δz, respectively. The nominal length of the bar OB_i is l_i, but the bar may present an error of fabrication so there exists a deviation δ_i^* of its nominal length. The modulus of elasticity of the bar is E_i, while the area of the cross-section of the bar is A_i.

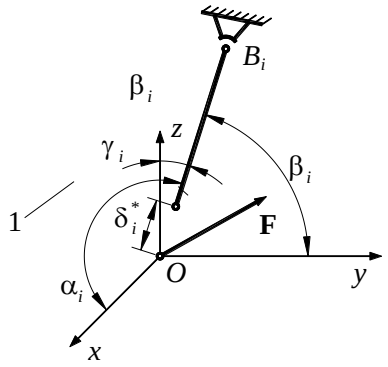

Figure 1: Mathematical model

Proceeding as in [1] one may establish the following system of equations of equilibrium

$$\left(\sum_{i=1}^{n} k_i \cos^2\alpha_i + k_{n+1}\cos^2\alpha_{n+1}\right)\Delta x + \left(\sum_{i=1}^{n} k_i \cos\alpha_i \cos\beta_i + k_{n+1}\cos\alpha_{n+1}\cos\beta_{n+1}\right)\Delta y + \left(\sum_{i=1}^{n} k_i \cos\alpha_i \cos\gamma_i + k_{n+1}\cos\alpha_{n+1}\cos\gamma_{n+1}\right)\Delta z = F_x + \sum_{i=1}^{n} k_i\delta_i^* \cos\alpha_i + k_{n+1}\delta_{n+1}^*\cos\alpha_{n+1}, \tag{1a}$$

$$\left(\sum_{i=1}^{n} k_i \cos\beta_i \cos\alpha_i + k_{n+1}\cos\beta_{n+1}\cos\alpha_{n+1}\right)\Delta x + \left(\sum_{i=1}^{n} k_i \cos^2\beta_i + k_{n+1}\cos^2\beta_{n+1}\right)\Delta y + \left(\sum_{i=1}^{n} k_i \cos\beta_i \cos\gamma_i + k_{n+1}\cos\beta_{n+1}\cos\gamma_{n+1}\right)\Delta z = F_y + \sum_{i=1}^{n} k_i\delta_i^* \cos\beta_i + k_{n+1}\delta_{n+1}^*\cos\beta_{n+1}, \tag{1b}$$

$$\left(\sum_{i=1}^{n} k_i \cos\gamma_i \cos\alpha_i + k_{n+1}\cos\gamma_{n+1}\cos\alpha_{n+1}\right)\Delta x + \left(\sum_{i=1}^{n} k_i \cos\gamma_i \cos\beta_i + k_{n+1}\cos\gamma_{n+1}\cos\beta_{n+1}\right)\Delta y + \left(\sum_{i=1}^{n} k_i \cos^2\gamma_i + k_{n+1}\cos^2\gamma_{n+1}\right)\Delta z = F_z + \sum_{i=1}^{n} k_i\delta_i^* \cos\gamma_i + k_{n+1}\delta_{n+1}^*\cos\gamma_{n+1}, \tag{1c}$$

where we considered that the extra bar is denoted by $n+1$, while

$$k_i = \frac{E_i A_i}{l_i},\ i = \overline{1, n+1}. \tag{2}$$

3. NUMERICAL SPATIAL SIMULATIONS

In the simulations we will consider that the original system has four bars, while the fifth bar is the added one.

In the first case of spatial system of bars the following values are selected: (modulii of elasticity of the five bars) $E_1 = 2.11\times10^{11}\left[\mathrm{N/m^2}\right]$, $E_2 = 2.11\times10^{11}\left[\mathrm{N/m^2}\right]$,

$E_3 = 10^{11}[\mathrm{N/m^2}]$, $E_4 = 1.5\times10^{11}[\mathrm{N/m^2}]$, $E_5 = 1.3\times10^{11}[\mathrm{N/m^2}]$, (the components of the force $\mathbf{F}$) $F_x = 10^6[\mathrm{N}]$, $F_y = 1.3\times10^6[\mathrm{N}]$, $F_z = -1.5\times10^6[\mathrm{N}]$, (the variations of the lengths of the five bars with respect to their nominal lengths) $\delta_1^* = 2\times10^{-3}[\mathrm{m}]$, $\delta_2^* = 0[\mathrm{m}]$, $\delta_3^* = -1\times10^{-3}[\mathrm{m}]$, $\delta_4^* = 0[\mathrm{m}]$, $\delta_5^* = 1.1\times10^{-3}[\mathrm{m}]$, (the diameters of the cross section of the five bars) $d_1 = 20\times10^{-3}[\mathrm{m}]$, $d_2 = 25\times10^{-3}[\mathrm{m}]$, $d_3 = 40\times10^{-3}[\mathrm{m}]$, $d_4 = 45\times10^{-3}[\mathrm{m}]$, $d_5 = 35\times10^{-3}[\mathrm{m}]$, (the nominal lengths of the first four bars) $l_1 = 1[\mathrm{m}]$, $l_2 = 0.9[\mathrm{m}]$, $l_3 = 1.2[\mathrm{m}]$, $l_4 = 0.75[\mathrm{m}]$, (the angles between the first four bars and the axes of coordinates) $\alpha_1 = \frac{\pi}{6}[\mathrm{rad}]$, $\beta_1 = \frac{\pi}{2}[\mathrm{rad}]$, $\gamma_1 = \frac{\pi}{3}[\mathrm{rad}]$, $\alpha_2 = \frac{5\pi}{3}[\mathrm{rad}]$, $\beta_2 = \frac{2\pi}{3}[\mathrm{rad}]$, $\gamma_2 = \frac{\pi}{4}[\mathrm{rad}]$, $\alpha_3 = \frac{7\pi}{5}[\mathrm{rad}]$, $\beta_3 = \frac{2\pi}{3}[\mathrm{rad}]$, $\gamma_3 = 1.1668221882[\mathrm{rad}]$, $\alpha_4 = \frac{\pi}{4}[\mathrm{rad}]$, $\beta_4 = -\frac{\pi}{3}[\mathrm{rad}]$, $\gamma_4 = \frac{\pi}{3}[\mathrm{rad}]$, (the elastic constants of the bars, the formula for the fifth one is similar but its length is not known at the beginning) $k_i = \frac{\pi d_i^2}{4l_i}E_i$, $i = \overline{1,4}$, $x_{5\min} = 0.1[\mathrm{m}]$, $x_{5\max} = 0.5[\mathrm{m}]$, $y_{5\min} = 0.3[\mathrm{m}]$, $y_{5\max} = 0.6[\mathrm{m}]$, $z_{5\min} = 1.2[\mathrm{m}]$, $z_{5\max} = 1.3[\mathrm{m}]$ (the minimum and maximum values along the three axes inside which the point B_5 can be situated), $\mathrm{d}x = 10^{-3}[\mathrm{m}]$, $\mathrm{d}y = 10^{-3}[\mathrm{m}]$, $\mathrm{d}z = 10^{-3}[\mathrm{m}]$ (the incremental steps along the three axes).

The second case of simulation is characterized by: $E_1 = 2.11\times10^{11}[\mathrm{N/m^2}]$, $E_2 = 2.11\times10^{11}[\mathrm{N/m^2}]$, $E_3 = 10^{11}[\mathrm{N/m^2}]$, $E_4 = 1.5\times10^{11}[\mathrm{N/m^2}]$, $E_5 = 1.3\times10^{11}[\mathrm{N/m^2}]$, $F_x = -1.3\times10^6[\mathrm{N}]$, $F_y = 2\times10^6[\mathrm{N}]$, $F_z = 2.5\times10^6[\mathrm{N}]$, $\delta_1^* = 2\times10^{-3}[\mathrm{m}]$, $\delta_2^* = 0[\mathrm{m}]$, $\delta_3^* = -1\times10^{-3}[\mathrm{m}]$, $\delta_4^* = 0[\mathrm{m}]$, $\delta_5^* = 1.1\times10^{-3}[\mathrm{m}]$, $d_1 = 20\times10^{-3}[\mathrm{m}]$, $d_2 = 25\times10^{-3}[\mathrm{m}]$, $d_3 = 40\times10^{-3}[\mathrm{m}]$, $d_4 = 45\times10^{-3}[\mathrm{m}]$, $d_5 = 35\times10^{-3}[\mathrm{m}]$, $l_1 = 1[\mathrm{m}]$, $l_2 = 0.9[\mathrm{m}]$, $l_3 = 1.2[\mathrm{m}]$, $l_4 = 0.75[\mathrm{m}]$, $\alpha_1 = \frac{\pi}{6}[\mathrm{rad}]$, $\beta_1 = \frac{\pi}{2}[\mathrm{rad}]$, $\gamma_1 = \frac{\pi}{3}[\mathrm{rad}]$, $\alpha_2 = \frac{5\pi}{3}[\mathrm{rad}]$, $\beta_2 = \frac{2\pi}{3}[\mathrm{rad}]$, $\gamma_2 = \frac{\pi}{4}[\mathrm{rad}]$, $\alpha_3 = \frac{7\pi}{5}[\mathrm{rad}]$, $\beta_3 = \frac{2\pi}{3}[\mathrm{rad}]$, $\gamma_3 = 1.1668221882[\mathrm{rad}]$, $\alpha_4 = \frac{\pi}{4}[\mathrm{rad}]$, $\beta_4 = -\frac{\pi}{3}[\mathrm{rad}]$, $\gamma_4 = \frac{\pi}{3}[\mathrm{rad}]$, $k_i = \frac{\pi d_i^2}{4l_i}E_i$, $i = \overline{1,4}$, $x_{5\min} = 0.3[\mathrm{m}]$, $x_{5\max} = 0.7[\mathrm{m}]$, $y_{5\min} = 0.2[\mathrm{m}]$, $y_{5\max} = 0.8[\mathrm{m}]$, $z_{5\min} = 1.1[\mathrm{m}]$, $\mathrm{d}x = 10^{-3}[\mathrm{m}]$, $\mathrm{d}y = 10^{-3}[\mathrm{m}]$, $\mathrm{d}z = 10^{-3}[\mathrm{m}]$.

In the first case the answers are as follows: $|\Delta x|_{\min} = 0.000042[\mathrm{m}]$ for $\alpha_5 = 1.490467[\mathrm{rad}]$, $\beta_5 = 1.310279[\mathrm{rad}]$, and $\gamma_5 = 0.273175[\mathrm{rad}]$; $|\Delta y|_{\min} = 0.000060[\mathrm{m}]$ for $\alpha_5 = 1.490417[\mathrm{rad}]$, $\beta_5 = 1.312606[\mathrm{rad}]$, and $\gamma_5 = 0.270962[\mathrm{rad}]$; $|\Delta z|_{\min} = 0.0000000095[\mathrm{m}]$ for $\alpha_5 = 1.485617[\mathrm{rad}]$, $\beta_5 = 1.312711[\mathrm{rad}]$, and $\gamma_5 = 0.272392[\mathrm{rad}]$; $\left(\sqrt{(\Delta x)^2 + (\Delta y)^2 + (\Delta z)^2}\right)_{\min} = 0.002778[\mathrm{m}]$ for $\alpha_5 = 1.214063[\mathrm{rad}]$, $\beta_5 = 1.138389[\mathrm{rad}]$, and $\gamma_5 = 0.576975[\mathrm{rad}]$; $|N_1|_{\min} = 0.047432[\mathrm{N}]$ for $\alpha_5 = 1.350652[\mathrm{rad}]$, $\beta_5 = 1.279145[\mathrm{rad}]$, and $\gamma_5 = 0.369401[\mathrm{rad}]$; $|N_2|_{\min} = 0.163784[\mathrm{N}]$ for $\alpha_5 = 1.358946[\mathrm{rad}]$, $\beta_5 = 1.150587[\mathrm{rad}]$, and

$\gamma_5 = 0.47681[\text{rad}]$; $|N_3|_{\min} = 975.8196[\text{N}]$ for $\alpha_5 = 1.490843[\text{rad}]$, $\beta_5 = 1.29330[\text{rad}]$, and $\gamma_5 = 0.28937[\text{rad}]$; $|N_4|_{\min} = 20013.398[\text{N}]$ for $\alpha_5 = 1.490286[\text{rad}]$, $\beta_5 = 1.318827[\text{rad}]$, and $\gamma_5 = 0.265055[\text{rad}]$; $|N_5|_{\min} = 0.003685[\text{N}]$ for $\alpha_5 = 1.267035[\text{rad}]$, $\beta_5 = 1.255546[\text{rad}]$, and $\gamma_5 = 0.445395[\text{rad}]$; $\left(\sum_{i=1}^{5}|N_i|\right)_{\min} = 869505.071[\text{N}]$ for $\alpha_5 = 1.193347[\text{rad}]$, $\beta_5 = 1.280752[\text{rad}]$ and $\gamma_5 = 0.485330[\text{rad}]$.

For the second case one obtains: $|\Delta x|_{\min} = 0.000001[\text{m}]$ for $\alpha_5 = 1.310287[\text{rad}]$, $\beta_5 = 1.350817[\text{rad}]$, and $\gamma_5 = 0.344343[\text{rad}]$; $|\Delta y|_{\min} = 0.000539[\text{m}]$ for $\alpha_5 = 1.314115[\text{rad}]$, $\beta_5 = 0.965626[\text{rad}]$, and $\gamma_5 = 0.672543[\text{rad}]$; $|\Delta z|_{\min} = 0.00000569[\text{m}]$ for $\alpha_5 = 1.279858[\text{rad}]$, $\beta_5 = 1.219041[\text{rad}]$, and $\gamma_5 = 0.464891[\text{rad}]$; $\left(\sqrt{(\Delta x)^2 + (\Delta y)^2 + (\Delta z)^2}\right)_{\min} = 0.002187[\text{m}]$ for $\alpha_5 = 1.095497[\text{rad}]$, $\beta_5 = 1.020457[\text{rad}]$, and $\gamma_5 = 0.763008[\text{rad}]$; $|N_1|_{\min} = 0.008567[\text{N}]$ for $\alpha_5 = 1.100687[\text{rad}]$, $\beta_5 = 1.387306[\text{rad}]$, and $\gamma_5 = 0.510199[\text{rad}]$; $|N_2|_{\min} = 1.137601[\text{N}]$ for $\alpha_5 = 1.350476[\text{rad}]$, $\beta_5 = 0.971034[\text{rad}]$, and $\gamma_5 = 0.650114[\text{rad}]$; $|N_3|_{\min} = 14419.090[\text{N}]$ for $\alpha_5 = 1.095739[\text{rad}]$, $\beta_5 = 1.020745[\text{rad}]$, and $\gamma_5 = 0.767847[\text{rad}]$; $|N_4|_{\min} = 74.96161[\text{N}]$ for $\alpha_5 = 1.323615[\text{rad}]$, $\beta_5 = 1.194129[\text{rad}]$, and $\gamma_5 = 0.457567[\text{rad}]$; $|N_5|_{\min} = 0.000041[\text{N}]$ for $\alpha_5 = 1.288224[\text{rad}]$, $\beta_5 = 1.006448[\text{rad}]$, and $\gamma_5 = 0.647810[\text{rad}]$; $\left(\sum_{i=1}^{5}|N_i|\right)_{\min} = 680762.2[\text{N}]$ for $\alpha_5 = 1.296042[\text{rad}]$, $\beta_5 = 0.971863[\text{rad}]$ and $\gamma_5 = 0.675963[\text{rad}]$.

4. CONCLUSIONS

In this paper we have studied the minimization of the displacements (along one direction or considering it by Euclidian norm) and of modulii of the tensions in one particular bar or as sum of modulii. The reader may observe that even in the particular cases the problem has an analytical solution, the only possibility to obtain a solution being by use of numerical calculation. The additional bar can have an end in a zone of space defined by a parallelepiped for which one knows $x_{\min}$, …, $z_{\max}$. Of course, depending on the problem this zone may be another particular one (not necessary a parallelepiped, but a sphere, an ellipsoid etc.) or may be a reunion of particular zones. The problem may simplify in the planar case when only two equations are obtained, but neither in this case may an analytical solution be obtained in the general situation. In fact, analytical solution looks to be possible only for very particular systems of bars.

REFERENCES

[1] Răcășan V., Stănescu N-D, On spatial systems of bars spherically jointed at their ends and having one common end. *Mathematics* 2024, *12(17)*, 2680.

[2] Răcășan V., Pandrea N., Stănescu N.-D., On the rigid hung by elastic bars subjected to axial forces, Proceedings of the 29th International Congress on Sound and Vibration, Prague, Czech Republic, 9-13 July, 2023.

[3] Hwang Y.-L., Dynamic recursive decoupling method for closed-loop flexible mechanical systems. *International Journal of Non-Linear Mechanics* 2006, *41*, 1181-1190.

[4] Marques F., Roupa I., Silva M. T., Flores P., Lankarani H. M., Examination and comparison of different methods to model closed loop kinematic chains using Lagrangian formulation with cut joint, clearance joint constraint and elastic joint approaches. *Mechanism and Machine Theory* 2021, *160*, 104294.

[5] Sorgonà O., Cirelli M., Giannini O., Verotti M., Comparison of flexibility models for the multibody simulation of compliant mechanisms. *Multibody System Dynamics* 2024 (online).

[6] Chen J., Chen Q., Liang D., Mo J., Solution of geometrico-static problems and motion experiments for a suspended under-constrained parallel mechanism driven by two flexible cables. *Journal of Mechanical Science and Technology* 2024, 38(8), 4365-4376.

[7] Gallardo-Alvarado J., Jerk distribution of a 6-3 Gough-Stewart platform, *Proceedings of the Institution of Mechanical Engineers, Part K: Journal of Multi-body Dynamics* 2013, *217 (1)*, 77-84.

[8] Zhou H., Cao Y., Li B., Wu M., Yu J., Chen H., Position-Singularity Analysis of a Class of the 3/6-Gough-Stewart Manipulators based on Singularity-Equivalent-Mechanism. *International Journal of Advanced Robotic Systems* 2012, *9 (9)*, 1-9.

[9] Ding X., Isaksson M., Quantitative analysis of decoupling and spatial isotropy of a generalised rotation-symmetric 6-DOF Stewart platform. *Mechanism and Machine Theory* 2023, 180, 105156.

[10] Šika Z., Krivošej J., Vyhlídal T., Three dimensional delayed resonator of Stewart platform type for entire absorption of fully spatial vibration. *Journal of Sound and Vibration* 2024, *571*, 118154.

[11] Hajimirzaallan H., Ferraresi C., Moosavi H., Massah M., An analytical method for the inverse dynamic analysis of the Stewart platform with asymmetric-adjustable payload. *Proceedings of the International Institution of Mechanical Engineers Part K: Journal of Multi-body Dynamics* 2013, *227(2)*, 162-171.

[12] Leonov G. A., Zegzhda S. A., Zuev S. M., Ershov B. A., Kazunin D. V., Kostygova D. M., Kuznetsov N. V., Tovstik P. E., Tovstik T. P., Yushkov M. P., Dynamics and Control of the Stewart platform. *Doklady Physics* 2014, *59(9)*, 405-410.

[13] Korkealaakso P., Mikkola A., Rantalainen T., Rouvinen A., Description of joint constraints in the floating frame of reference formulation. *Proceedings of the Institution of Mechanical Engineers, Part K: Journal of Multi-body Dynamics* 2009, *223*, 133-145.

[14] Bouzgarrou B. C., Ray P., Gogu G., New approach for dynamic modeling of flexible manipulators. *Proceedings of the Institution of Mechanical Engineers, Part K: Journal of Multi-body Dynamics* 2005, *219*, 285-298.

[15] Huang Z., Zhao Y., Liu J., Kinetostatic Analysis of 4-R (CRR) Parallel Manipulator with Overconstraints via Reciprocal-Screw Theory. *Advances in Mechanical Engineering* 2010, 404960.

[16] Stan A.-F., Pandrea N., Stănescu N.-D., Munteanu L., Chiroiu V., On the vibrations of a Rigid Solid Hung by Kinematic Chains, Symmetry, 2022, 14 (4), 1-56.

[17] Hu Y., Zhang H., Wang K., Fang Y., Ma C., Analytical analysis of vibration isolation characteristics of quasi-zero stiffness suspension backpack. *International Journal of Dynamics and Control* 2024. (online)

[18] Chen W., Wang S., Li J., Lin C., Yang Y., Ren A., Li W., Zhao X., Zhang W., Guo W., Gao F., An ADRC-based triple-loop control strategy of ship-mounted Stewart platform for six-DOF wave compensation. *Mechanism and Machine Theory* 2023, *184*, 105289

[19] Yang S., Xu P., Li B., Design and rigid-flexible dynamic analysis of a morphing wing eight-bar mechanism. *Nonlinear Dynamics* 2024, *112*, 15025–15060.

[20] Chen G., Rui X., Abbas L.K., Wang G., Yang F., Zhu W., A novel method for the dynamic modeling of Stewart parallel mechanism. *Mechanism and Machine Theory* 2018, *126*, 397–412.

[21] Xu A., Xu Z., Zhang H., He S., Wang L., Novel coarse and fine stage parallel vibration isolation pointing platform for space optics payload. *Mechanical Systems and Signal Processing* 2024, *213*, 111359.

[22] Jiang Y., Xiao H., Yang G., Guo H., Liu R., Deng Z., Study on transient dynamics of the pyrotechnic-driven large flexible expansion mechanism. *Nonlinear Dynamics* 2024, *112*, 15917–15932.

[24] Pandrea N., Elements of mechanics of rigid solids in plűckerian coordinates, The Romanian Academy Publishing House, Bucharest, 2000.

[25] Răcășan V., Stănescu N.-D., Minimization of the small deformations for a planar system of concurrent bars jointed at their ends, Proceedings of the 30th International Congress on Sound and Vibration, Amsterdam, Netherlands, 8-11 July, 2024.

COMAT The 10th International Conference on ADVANCED COMPOSITE MATERIALS ENGINEERING

Transilvania University of Brasov
FACULTY OF MECHANICAL ENGINEERING

30-31 October 2024

Hybrid biocomposites: properties and performance for exoskeleton applications

Savin A.*[1], Steigmann R. [1], Dobrescu S.G.[1], Moraras C.[2]

1. Nondestructive testing Department, National Institute of R&D for Technical Physics, Iasi, Romania; steigmann@phys-iasi.ro; gdobrescu@phys-iasi.ro
2. Faculty of Mechanical Engineering, Technical University Gh. Asachi Iasi, Romania, ciprian-ionut.moraras@academic.tuiasi.ro

*Corresponding author: asavin@phys-iasi.ro

Abstract: *Bio composites are biocompatible composites, having organic or inorganic components in their composition. A 100% ecological bio composite material consists of a matrix (resin) and reinforcement represented by natural fibers. The matrix can be from two resources, i.e. renewable or non-renewable polymers. The matrix has a major importance in protecting the reinforcement against exposure to the environment through mechanical and/or chemical damage and for supporting the loads. The paper analysis the hybrid (basalt/flax) bio composites for determination of mechanical properties on DMA tests, in order to evaluate possibility to use the composite bio basalt/flax made of 8-ply flat woven laminates for realizing exoskeleton for transport and weights handling and to compare the performance for the stacking configurations considered.*
Keywords: *bio composites, natural fibers, mechanical, DMA*

1. INTRODUCTION

The composites industry is in a permanent modeling, led by the market, by the component materials and by their technology. The components of a composite, the matrix and the fibers, play a significant role in the structure and contribute greatly to the remaining on the market. Biocomposites are considered as new materials from the fourth generation, having organic or inorganic components [1]. Biocomposites have natural fibers as reinforcement in their structure, being an alternative to composites reinforced with synthetic fibers (glass, carbon)[2]. Depending on their origin, natural fibers can be obtained from plants, animals or minerals. Used alone or in hybrid combinations with already tested materials (glass fibers or carbon fibers), the organic materials can improve quality by being lighter and visually attractive. Thus, flax can compete with glass fibers due to the breaking resistance given by the long cellulose fibers inside the stems of the plant. Natural fibers have good sustainability [3] but they have disadvantages (sensitivity to moisture, their structure depends on the growing conditions and the harvesting period), leading to an uncertainty of the final properties as low thermal stability. Adherence to matrix and the tendency to form agglomerates with resins implies the solutioning of

manufacturing technological problems and a control of the behavior in the intended applications [4]. Basalt fiber with mineral origin from volcanic rock is obtained by extruding the melted material into fine fibers, used for reinforcing composite with durability and good heat resistance.

The transport industry requires the movement and handling of heavy materials. Adding a wearable could assist the transport activity or workflow in some areas. Thus, the optimal design of the bio-composites used in exoskeleton construction (for transport and weights handling), require to know the mechanical properties of the component materials. For this, the influence of the orientation and stacking sequences of the basalt and flax layers over mechanical properties were evaluated, the results were compared with those of carbon fiber reinforces plastics with same characteristics.

2. SPECIMEN PREPARATION AND METHODS

The influence of stacking sequences on the mechanical properties of composites is recognized [5], the elastic properties of the composite are dependent on the significant differences in the packaging of the laminae as well as the laminae themself [6]. The fibers provide strength and rigidity and act as reinforcement in composites and determine their properties. The unidirectional fibers in the fabric structure obtained in two layers sewn together give it improved mechanical properties. The rigidity of the laminate is given by the twill 2/2 fabric and the twist-free threads. In the case of basalt, the multiaxial fabric leads to a significant increase in the modulus of elasticity and resistance, promoting them to construction of ships, cars, high-speed trains, wind blades.

In the case of the studied biocomposites, for the evaluation of their mechanical performances, plates having 295x205 mm^2 with a thickness of 5.38 mm for flax and 3.45 mm for basalt were made by the vacuum infusion process with eight layers of fabric for both types of fibers. The stacking order for flax was $[0^o]_8$ and $[45^o]_8$ and for basalt it was $[+45^o/-45^o]_4$ respectively $[0^o/90^o]_4$. For both materials, bioepoxy with 56% of plant source GreenPoxy 56 and multi-purpose hardener series SD7561 with a high carbon content of vegetable origin were used. In order to compare the performance of bio composites with those of the carbon fiber reinforced polymer (CFRP), plates with dimensions of 295x205x3.20mm^3 were made by the same process. The multilayer stacking sequence of the T240 type pre-impregnated carbon fibers for FRP plates is face and opposite surface $[0^o/90^o]$ with intermediate layers $\{[0^o]_3$ and $[+45^o/-45^o]_2\}$. Table 1 shows mechanical properties of different bio fibers/CF.

Tables1. Mechanical properties of different bio fibers/CF

Materials/ width (mm)	V_f (%)	Areal weight (g/m2)	Tensile Strength of filament (MPa)	Young's modulus (GPa)	Elongation at break (%)
Flax- 5.38	30-35	200-350	500-900	50-70	1.5-4.0
Basalt – 3.45	50	620	3000-4840	79.3-110	3.1-3.2
CF – 3.43	45	193	3600-4100	235	2.8

Changing the stacking sequence generally modifies the parameters of the composite and joining with adhesives generates a behavior that is influenced

both by the total stacking sequence, the sequence and the local distribution of the layers near the interfaces. Dynamic mechanical analysis (DMA) specimens were prepared in accordance with ASTM D5023 ~~[14]~~ for testing with DMA 242C – Netzsch Germany, three-point bending test using Protheus software v.4.8.5 under sinusoidal cyclic loading. The maximum allowed dimensions of the specimens are 50x10x5mm^3. The viscoelastic properties of the specimens as complex modulus of elasticity E', the loss modulus E'', the damping or loss factor, tan δ, depending on the temperature were determined in the range of 25^{o}C-250^{o}C. The parameters obtained provide information on vitrification, referred to T_g (glass transition), resulting from the cross-linking reaction. The apparent activation energy for the glass transition process, at a preload of 6N was determined for 1 and 5Hz in a temperature-controlled room.

The absence/presence of porosity in the samples were analyzed using the US method. For this, the PHASOR XS equipment coupled with a phased array with 32 US sensors working at a frequency of 5MHz and a delay line was used.

3. RESULTS AND DISCUSSION

Through their microscopic structure, bio composites are made of fibers embedded in a matrix, arranged with different orientations to the longitudinal axis, forming a layered composite. Figure 1 shows the non-crimp biax fabric used as reinforcements in bio-composites.


a


b

Figure 1: Reinforcements used a) bidirectional flax 0/90; b) basalt woven fibers 0/90/±45

Composite interaction with the ultrasounds (US) depends on the US energy but also on its structure as the dimensions and cohesion of the fibers, the quality and composition of the bio-resin, the moisture content, the temperature of the environment and, in particular, the orientation of the wrapping sequences in relation to US source. The time-of-flight method is the common technique in US testing. From the time interval between transmission and reception, either the speed of sound or the distance traveled is obtained. The effect of the percentage of fibers (V_f) in the composite mass and the orientation of the fibers correlates with the speed of the longitudinal US waves as well as with the attenuation of the US wave [7]. For the fiber content for flax alkali treated, c_f=2764m/s was obtained and for basalt c_b=2556m/s. The porosity content of the material is directly related to the pressure applied during the hardening of the composite. The pressure regulation can control the volume of void content in the first sequence. Here, the porosity was assessed by image analysis, knowing that the degree of porosity is in linear correlation with the US attenuation in composites (Figure 2). The displacement of the transducer and establishing the tested location was achieved using an encoder.

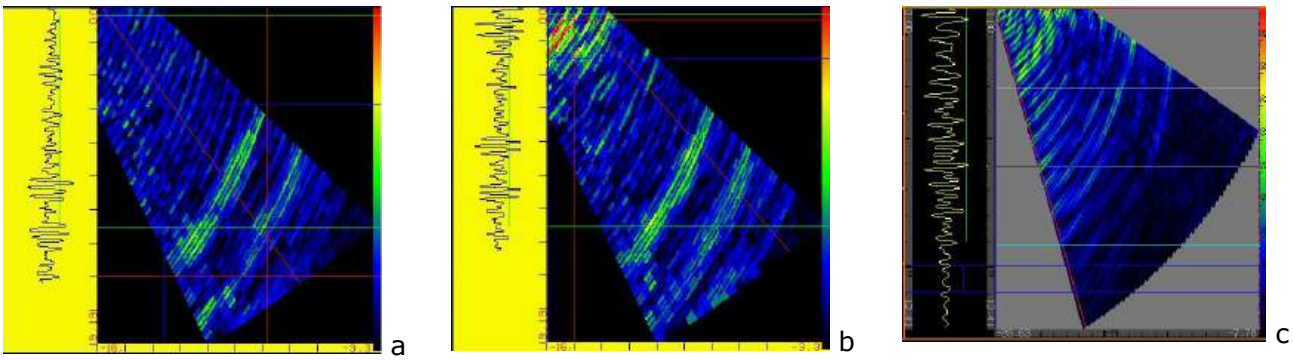

Figure 2: Combined A-scan and sectorial scan views for: a) flax; b) basalt; c) CF

The US tests were performed in approximately 20-25 areas of the bio and carbon epoxy composites. It is possible to evaluate the way of distribution of the fibers as well as the lack of delaminations/gaps. Thus, from figure 1b, it can be seen that the basalt has a different arrangement of fibers near the surface compared to those in the volume. It is found that flax and basalt fibers have a higher attenuation compared to FRP, the US absorption coefficient is defined as the energy absorbed reported to the total energy used [8].

The DMA tests performed for the samples show that the changes in the dynamic mode of the materials under the vibration load with temperature differ for the type of bio-composites compared to the carbon-based composites. The mechanical properties as well as the effect of the frequency on the viscoelastic properties of the composites are presented in figures 3-5.

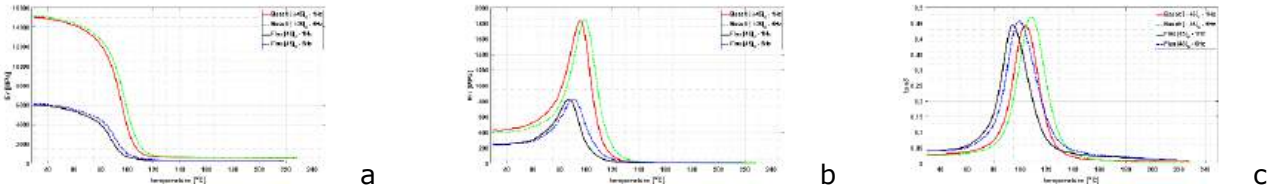

Figure 3: Basalts and flax samples with stacking sequence $[\pm 45]_4$: a) E'; b) E"; c) (tanδ)

The loss modulus E' (figure 3) measures the energy absorbed by the composite during the oscillation cycle. For V_f=50% fibers E'=6GPa for flax and 15.8GPa for basalts. It can be observed that, at the same stacking sequence, the modulus of elasticity for basalt decreases much faster in the range of 80-100°C compared to flax, while the loss modulus also for basalt fluctuated violently for the same temperature range. This indicates that temperature has a significant role on the interface's properties and adhesion activity of the resin. The stress is distributed equally in both directions. It is observed that the variation of E' of the biocomposites is greater in the glassy region, so that later at a temperature of 80°C it decreases due to the reinforced fiber that loses its rigidity at elevated temperatures. The difference between the properties of the composites with flax and basalt fibers after the temperature of 100°C is no longer significant. The transition temperature to the vitreous state for both types of fibers in this packaging does not differ significantly with frequency, thus at 1 and 5 Hz for basalt T_g={85.2; 86.6}°C and for flax T_g={80.4; 82.2}°C. The analysis shows that T_g represents the critical limit of good functioning of the composite material. The advanced characterization provides data for knowing the performance/limits of the use of bio-epoxy composites.

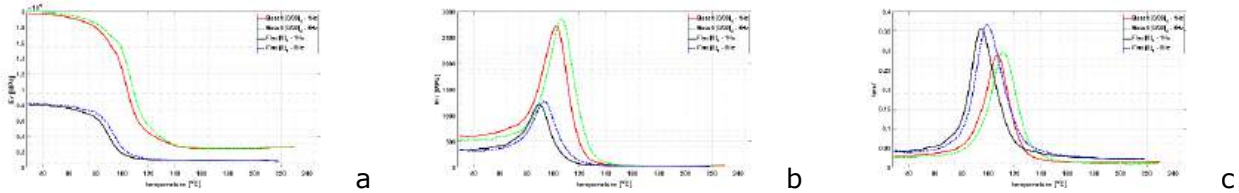

Figure 4: Basalts and flax samples with stacking sequence [(0/90)]: a) E'; b) E"; c) (tanδ)

In relation to the packing mode, it can be observed that due to the presence of fibers with $[0/90]_4$ orientation, the flax and basalt composites in the vitreous region have an increased storage modulus compared to figure 3. The same behavior is noted for the E' and E" values at the 80-100°C range for the glass transition region, E" provides information on the amount of energy dissipated in the form of heat per oscillation cycle. The increased values may be due to the 0° orientation of the fibers, knowing that the unidirectional shows an increased stiffness. A slight increase in T_g={91.4; 92.8}°C for basalt and T_g={83.6; 86.5}°C for flax at 1 and 5 Hz. As the material passes from the vitreous state to the "highly elastic" state, the properties of the biopolymer become predominant. Tanδ (damping) measures the impact properties of the biocomposite. Tanδ for $[0/90]_4$ has a lower value, because the bioepoxy resin has a high molecular mobility that is stopped by the incorporation of fibers in the given structure. Thus, the strong adhesion of the fibers to the matrix is established, resulting in a uniformly distributed tension. The lower damping curve for flax compared to basalt indicates that the material can absorb more energy, becoming stiffer at a slightly higher temperature. The curves have a high peak as the frequency increases. The DMA analysis of FRP in the presented stacking mode, shows that as the temperature increases and at the two vibration frequencies, the loss modulus E' respects the three transition zones of the phases.

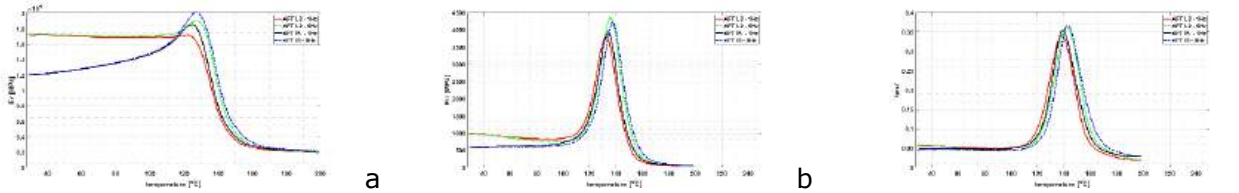

Figure 5: FRP samples. a) E'; b) E"; c) (tanδ)

The vitrous state remains approximately constant up to 80°C so that then in the vitreous state a slight increase can be noticed at a temperature of 125°C, after which it decreases in the range [130-150°C]. For both directions of FRP testing (given by the layout of the layers) the transition temperature to the vitreous state is T_g={115.8; 119.3°C}.The orientation of the fibers seems to reduce the variation range of T_g by a few degrees and therefore increases T_g as the critical upper limit for safe design. The same behavior of rapid decrease of E' is noted due to the reaction of the resin groups in the matrix. The loss modulus curve fluctuates violently with temperature between [110-150°C], the area demonstrating a high energy dissipation, the synthetic epoxy sample has the peak at a higher temperature than the bio epoxy samples but having close transition temperatures. FRP has a narrower width of the E" curve compared to bio-composites. Tanδ which provides information on the fiber and matrix interaction, measures the impact properties of FRP. The peak value is close to that of the flax biocomposites with the sequence $[0]_8$, demonstrating a high

molecular mobility that is stopped by the incorporation of fibers in the given structure. The strong adhesion of the fibers with the matrix, in the created structure, results in a uniformly distributed tension.

4. CONCLUSIONS

The research demonstrated that the use of biocomposites with natural fibers ie flax or basalts with the volume of fibers Vf=50% could replace with good results the composites reinforced with carbon fibers in the face and opposite surface structure [0^o/90^o] with intermediate layers {[0^o]$_3$ and [+45^o/-45^o]$_2$} in making the exoskeleton for transport and baggage handling. The prospects of using basalt and flax fibers for the production of bio composite materials with a complex of improved mechanical properties were highlighted. The volume fraction of flax fiber/basalts is very important for establishing the quality of the biocomposite designed for exoskeleton application. It directly affects both mechanical performance and vibration resistance. The width of the curve could suggest the degree of homogeneity of the composite. The informative characterization parameters were analyzed the complex modulus of elasticity E, the loss modulus E'', which represents the viscous component of the material and the damping or loss factor, tan δ, in a temperature range following the dynamic behavior of the biocomposite after passing over transition temperature to the vitreous state. The integration of monitoring improves the understanding of the mechanical behavior of biocomposites, the correlation of dynamic parameters with the dominant stresses in the realization of the exoskeleton for transport and baggage handling could offer possibilities for stress/damage prediction in these applications.

Acknowledgements

This work was supported by MCID Nucleu (PN 23 11 01 02) and PFE (Contract No. 5PFE/2022) Programs.

References

[1] Faruk O., Bledzki A.K., Fink H.P. and Sain M., 2012. Biocomposites reinforced with natural fibers: 2000–2010. Progress in polymer science, 37(11), pp. 1552-1596.

[2] Akampumuza O., et al., 2017. Review of the applications of biocomposites in the automotive industry. Polymer composites, 38(11), pp.2553-2569.

[3] Bogard F., et al., 2022. A comparative review of Nettle and Ramie fiber and their use in biocomposites, particularly with a PLA matrix. Journal of Natural Fibers, 19(14), pp.8205-8229.

[4] Xu X., Hu D. and Ma W., 2021. Synergistic improvement of mechanical and thermal properties in epoxy composites via polyimide microspheres. Journal of Applied Polymer Science, 138(35), p.50869.

[5] Mohanavel V., et al. 2022. Influence of stacking sequence and fiber content on the mechanical properties of natural and synthetic fibers reinforced penta-layered hybrid composites. Journal of Natural Fibers, 19(13), 5258-5270.

[6] NagarajaGanesh B. and Rekha B., 2020. Intrinsic cellulosic fiber architecture and their effect on the mechanical properties of hybrid composites. Archives of Civil and Mechanical Engineering, 20, pp.1-12.

[7] Faktorová, D., et al. (2024). Analysis of the Anisotropy of Sound Propagation Velocity in Thin Wooden Plates Using Lamb Waves. Polymers, 16(6), 753.

[8] Markiewicz E, PauksztaDand Borysiak S 2012 Acoustic and dielectric properties of polypropylene-lignocellulosic materials composites, Polypropylene InTech. 30:193-217.

COMAT The 10th International Conference on ADVANCED COMPOSITE MATERIALS ENGINEERING

Transilvania University of Brasov
FACULTY OF MECHANICAL ENGINEERING

30-31 October 2024

Assessment of zirconia thermal barrier coatings on austenitic steel

Savin A.*[1], Steigmann R.[1], Faktorova D.[2]

1. Nondestructive testing Department, National Institute of R&D for Technical Physics, Iasi, Romania; steigmann@phys-iasi.ro
2. Faculty of Special Technology, Alexander Dubcek University of Trenčín, Trenčín, Slovakia; dagmar.faktorova@tnuni.sk

*Corresponding author: asavin@phys-iasi.ro

Abstract: *The need to increase the efficiency of aerodynamic engines and last generation turbines (t>1200° C) have imposed new types of materials and coating techniques for the realization of thermal barriers (TBCs). Yttria-doped zirconia (YSZ)-based TBCs are now competing with new materials to provide durability and reliability. The research is focused on the development of new TBC manufacturing techniques to improve the performance of YSZ. A layer of zirconia, without intermediate thermally grown oxide (TGO), with micrometric thickness of the deposition on an austenitic steel support, multilayered and doped with nanometric particles in two phases, was investigated non-destructively. The results obtained on the quality and adhesion to the support obtained by X ray diffraction (XRD) and scanning electron microscopy (SEM) are compared with the electromagnetic ones (EM).*
Keywords: *ZrO_2-ceramic coating, yttria, SEM, XRD, nondestructive testing*

1. INTRODUCTION

In the evolution of industrial sectors involving gas turbines, the innovative advances related to ceramic protective coatings at high temperatures, Thermal Barrier Coatings (TBCs) are of particular importance. The literature includes a large number of specialized works that provide information on some aspects of the behavior of TBCs [1-3] at high temperatures. Among them, we also find those focused on the comprehensive analysis of the mechanisms underlying spalling ceramic zirconia ceramic as TBCs, in terms of material selection, deposition techniques, performance evaluation, etc. TBCs are the most difficult and delicate structures that must ensure the protection of engines from the unwanted effects of extreme operating temperatures in power generating units[4]. New generations of materials based on rare earths have been developed in the manufacture of TBCs aiming to increase efficiency, improve durability and reduce the cost of the life cycle [5],[6]. Ceramic coating (CC) part of TBC creates a protective layer and together with the base material forms a layered composite of refractory oxide with a small thickness (approx. 120-400μm). The typical CC architecture has two layers, a top coating layer that ensures thermal insulation, usually a ceramic with a low thermal conductivity, and an antioxidized layer that ensures adhesion to the superalloy

substrate (bond coat BC). TBC can be obtained through the atmospheric plasma spraying (APS) process [7] or electron beam physical vapor deposition (EB-PVD) technology in bi- or multi-layered structures and represent favorable models for coatings [4]. Whatever the advantages/disadvantages of high-performance TBC deposition methods, they must ensure superior resistance to thermal shocks, erosion and excellent thermal efficiency. Besides these, the implementation of TBC has the advantage of reducing the possibility of using a variety of fuels (especially for stationary gas turbines). Zirconia (ZrO_2) stabilized with yttria (YSZ) is most often used as a material for thermal coatings in engines due to its high resistance to thermal shocks, high oxidation and thermal fatigue resistance up to 1150^{o}C. The objective of the work is to emphasize, by combining non-destructive evaluation (NDT) techniques (electromagnetic EM, X-ray diffraction and SEM with Dispersive X-ray spectroscopy), the effect of doping with nano particles Y_2O_3 of the YSZ ceramic structure used as TBC.

2. MATERIALS AND METHODS

The most vulnerable part of a thermal barrier (TB) is the ceramic substrate interface. Cracking due to high temperatures and intergranular stress of 316L and 304L stainless steel is a critical problem. In the present case, the AISI 316L austenitic steel alloy (<0.03 %C as EN 14404), susceptible to intergranular corrosion, is covered with YSZ ceramics considered TBC [8]. The laminar structures of YSZ as TBC are analyzed to emphasize the improvement of Zr coating-based ceramics properties as a function of addition of Re_2O_3 in the structure of the original ceramics. Ceramics ZrO_2 doped with rare earths (RE) oxides is considered a good TBC material due to their advanced mechanical properties such as low thermal conductivity (2.0 $m^{-1}K^{-1}$ at 1100^o C), refractory, corrosion resistance, as high-fracture toughness and bulk modulus, chemical inertness, and compatible thermal expansion coefficient] with metallic support [9]. At the nanoscale, the main method of stabilizing the tetragonal phase (t) is the introduction of Ce or Y as stabilizing component. Pure yttrium oxide has high melting point; it is chemically inert and has an excellent electrical insulation. In a deposition like TBC, the most sensitive part is the substrate-ceramic interface, where t→m transformations occur that can generate fractures under the influence of thermal shock. For YSZ ceramics, a superior layer quality can be obtained by glazing when the surface can be densified. CC were deposited onto AISI 316L samples [8], with 80x20x2mm^3 and were investigated through XRD, structure and SEM. The samples were sandblasted using 50-80 grit alumina to improve adhesion of the deposition to the substrate as well as to remove possible residues from the metal surface [10]. The formation and evolution of flaws (dislocations, cracks, voids, amorphous phases), as well as the interaction between grain boundaries (GB) and flaws are of interest to the ZrO_2. Among the intrinsic factors that govern the superplastic response of ZrO_2 ceramics, chemical bonding state at GBs has been reported, the research being focused on the intergranular fracture surfaces of polycrystalline YSTZ [11]. Using YSZ ceramics, the quality of the CC applied to the metal surface of the substrate increases. Figure 1 shows the image of the ZrO_2 coating on AISI surface, emphasizing the region formed by the CC before and after spraying with nano powder Y_2O_3. It can be considered that the densification obtained by spraying closes the voids that affect the

sandwich surface of the ceramic (figure 1b) which can lead to an increase in thermal conductivity [12]. These regions that create a densification can also be distinguished by microscopic visualization.

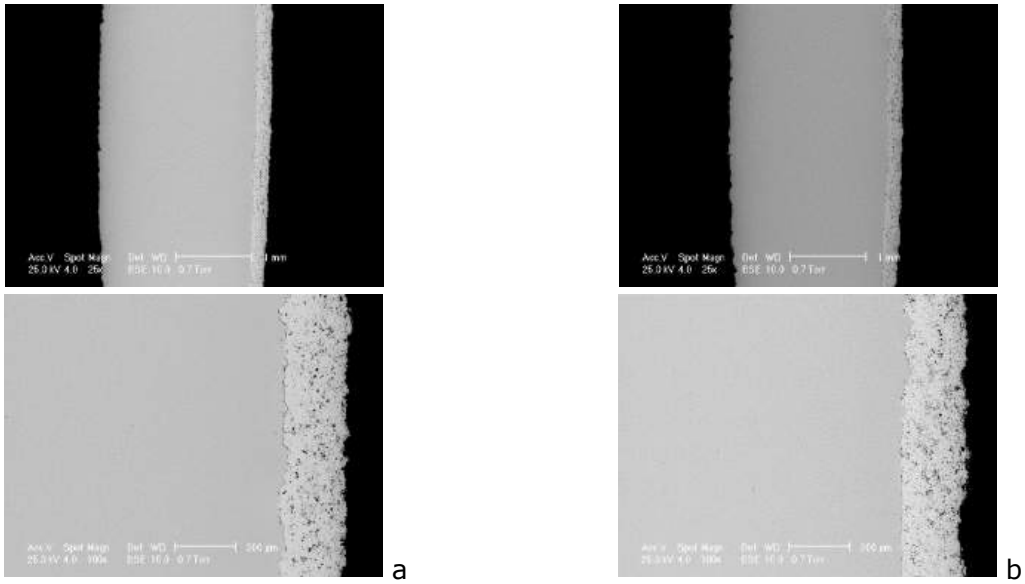

a b

Figure 1: Support AISI 316L and sandwich of zirconia (a) for specimen with 0.2 mm thin monolithic coating ZrO_2 with addition of 20 % Y_2O_3; and (b) for specimen with sandwich coating 0.25 mm ZrO_2 with addition of 20 % Y_2O_3 and 0.005 mm Y_2O_3.

3. RESULTS AND DISCUSSIONS

3.1. Microscopy and XRD analyses

The structures of YSZ layers appear porous (Figure 1a). The information about the action of sandwich coating nano powder 0.005mm Y_2O_3 on the densification and adhesion to the support of CC on SS was obtained from Secondary Electrons (SE) images, as well as Backscattered Electrons (BSE) images (Figures 2 a;b).

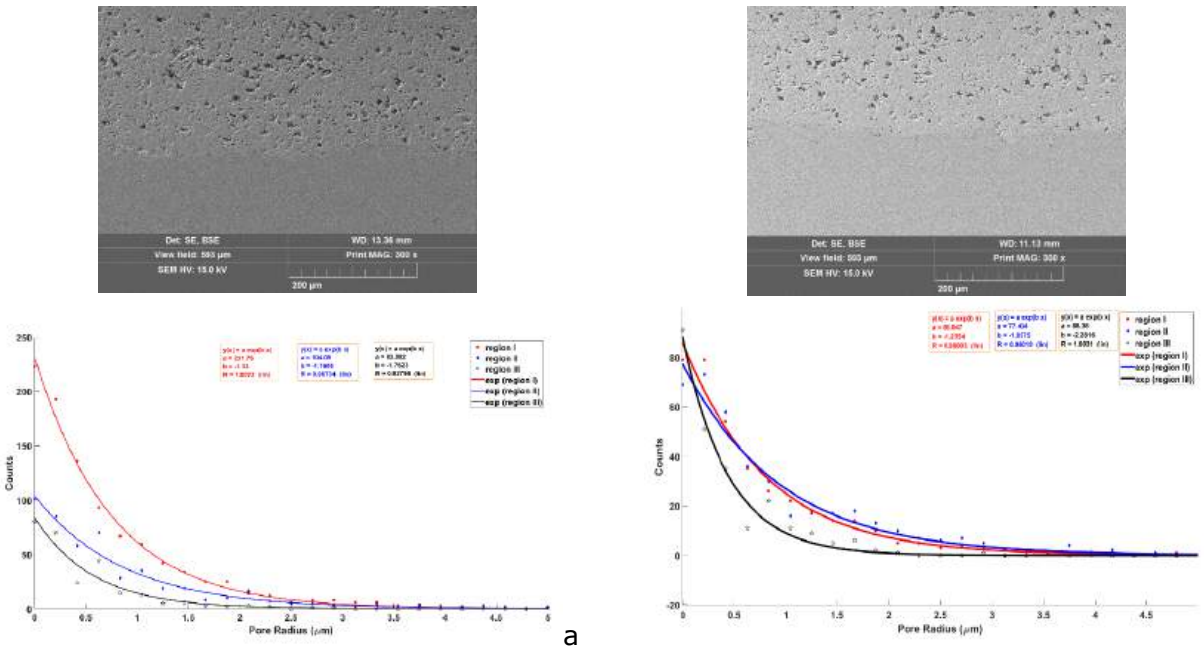

a b

Figure 2: SEM images specimen with voids counting for (a) coating 0.25 mm thick monolithic coating ZrO_2 with addition of 20 % Y_2O_3 and (b) sandwich coating 0.25 mm ZrO_2 with addition of 20 % Y_2O_3 and 0.005 mm Y_2O_3.

In order to establish the pore distribution, the obtained image was divided equally to obtain three regions; region III includes the adhesion layer to the support. The doping with Y_2O_3 caused a decrease in the number of large pores, and in the middle of the coating layer (region II), a densification can be observed. XRD experiments were performed at room temperature using a Philips diffractometer. The phase composition and microstructural parameters were determined using Fullprof software, Ceckcell was used for the spatial group and network constants.

The diffractogram for the sample containing the layer of ZrO_2 doped withY_2O_3 on the SS support and the ZrO_2 one doped withY_2O_3 were traced.

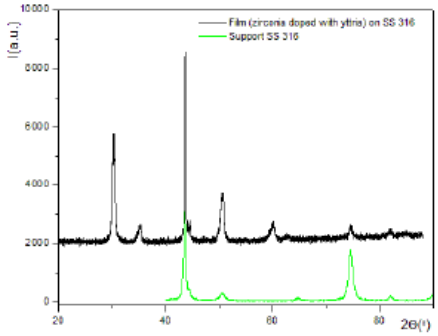

Figure 3: XRD of films and SS 316 support

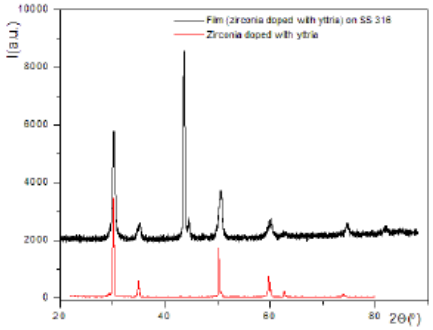

Figure 4: XRD of films and ZrO_2 with yttria

These allowed the identification of the austenite maximumγ(Figure 3) and of the doping maxima t ZrO_2 (Figure 4). The composition as shown in figures 5 and 6 were obtained using Energy Dispersive X-ray spectroscopy (EDXS).

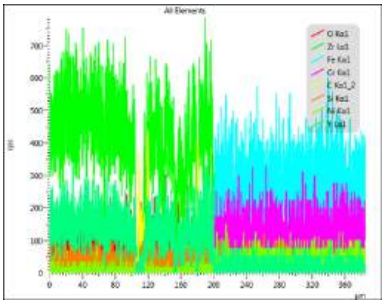

Figure 5: EDXS of (ZrO_2 + 20 % Y_2O_3 coating thick monolithic sandwich - 0.2mm)

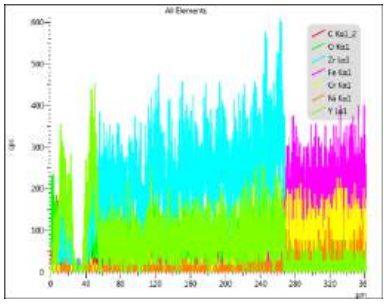

Figure 6: EDXS of (ZrO_2+20%Y_2O_3 coating and 0.005 mm Y_2O_3)

3.2. Electromagnetic methods

NDT is based on the EM method, which is a method applied to conductive materials. The EM method consists in evaluating the interaction of the EM field and the material, the dependence of the transducer impedance on the material properties being known. Advantages such as high sensitivity automated scanning, non-contact inspection and detection of material discontinuities make this technique complementary to classical methods. The impedance changes due to the densification of ceramics or small variation of thickness are incoherent whereas the impedance changes due to defect extended spatially (adherence to the support) of eddy current of the transducer used are significantly. Experimental set-up is presented in figure 7. The working frequency of the transducer is 105MHz provided by Agilent 4395A, the data is acquired and stored on PC. Cracks may appear in the ceramic layer after deposition due to the relaxation of residual stresses.

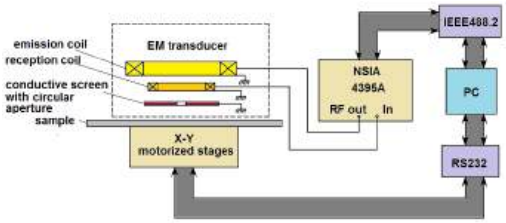

Figure 7: Experimental set-up

The microstructure can present lamellar washes or flattened with microcracks through washes or inter-washes. When scanning the surface of the sample, the image provided through the transducer is amplified. The EM field generated by the transducer propagates in the material as a wave with the wavelength $\lambda=2\pi\delta$ where $\delta=\sqrt{2/\omega\mu_0\sigma}$, $\omega=2f$ angular frequency, σ electrical conductivity, μ_0 vacuum magnetic permeability. The detection principle is similar to that of near-field EM scanning microscopy [13].

In essence, it is about the technique of electron emission from the tip of the transducer and the interaction with the sample. As a result, the extracted electrons are ejected from the sample surface and detected by the transducer. The "topographic images" determined by the intensity variations of the secondary and backscattered electrons give a vertical resolution at the atomic scale and a small nanometric lateral one. The transducer works as a detection antenna transforming localized energy into electromotive forces.

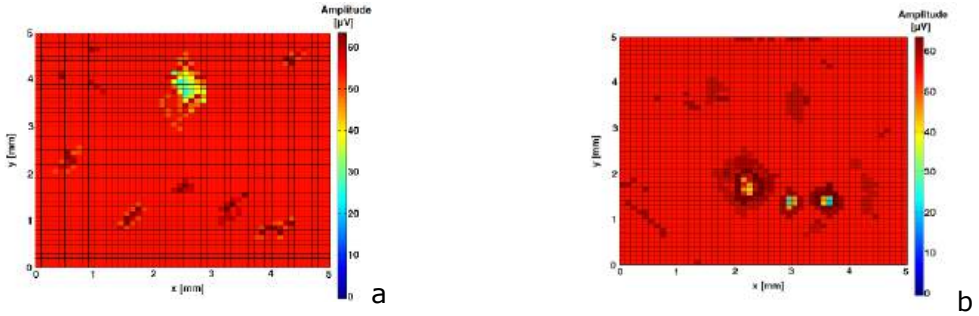

Figure 8: The amplitude of the emf induced in the reception coil of the EM transducer at the scanning of the specimens: a) 0.25 mm thick coating ZrO_2+20 % Y_2O_3; b) sandwich coating 0.25 mm ZrO2 + 20 %Y_2O_3 and 0.005mm Y_2O_3

The images show the amplitude of the emf induced in the reception coil of the EM transducer at the scanning of the surface of analyzed specimens. The image in Figure 8a corresponds to 0.25mm thick monolithic coating ZrO_2+20% Y_2O_3, and shows, in addition to the lack of adhesion to the support, some inhomogeneities of the microstructure, possibly both in CC and on the surface of the support (SS AISI 316L). The image corresponding to the CC structure with 0.25mm ZrO_2+20%Y_2O_3 and 0.005mm Y_2O_3, shows that doping with yttrium nanopowder makes the voids more extensive while decreasing their number, an observation in agreement with the SEM results (Figure 2).

4. CONCLUSIONS

The performance of CC based on zirconia doped with yttria can be increased by densifying the ceramic coating with yttria nanopowders. The multilayered

ceramic nanocomposite (realized as TBC) obtained by doping in two phases with yttria and structured in a gradient presents special characteristics compared to the ceramic coating realized as a thermal barrier through traditional YSZ. The reduction of the number of voids in the CC layer was highlighted as well as a good adhesion to the support, without thermally grown oxide (TGO) intermediate, of the CC layer with a micrometric thickness. The optimization of the TBC deposition methods and the evaluation of the CC performances, involves the analysis of the adhesion to the support and the increase of the life span. Additional tests are needed on a larger number of samples having CC with variable thicknesses and subjected to different thermal treatments to establish the accuracy of the results. It is necessary to establish a correlation between the decreasing number of voids and the concentration of yttria nanoparticles.

Acknowledgements

This work was supported by MCID Nucleu (PN 23 11 01 02) and PFE (Contract No. 5PFE/2022) Programs.

References

[1] Wei Z.Y., et al. (2022). Progress in ceramic materials and structure design towards advanced thermal barrier coatings. Journal of Advanced Ceramics, 11(7), 985-1068

[2] Mehta, A., et al. (2022). Processing and advances in the development of thermal barrier coatings: a review. Coatings, 12(9), 1318.

[3] Thakare, JG, Pandey, C., Mahapatra, MM, & Mulik, RS (2021). Thermal barrier coatings—A state of the art review. Metals and Materials International, 27, 1947-1968.

[4] Pakseresht, A., et al. (2022). Failure mechanisms and structure tailoring of YSZ and new candidates for thermal barrier coatings: A systematic review. Materials & Design, 222, 111044.

[5] Meghwal, A., Anupam, A., Murty, BS, Berndt, CC, Kottada, RS, & Ang, ASM (2020). Thermal spray high-entropy alloy coatings: a review. Journal of Thermal Spray Technology, 29, 857-893.

[6] Sudarshan, R., Venkatesh, S., & Balasubramanian, K. (2020). Thermal Barrier Coatings for Gas-Turbine Engine Applications-A Review. PalArch's Journal of Archeology of Egypt/Egyptology, 17(6), 15487-15500.

[7] Vaßen, R., Mack, DE, Tandler, M., Sohn, YJ, Sebold, D., & Guillon, O. (2021). Unique performance of thermal barrier coatings made of yttria-stabilized zirconia at extreme temperatures (> 1500°C). Journal of the American Ceramic Society, 104(1), 463-471.

[8] Savin, A., et al (2018). Complementary Methods for Evaluation of Yttria Stabilized Zirconia Coatings used as Thermal Barrier Coating. Journal of Mechanical Engineering/Strojniški Vestnik, 64(11).

[9] Dudnik, EV, Lakiza, SN, Hrechanyuk, IN, Ruban, AK, Redko, VP, Marek, IO, ... & Hrechanyuk, NI (2020).Thermal barrier coatings based on ZrO 2 solid solutions. Powder Metallurgy and Metal Ceramics, 59, 179-200.

[10] Faktorova, D., Novy, F., Fintova, S., Savin, A., Steigmann, R., Iftimie, N., Turchenko, V. and Craus, M.L., 2016. Evaluation of zirconia coatings deposited on stainless steel substrate. In Electromagnetic Nondestructive Evaluation (XIX) (pp. 254-262). IOS Press.

[11] Wang, Y., Bai, Y., Liu, GH, Sun, J., Zheng, QS, Yu, FL, ... & Wang, HD (2024). Wide-velocity range high-energy plasma sprayed yttria-stabilized zirconia thermal barrier coating—Part II: Structural defects and thermal-bonding properties. Surface and Coatings Technology, 476, 130203.

[12] Qadir, D., Sharif, R., Nasir, R., Awad, A., & Mannan, HA (2024). A review on coatings through thermal spraying. Chemical Papers, 78(1), 71-91.

[13] Asakura, T. and Akamatsu, I., 1972. Fresnel diffraction by a circular aperture illuminated with partially coherent light. I. Optica Acta: International Journal of Optics, 19(9), pp.749-763.

COMAT The 10th International Conference on ADVANCED COMPOSITE MATERIALS ENGINEERING

Transilvania University of Brasov
FACULTY OF MECHANICAL ENGINEERING

22-23 October 2024

ANALYSIS OF A 3D PRINTED EYEGLASSES FRAME - EXPERIMENTAL STUDY

Stanciu Anca*1, Bencze Andrei 2

1. University Transilvania of Brașov, Brașov, Romania, anca.stanciu@unitbv.ro
2. University Transilvania of Brașov, Brașov, Romania, andrei.bencze@unitbv.ro
*Corresponding author: anca.stanciu@unitbv.ro

Abstract: *In this paper is presented a comparative study for an eyeglass frame realized from 3D printed materials (PLA and PETG), as well as from existing eyeglasses frames on the market made of plastic materials, which are the most widespread. For these frames, designed and printed from new materials, made with the help of the Prusa type 3D printer, an optimal weight to strength ratio could be obtained by using a corresponding printed material density. Both the frames that are on the market and the printed ones were subjected to mechanical bending tests, thus having a comparative analysis of the mechanical properties. PLA's benefit as a bio-plastic is its versatility and the fact that it naturally degrades when exposed to the environment. PETG is a material with a unique mixture of qualities, it is readily available and relatively cheap, with a high allowable stress, being easily recycled, transformed into the original resin, and also it is very glossy.*

Keywords: *bending test; eyeglasses frame, 3D printing material, stress, PLA and PETG*

1. INTRODUCTION

Plastic materials are macromolecular synthetic products, used in industry due to the high plasticity and favorable properties of the processed parts, having as advantages: low volumetric mass, good electrical and thermal insulation properties, high resistance to the action of chemical agents, increased capability of processing through multiple technological processes, low price. At the same time, their use is limited, with certain disadvantages: relatively low mechanical properties, non-degradable, which creates serious pollution problems, the properties are not preserved at high temperatures, relatively high expansion coefficients, by burning they release toxic products.

Plastic is also used in the manufacture of eyeglass frames. Eyeglass frames made of plastic are available in a wide variety of designs, shapes and colors. Several types of plastic are available. A big advantage of plastic frames is that they are lightweight and can be found in different shapes and colors.

Poly-lactic acid or PLA is a biodegradable and bioactive thermoplastic derived from renewable sources such as corn starch or sugar cane. It is formed by the polymerization of lactic acid and stands out from conventional plastics due to its exceptional biodegradability and due to the fact that it can be turned into compost.

Another studied material, PETG Print filament, is tougher. It has a very high impact resistance and good flexibility. This filament does not release toxic or irritating vapors when printing. PETG Print has good adhesion between layers, which makes printing extremely easy. Due to the high quality and lack of additives, this filament can be printed in a wide temperature range.

Table 1 presents the comparison between the selected materials, based on [1].

Table1. Comparison of traditional plastic, PLA, PETG [1]

Material properties	Plastic	PLA	PETG
Biodegradability	No	Yes	No
Transparency	Low	High	High
Strength and rigidity	Good	Good	Excellent
Heat resistance	High	Moderate	High
Production source	Fossil fuels (Petrol)	Renewable Sources (Plants)	Fossil fuels (Petrol)
Environmental Impact	Increased carbon footprint	Reduced carbon footprint	Increased carbon footprint

2. EXPERIMENTAL BENDING ANALYSIS OF SELECTED MATERIALS

In the framework of the tests presented in this paper, the mechanical properties [2] for the glasses frames were obtained. Existing plastic frames on the market and frames made with 3D printing, using PLA and PET-G materials, were tested. All the frames were submitted to the bending test.

Figure 1 presents samples of glasses frames subjected to bending test.

Figure 1: Glasses frames and arms subjected to bending test

In the case of bending, the results were obtained automatically in the program used by the bending test machine. This software allowed the statistical calculation of average values for: longitudinal modulus of elasticity E, bending stiffness, admissible stress at maximum load, specific deformation of the specimen, deformation (from the initial value to the maximum value), mechanical work performed (of to the initial value to the maximum), the load at breaking, the stress at breaking, the deformation at breaking, the stress at maximum deformation.

Additionally, a theoretical study (with the Finite Element Models - FEM) was carried out for the 2 printed materials, so that a result can be obtained much faster regarding the changes that appear in the material.

The results for the finite elements analysis and for the tests are presented in Table 2 and Table 3.

Table2. Finite elements model analysis results

Material	PETG	PLA
Maximum deformation [mm] at 10 N applied force	2.19	1.41
Maximum deformation [mm] extrapolated to test maximal load	2.10x67/10= 14.67	1.41x70/10=9.87
Maximum stress [MPa]	5.86	5.87

Table3. Test analysis results

Material	PETG	PLA
Maximum deformation [mm] (linear elastic zone)	15	10
Maximum load [N] (linear elastic zone)	67	70

2.1. FE Model - Geometry

The finite elements model (FEM) pre-processing and post-processing are realized in MSC Patran 2019, while the static linear analysis (SOL 101) is carried out in MSC Nastran 2019.

The mesh is done on the median surface of the geometry presented in Figure 2. The median surface is meshed with 2D Shell elements (with hybrid quad4 and tria3 topology) and has a general global element edge length of 1 mm. Plate thickness, defined in the FE properties is 5 mm. Since the material properties are not varying with the thickness, the shell approach is applicable.

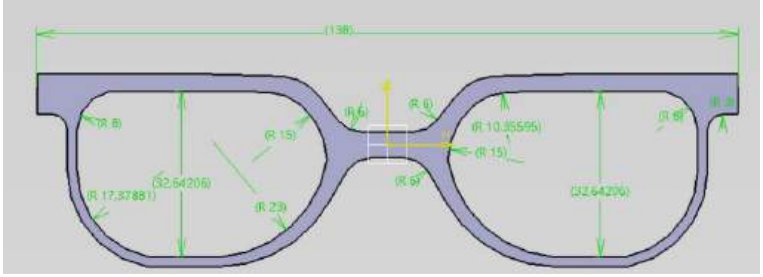

Figure 2: Model geometry

The selected materials are defined as isotropic materials based on the technical sheets provided by the manufacturers:

Prusament PLA / Prusa Polymers, named hereafter PLA
- Longitudinal elasticity Modulus 2200 MPa
- Tensile Yield Allowable Strength = 50.8 MPa

Prusament PETG / Prusa Polymers, named hereafter PETG
- Longitudinal elasticity Modulus 1500 MPa
- Tensile Yield Allowable Strength = 47.0 MPa

For an improved modelling, the PLA material is defined additionally also as a composite material (laminate material), with a stacking layup of 10 plies of 0.5mm each, with different orientations as presented in the Table 4. The plies at 0 degrees are aligned with the longitudinal direction.

Table4. Layup of the PLA composite material model

Material	Ply orientation in stacking [deg.]
Layup 1	0 / 45 / 0 / -45 / 90 / 90 / 45 / 0 / -45 / 0

2.2. FE Model - Loads

Two load cases are defined, based on a selection of possible realistic scenarios, considering ear and nose side loading and clamping.

In both selected scenarios, a load of 10 N (equivalent of a force exerted by a 1 kilogram weight) is applied in a specific location as presented in Table 5. Function of the load application point, the model is constricted (movement is restricted for all 6 degrees of freedom) at critical locations, as presented in Figure 3, leading to a conservative analysis.

Table4. Layup of the PLA composite material model

Load Case	Fixations – Blocked DOFs	Fixations – Area (Zone)	Load Value	Load Direction	Load Area (Zone)
1	All 6	nodes in A	9x1.11=10N	negative Z	nodes in B
2	All 6	nodes in C	6*1.66=10N	negative Z	nodes in D

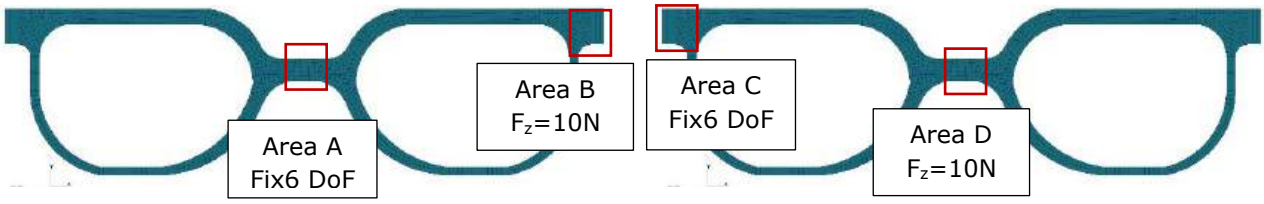

Figure 3: FE Model - Load cases definition

2.3. FE Model - Results

At post-processing stage, the von Mises stresses are extracted for each material and each load case listed above, and the results are summarized in Table 5. The Figures 4, 5 and 6 present typical deformations and stresses for the 2 selected load cases.

Table5. FE Model results

Load Case	Material	Material Definition	Thickness [mm]	Maximum Displacement [mm]	Von Mises Stress Z1/Z2 [MPa]	Allowable Stress [MPa]
1	PETG	Isotrop	5.0	8.03	37.62	47.0
1	PLA	Isotrop	5.0	5.49	37.75	50.8
1	PLA	2D Composite	0.5x10	5.49	30.13	50.8
2	PETG	Isotrop	5.0	18.54	35.97	47.0
2	PLA	Isotrop	5.0	12.65	36.00	50.8
2	PLA	2D Composite	0.5x10	12.65	30.69	50.8

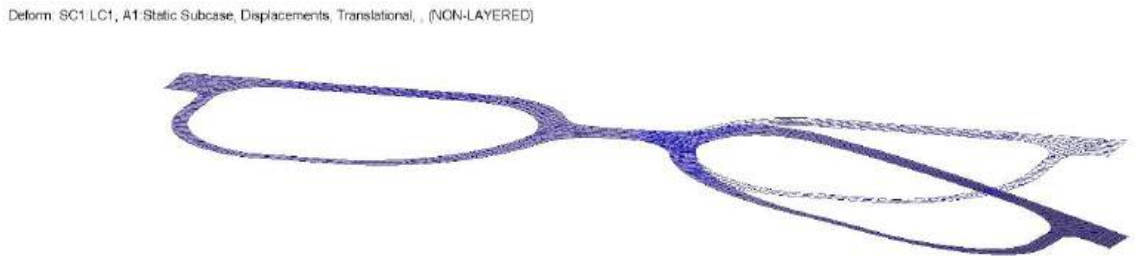

Figure 4: Deformation – Load Case 1 (side and isometric view), PLA material, 2D isotropic

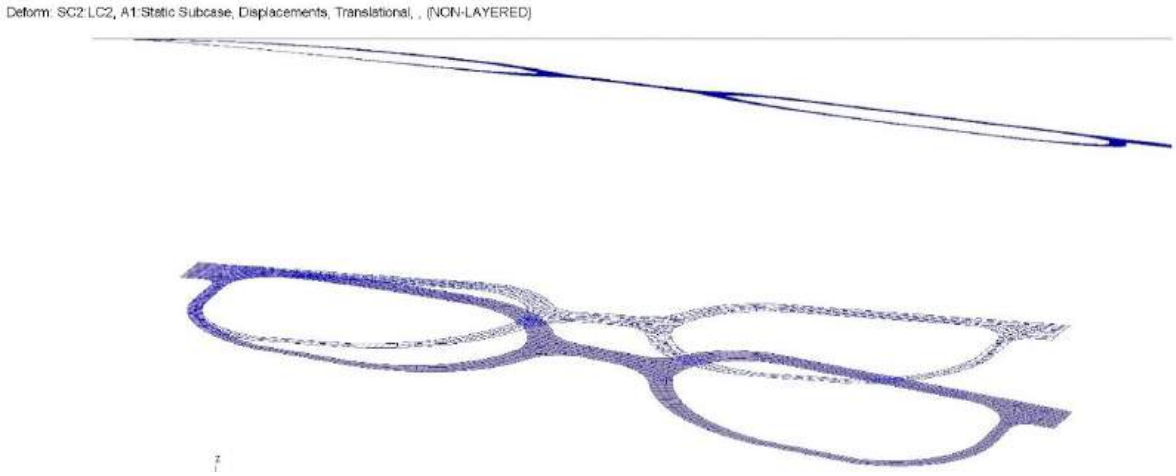

Figure 5: Deformation – Load case 2(side and isometric view), PLA material, 2D isotropic

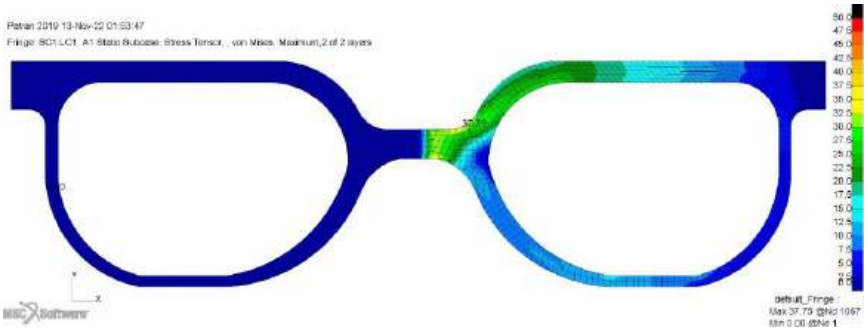

Figure 6: Von Mises Stress – Load Case 1, PLA material, 2D isotropic

3. CONCLUSIONS

The eyeglass frames, both made of plastic materials and printed with the help of the 3D printer, were subjected to the bending test, thus obtaining their mechanical properties (Yield tension allowable Fty, Longitudinal Elasticity Modulus E, Strain and Stress).

Finite element method (FEM) analysis is a complex process, which involves going through some well-defined stages. Another important aspect is to have the technical sheet of the material, so that depending on its structure, the product can be analyzed, thus replacing the experimental analysis, reducing the time required, as well as the consumption of materials.

Also, care must be taken not to exceed the admissible yield stress, because above this value, the material enters the yield zone and residual deformations occur, possibly causing cracks between the layers.

Both quantitatively and qualitatively, the solutions offered by the finite element method are close to the real behavior of the piece, but depend to a great extent on the modeling and solving capabilities offered by the used software.

BIBLIOGRAPHY

[1] PMS,https://plasticmoldingsolutions.com/ro/polylactic-acid-pla/#elementor-toc__heading-anchor-1

[2] Callister W., Fundamentals of Materials Science and Engineering, John Wiley & Sons, New York, 2001

COMAT The 10th International Conference on ADVANCED COMPOSITE MATERIALS ENGINEERING

Transilvania University of Brasov
FACULTY OF MECHANICAL ENGINEERING

22-23 October 2024

Study Regarding the Influence of the Build Plate Temperature and the Filament Color on the Tensile Strength of FDM Printed PLA Specimens

Raul-Rusalin Turiac[1], Ionuț-Sebastian Gheorghe[2], Deian Ardeljan[3], Nicoleta Băcescu[*4]

1. Babeș-Bolyai University, Reșița, Romania, raul.turiac@ubbcluj.ro
2. Babeș-Bolyai University, Reșița, Romania, ionut.gheorghe@stud.ubbcluj.ro
3. Babeș-Bolyai University, Reșița, Romania, deian.ardeljan@stud.ubbcluj.ro
4. Babeș-Bolyai University, Reșița, Romania, nicoleta.bacescu@ubbcluj.ro

[*]Corresponding author: nicoleta.bacescu@ubbcluj.ro

Abstract: *This study investigates the effect of the build plate temperature on the tensile strength of PLA products manufactured by FDM 3D printing. Tensile tests were conducted on specimens printed at 40°C, 60°C, 80°C, and 100°C using different colored PLA filaments (natural, black, red, and gray) aiming to analyze the combined influence of temperature and pigment. Results show that higher bed temperatures enhance interlayer adhesion, improving mechanical strength, but also increase the risk of deformation. The research provides recommendations for optimizing the printing parameters, contributing to the development of more sustainable and efficient 3D printing techniques for PLA.*

Keywords: *FDM (fused deposition modeling), build plate temperature, PLA (polylactic acid), filament color, tensile strength.*

1. INTRODUCTION

Additive manufacturing is increasingly being used for the production of functional components, allowing for a rapid transition from the 3D model to the physical part. Compared to other manufacturing technologies, 3D printing, which relies on layer-by-layer construction of objects, enables geometric optimization both externally and internally [1]. This provides flexibility in adjusting the material distribution according to the specific demands of the part.

The FDM (Fused Deposition Modeling) technology is one of the most accessible and popular 3D printing methods, due to its low cost and ease of use. This technology is widely used for producing prototypes and final components in various industries, including automotive, aerospace, electronics, and medical fields [2-4]. In this context, understanding how the process parameters used

in printing influence the mechanical properties of the final parts becomes essential.

Among the process parameters that directly influence the properties of printed parts is the print bed temperature. An appropriate bed temperature can improve the adhesion of the first layer to the surface, preventing warping or detachment of the part during the printing process. Additionally, the cooling speed of the filament is essential for forming the crystalline structure of the material. Cooling too quickly can lead to a disordered crystalline structure, thus weakening the strength of the final part. Moreover, temperature variations can generate internal stresses, affecting the mechanical integrity of the part [5-14].

The color of the filament used also has a direct influence on the properties of printed parts. Previous research [15,16] has revealed that the filament color affects the tensile strength of samples made from PLA (polylactic acid), making it an important parameter when aiming for high strength in printed parts.

The present work aims to investigate the influence of the print bed temperature and filament color on the tensile strength of samples made from PLA using FDM technology.

2. METHODS AND MATERIALS

For the tensile tests, we used "dogbone" type specimens in accordance with the ISO 5271:2019 standard, which we created in SolidWorks software and then imported into the Ultimaker Cura program. There, we established the process parameters and generated the numeric code for printing them. Figure 1 shows the dimensions of the specimen used for testing.

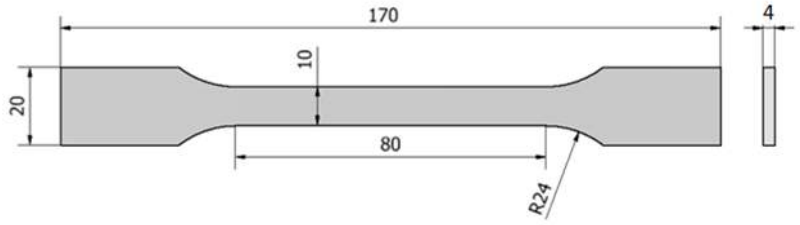

Figure 1: Testing specimen according to ISO 527-1:2019

For printing the specimens, we used an FLSUN V400 model printer, as shown in Figure 2a. The printing was conducted in a controlled environment (enclosed printing), using four filaments of different colors (natural, black, red, and aluminum grey) produced by Verbatim.

To highlight the influence of the print bed temperature and filament color on the tensile strength of samples made from PLA using FDM technology, we printed a batch of 80 specimens (20 specimens for each color). The process parameters are presented in Table 1. The process parameters were kept constants for all fabricated specimens, except for the print bed temperature, where we selected four critical temperatures for the study (40, 60, 80, and 100 °C), based on experience and the consulted literature.

Table 1. Process parameters used

Material	PLA Natural/transparent, black, red, gray
Filament diameter	1,75 mm
Nozzle diameter	0,4 mm
Printing head temperature	210 °C
Build plate temperature	40, 60, 80, 100 °C
Layer thickness	0,20 mm
Printing speed	50 mm/s
Orientation according to ISO/ASTM 52921:2013	YX
Raster angle, θ	45°/-45°
Infill density	100 %
Number of contour lines	2

To establish the influence of the print bed temperature and filament color on tensile strength, we subjected the entire batch of specimens to tensile testing using a Mecmesin MultiTest 2.5-dV machine (Figure 2b), with a testing speed of 10 mm/min.

a. FLSUN V400 model printer

b. Mecmesin MultiTest 2.5-dV

Figure 2: Equipment used

3. EXPERIMENTAL RESULTS

The experimental results obtained for the PLA specimens printed at different print bed temperatures reveal the following:

1) In the case of the transparent specimens, as the print bed temperature (Tp) increased, the tensile strength also increased, reaching a maximum UTS value at a temperature of 100°C (49,85 MPa). This value is 4,8% higher than that measured for Tp=40°C (47,57 MPa);

2) For the black samples, as the printing plate temperature increased, the tensile strength also increased, reaching a maximum UTS value at a temperature of 100°C (53.35 MPa), which is 2.3% higher than that measured for Tp=40°C (52.15 MPa);

3) Regarding the red specimens, as the print bed temperature increased, the tensile strength varied between 50,03 MPa (at Tp=60°C) and 53,19 MPa (at Tp=80°C). A maximum UTS value was recorded at a temperature of 80°C (53,19 MPa), which is 3,4% higher than that measured for Tp=40°C (51,42 MPa);

4) In the case of the gray specimens, as the print bed temperature increased, the tensile strength varied between 47,76 MPa (at Tp=40°C) and 49,41 MPa (at Tp=100°C), reaching a maximum UTS value at a temperature of 100°C (49,41 MPa). This value is 3,4% higher than that measured for Tp=40°C (47,76 MPa).

To highlight the influence of the filament colorant on the mechanical properties of the tensile specimens printed while varying a single printing parameter, the tensile strength values were represented on the same graph as a function of the set print bed temperature for the four colors of PLA filament (Figure 3).

The main findings resulted from analyzing Figure 3 and the experimental results are as follows:

- The color significantly influences the properties of PLA, as different UTS values are obtained for the same print bed temperature depending on the material color. The maximum differences were found to be 7,79% at a print bed temperature of 60°C (UTS PLA black/UTS PLA natural) and 10,67% at 80°C (UTS PLA red/UTS PLA gray).
- For print bed temperatures of 40-60°C, a higher UTS value was recorded for the black PLA specimens, while the lowest UTS value belonged to the transparent specimens.
- At a print bed temperature of 80°C, the best tensile strength was achieved by the red specimens (53,19 MPa), while at 100°C, the black specimens had the highest tensile strength (53,35 MPa). In contrast, the gray specimens recorded the lowest strengths within this temperature range (48,09 MPa at 80°C and 49,41 MPa at 100°C).

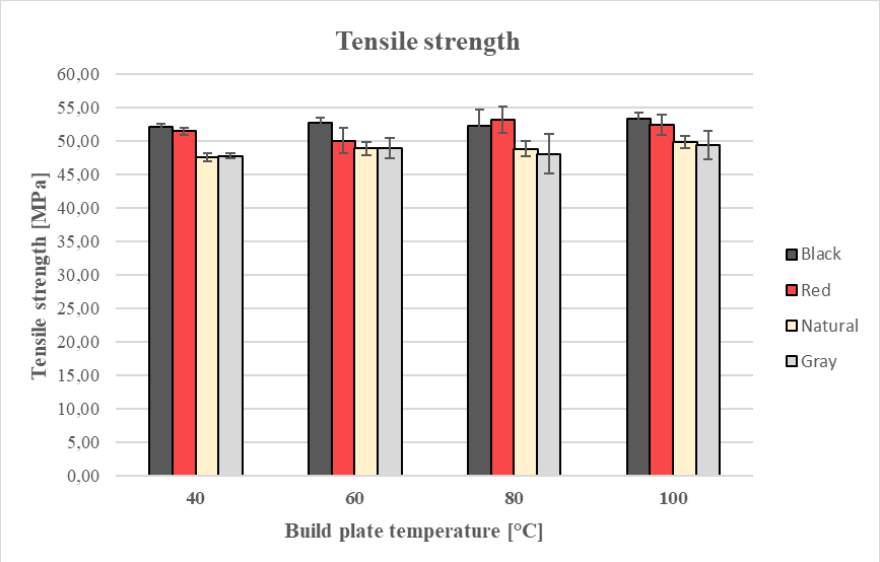

Figure 3: Variation of tensile strength as a function of print bed temperature

4. CONCLUSIONS

Summarizing the results obtained, the following conclusions can be drawn:

1) The temperature of the print bed significantly influences the tensile strength of FDM-printed products made from PLA. Generally, as the temperature increases, the mechanical strength also increases, but the increases relative to the reference temperature (40°C) are relatively small. In this study, these increases ranged from 2,3% (black PLA) to 4,8% (colorless PLA).

2) The color of the PLA filament has a significant influence on mechanical strength. For the same print bed temperature but different filament colors, differences in UTS values were obtained, ranging from 7,79% to 10,67%.

3) The choice of the optimal print bed temperature should be made in relation to the type of filament used. For the colors utilized in this study, the recommended temperatures to achieve maximum UTS values are:

   - Colorless PLA - 100°C;
   - Gray PLA - 100°C;
   - Red PLA - 80°C;
   - Black PLA - 100°C.

However, it should be noted that the experiments focused exclusively on tensile strength, without considering the correlation between print bed temperature and other properties of the printed products (such as, for example, dimensional accuracy).

BIBLIOGRAPHY

[1] Cojocaru V., Frunzaverde D., Miclosina C.O., Marginean G., The Influence of the Process Parameters on the Mechanical Properties of PLA Specimens Produced by Fused Filament Fabrication—A Review, Polymers, 2022

[2] Verma N., Awasthi P., Gupta A., Banerjee S., Fused Deposition Modeling of Polyolefins: Challenges and Opportunities, Macromol. Mater. Eng., 2022

[3] Bloju A.V., Korka Z.I., Bara A., Traistaru D.E., Sfetcu C.R., Precision assessment in additive manufacturing of plastic gears, The 9th International Conference on Advanced Composite Materials Engineering (COMAT), 2022

[4] Korka Z.I., Bloju A.V., Sfetcu C.R., Traistaru D.E., Bara A., Precision appraisal of PLA gears made by additive manufacturing, Annals of the „Constantin Brancusi" University of Targu Jiu, Engineering Series, no. 4, pp. 14-19, 2022

[5] Popescu D., Zapciua A., Amzab C., Baciuc F., Marinescu R., FDM process parameters infuence over the mechanical properties of polymer specimens: A review, Polymer Testing 69, 2018

[6] Hsueh M.H., Lai C.J., Wang S.H., Zeng Y.S., Hsieh C.H., Pan C.Y., Huang W.C., Effect of Printing Parameters on the Thermal and Mechanical Properties of 3D-Printed PLA and PETG Using Fused Deposition Modeling, Polymers, 2021

[7] Attolico M.A., Casavola C., Cazzato A., Moramarco V., Renna G., Effect of extrusion temperature on fused filament fabrication parts orthotropic behaviour, Rapid Prototyping Journal, 2020

[8] Harris M., Potgieter J., Archer R., Arif K.M., In-process thermal treatment of polylactic acid in fused deposition modelling, Mater. Manuf. Process., 2019

[9] Benwood C., Anstey A., Andrzejewski J., Misra M., Mohanty A.K., Improving the Impact Strength and Heat Resistance of 3D Printed Models: Structure, Property, and Processing Correlationships during Fused Deposition Modeling (FDM) of Poly (Lactic Acid), ACS Omega, 2018

[10] Vanaei H.R., Shirinbayan M., Vanaei S., Fitoussi J., Khelladi S., Tcharkhtchi A., Multi-scale damage analysis and fatigue behavior of PLA manufactured by fused deposition modeling (FDM), Rapid Prototyp. J., 2021

[11] Liparoti S., Sofia D., Romano A., Marra F., Pantani R., Fused Filament Deposition of PLA: The Role of Interlayer Adhesion in the Mechanical Performances, Polymers,2021

[12] Wach R.A., Wolszczak P., Adamus-Wlodarczyk A., Enhancement of Mechanical Properties of FDM-PLA Parts via Thermal Annealing, Macromol. Mater. Eng., 2018

[13] Wang S.H., Ma Y.B., Deng Z.C., Zhang S., Cai J.X., Effects of fused deposition modeling process parameters on tensile, dynamic mechanical properties of 3D printed polylactic acid materials. Polym. Test, 2020

[14] https://www.selfcad.com/blog/pla-bed-temperature - accessed on 21.09.2024

[15] Cojocaru V., Turiac R.R., Frunzaverde D., Trisca G., Bacescu N., Marginean G., Effect of the Printing Scenario on the Dimensional Accuracy and the Tensile Strength of Different Colored PLA Specimens Produced by Fused Deposition Modeling, Applied Sciences.,2024

[16] Frunzaverde D., Cojocaru V., Bacescu N., Ciubotariu C-R., Miclosina C-O., Turiac R.R., Marginean G., The Influence of the Layer Height and the Filament Color on the Dimensional Accuracy and the Tensile Strength of FDM-Printed PLA Specimens, Polymers, 2023

COMAT The 10th International Conference on ADVANCED COMPOSITE MATERIALS ENGINEERING

Transilvania University of Brasov
FACULTY OF MECHANICAL ENGINEERING

22-23 October 2024

The evolution of the eigenvalues for a rectangular plate with different aspect ratios

Zeno-Iosif Praisach[1], Nicoleta Băcescu*[2], Ionela Harea[3], Cristian TufișI[4]

1. Babeș-Bolyai University, Cluj-Napoca, Faculty of Engineering Reșița Romania, zeno.praisach@ubbcluj.ro
2. Babeș-Bolyai University, Cluj-Napoca, Faculty of Engineering Reșița Romania, nicoleta.bacescu@stud.ubbcluj.ro
   *Corresponding author: nicoleta.bacescu@stud.ubbcluj.ro
3. Babeș-Bolyai University, Cluj-Napoca, Faculty of Engineering Reșița Romania, ionela.moatar@ubbcluj.ro
4. Babeș-Bolyai University, Cluj-Napoca, Faculty of Engineering Reșița Romania, cristian.tufisi@ubbcluj.ro

Abstract: *The paper presents the analytical results obtained for the eigenvalues of a thin rectangular plate simply supported on two opposite sides and clamped on the other two for different ratios of the sides of the plate a/b, from 1/3 to 3. The obtained eigenvalues are necessary for the calculation of the natural frequencies of the plate and for the representation of the modal shapes. Considering the sides are simply supported at x=0 and x=a, the results indicate a strong change in the eigenvalues for ratios a/b<1, respectively a slight change for a/b>1, changes that influence the natural frequencies and the modal shapes of the plate.*

Keywords: *rectangular plate, eigenvalues, dynamic behavior*

1. INTRODUCTION

Plates are of particular importance in mechanical engineering, as many structures are made up of plates of various shapes and sizes [1]. A plate is a solid body that has one of its dimensions (thickness, noted with h) smaller than the other two (length and width, noted with a and b) and can be thought of as the materialization of a surface, just as a bar is the materialization of a line [2]. According to the literature, for a plate to be considered thin, the condition must be met: min(a, or b)/h>5. If this ratio is smaller than 5, then the plate is thick [3].

The paper presents the evolution of the eigenvalues for a thin rectangular plate simply supported on two opposite sides and clamped on the other two, for different values of the a/b ratio.

2. ANALYTICAL MODEL

Let's consider a thin rectangular plate (fig. 1), simply supported (SS) along the y direction at: x=0 and x=a. The thickness of the plate is denoted by h, and the other two dimensions are denoted by a and b, along the x and y directions. The plate is fixed (C) along the x direction at: y=0 and y=b.

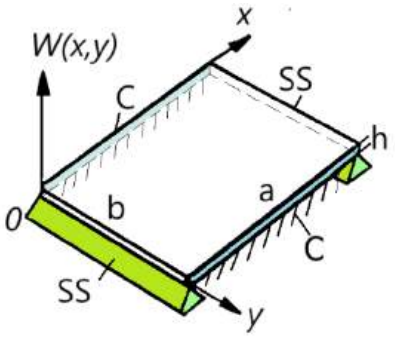

Figure 1: Rectangular plate simply supported (SS) along two opposing edges and clamped (C) on the other two.

In the case of flat plates, the equation of motion [1] is:

$$D\left(\frac{\partial^4 W(x,y)}{\partial x^4}+2\frac{\partial^4 W(x,y)}{\partial x^2\partial y^2}+\frac{\partial^4 W(x,y)}{\partial y^4}\right)-\rho h\omega^2 W(x,y)=0 \quad (1)$$

where,

W(x,y)=X(x)·Y(y) is the motion function along the x and y directions;

$D=\frac{Eh^3}{12(1-\nu^2)}$ [Nm] is the stiffness of the plate;

ν is Poisson's ratio;

E [N/m^2] is the longitudinal modulus of elasticity;

ρ [kg/m^3] is the density of the plate material;

ω [rad/s] is the pulsation;

X(x) and Y(y) are chosen as the fundamental modal shapes of the beams having the plate boundary conditions.

The boundary conditions for simply supported edges are:

$$W(0,y)=W(a,y)=\frac{\partial^2 W(0,y)}{\partial x^2}=\frac{\partial^2 W(a,y)}{\partial x^2}=0 \quad (2)$$

Solving the system of equations (2), it obtains the solution from the simply supported beam (3), respectively (4) for the plate [4]:

$$X(x)=sin\left(\frac{m\pi}{a}x\right) \quad (3)$$

$$W(x,y) = Y(y)\,sin\left(\frac{m\pi}{a}x\right) \tag{4}$$

Substituting (4) into relation (1), it can be written in the form:

$$\frac{d^4Y(y)}{dy^4} - 2\left(\frac{m\pi}{a}\right)^2\frac{d^2Y(y)}{dy^2} + \left[\left(\frac{m\pi}{a}\right)^4 - \frac{\rho h}{D}\omega^2\right]Y(y) = 0 \tag{5}$$

We make the substitution:

$$Y(y) = \sum_{i=1}^{4} C_i e^{\lambda_i \frac{y}{b}} \tag{6}$$

and inserted into (5), the following relation is obtained:

$$\left(\frac{\lambda_i}{b}\right)^2 = \left(\frac{m\pi}{a}\right)^2 \pm \sqrt{\frac{\rho h}{D}\omega^2} = \left(\frac{m\pi}{a}\right)^2\left[1 \pm \left(\frac{a}{m\pi}\right)^2\sqrt{\frac{\rho h}{D}\omega^2}\right] = \left(\frac{m\pi}{a}\right)^2[1 \pm K] \tag{7}$$

where,

$$K = \frac{\omega}{\left(\frac{m\pi}{a}\right)^2\sqrt{\frac{D}{\rho h}}} \tag{8}$$

represent the eigenvalues of the modal shapes, respectively of the natural frequencies, and:

$$\lambda_1 = \frac{b}{a}m\pi\sqrt{K+1} \qquad \lambda_2 = \frac{b}{a}m\pi\sqrt{K-1} \tag{9}$$

represent the dimensionless wave numbers. Under these conditions, the function Y(y) can be written:

$$Y(y) = Acosh\left(\lambda_1\frac{y}{b}\right) + Bsinh\left(\lambda_1\frac{y}{b}\right) + Ccos\left(\lambda_2\frac{y}{b}\right) + Dsin\left(\lambda_2\frac{y}{b}\right) \tag{10}$$

The boundary conditions for clamped edges are [5]:

$$Y(0) = Y(b) = \frac{dY(0)}{dy} = \frac{dY(b)}{dy} = 0 \tag{11}$$

and by solving the system (11) we obtain the frequency equation (12) whose solutions give us the eigenvalues (8) and the dimensionless wavenumbers (9):

$$2\lambda_1\lambda_2[cos(\lambda_2)cosh(\lambda_1) - 1] + \left(\lambda_2{}^2 - \lambda_1{}^2\right)sin(\lambda_2)sinh(\lambda_1) = 0 \tag{12}$$

3. RESULTS

To obtain the eigenvalues and the dimensionless wave numbers, the following steps are performed:

- in relation (9), consider m=1, give values to K, calculate λ_1 and λ_2 so that they are solutions for the characteristic equation (12);
- the first value of K that provides a solution for the characteristic equation corresponds to the vibration mode m=1, n=1; the second value of K that gives the solution to the characteristic equation corresponds to the vibration mode m=1, n=2, and so on, up to the desired n value;

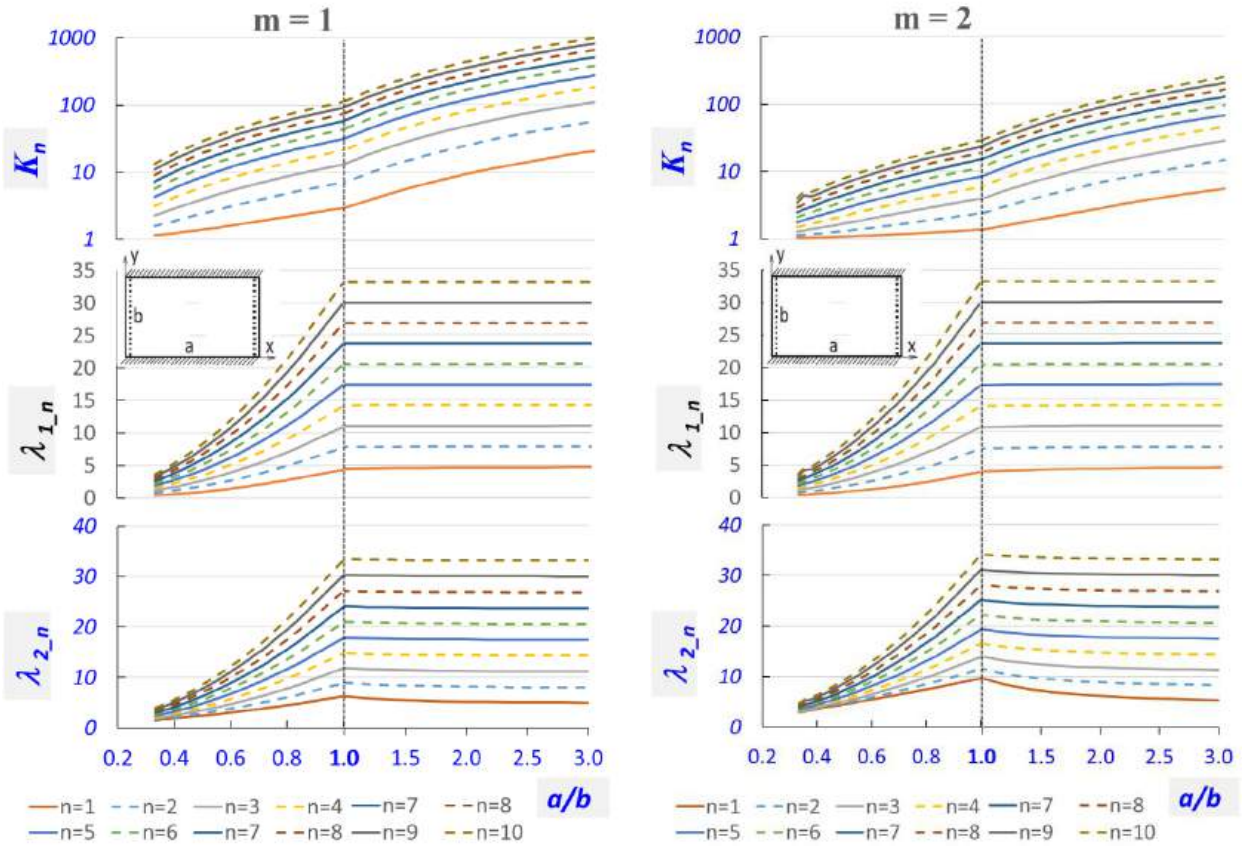

Figure 2: Eigenvalue and dimensionless wave numbers for m=1, m=2 and n=1, …, 10.

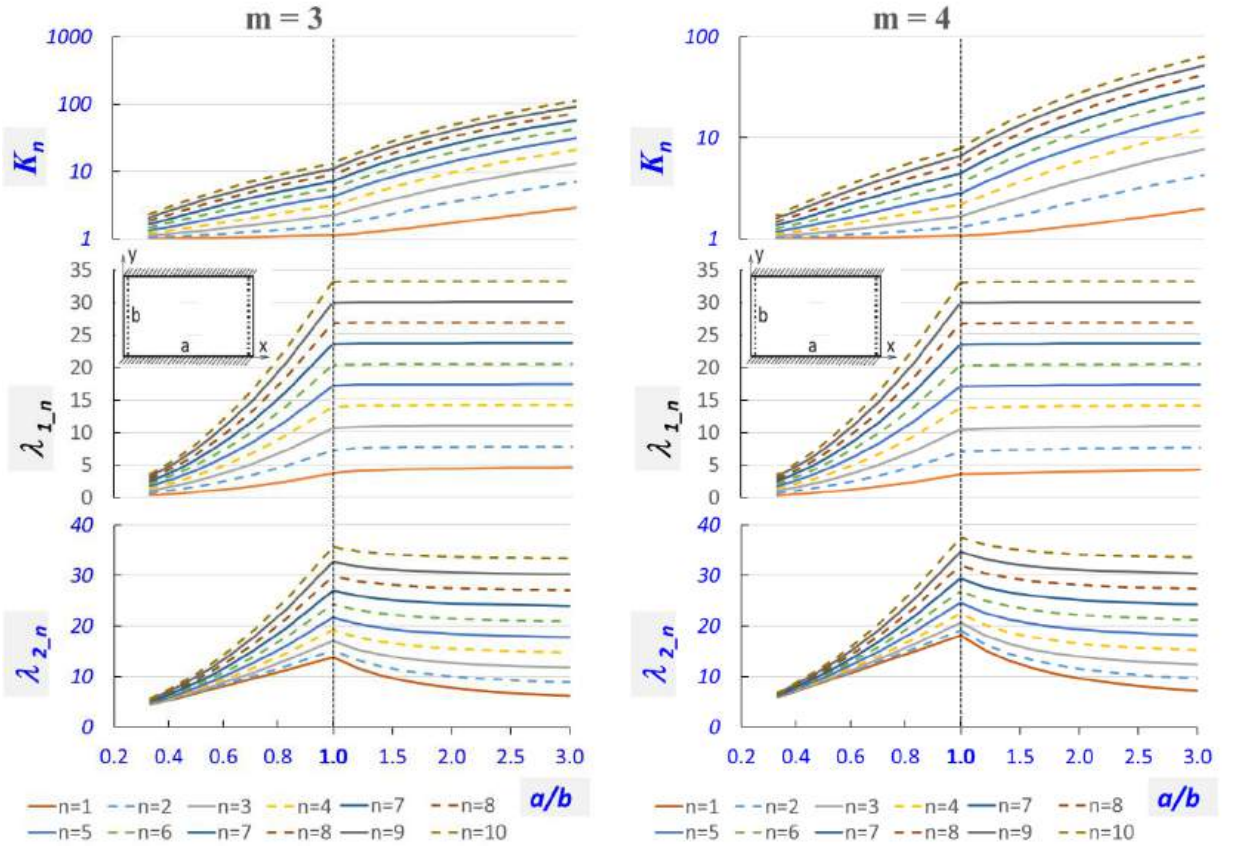

Figure 3: Eigenvalue and dimensionless wave numbers for m=3, m=4 and n=1, …, 10.

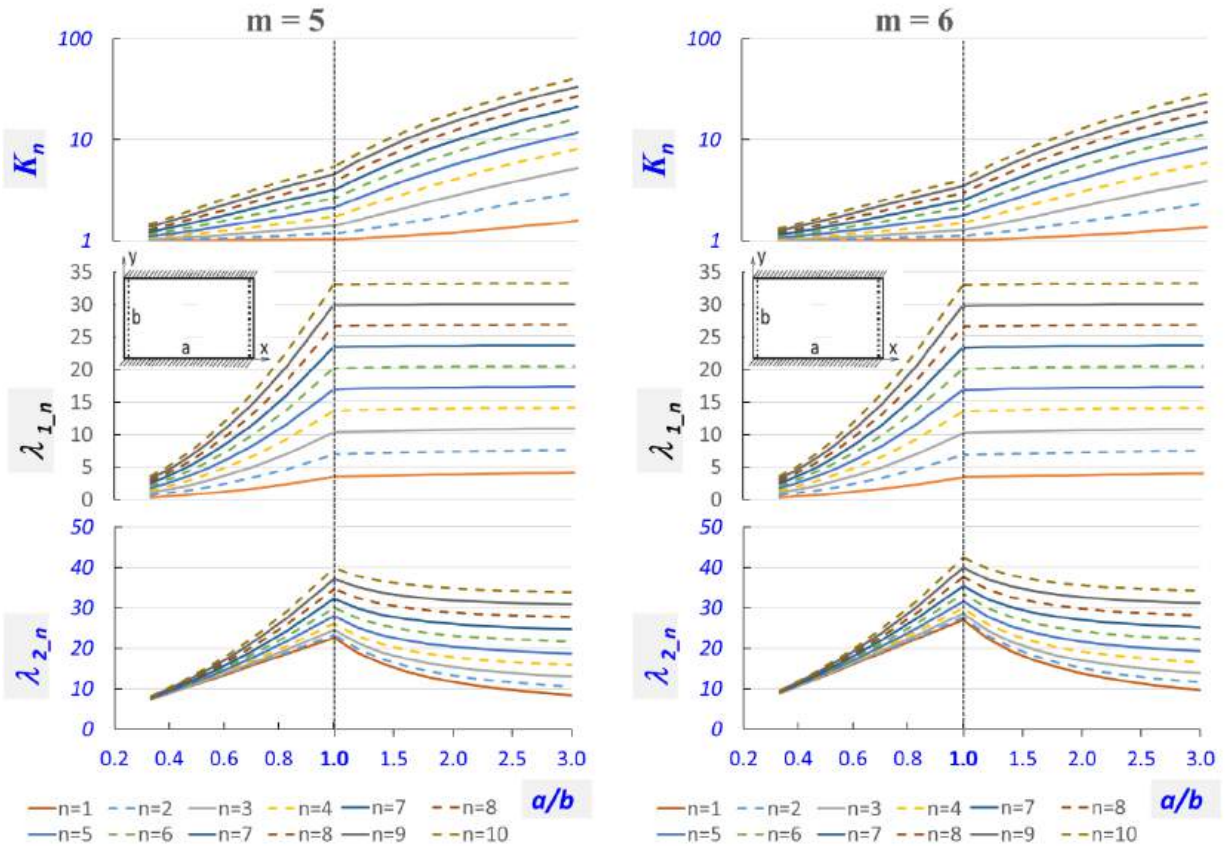

Figure 4: Eigenvalue and dimensionless wave numbers for m=5, m=6 and n=1, …, 10.

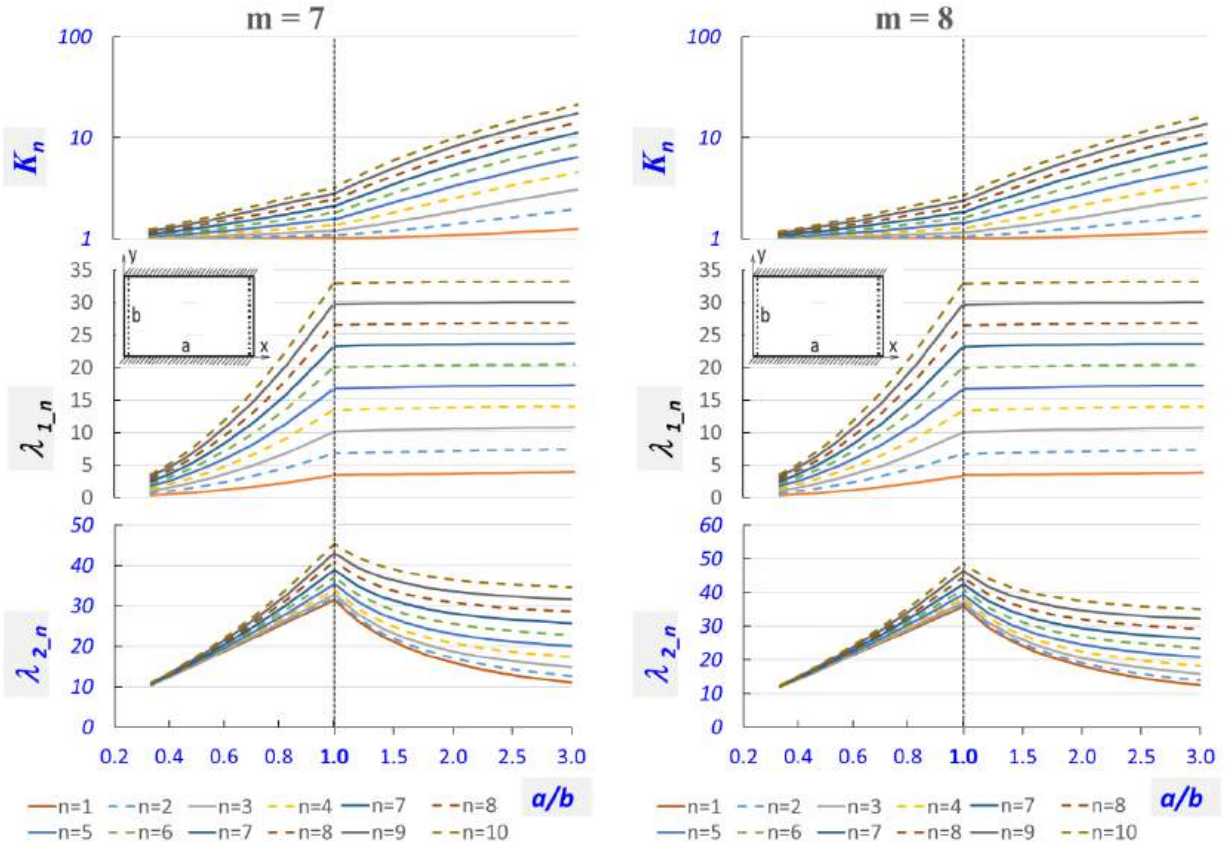

Figure 5: Eigenvalue and dimensionless wave numbers for m=7, m=8 and n=1, …, 10.

- in relation (9), consider m=2, give values to K, calculate λ_1 and λ_2 so that they are solutions for the characteristic equation (12) for vibration mode m=2, up to the desired vibration mode n;

- the process continues until the desired vibration mode m.

As can be seen from (9), the dimensionless wave numbers are a function of the aspect ratio of the rectangular plate, b/a. On this basis, the paper presents the evolution of the eigenvalues for the rectangular plate for a/b ratios from 3 to 1/3. On this basis, the paper presents the evolution of the eigenvalues for the rectangular plate for ratios a/b from 3 to 1/3, respectively for a/b=3, the edge a is clamped over a length three times greater than the simply supported side b, and for a/b=1/3, the edge a is clamped over a length three times smaller than the simply supported side b.

Figures 2 and 5 show the evolution of eigenvalues and dimensionless wavenumbers for vibration modes m=1, ..., 8 and n=1, ..., 10 for aspect ratios a/b from 1/3 to 3.

1. CONCLUSIONS

For the considered thin rectangular plate model, the following conclusions can be drawn from the analysis of the obtained results presented in the figures 2 to 5:

- eigenvalues and dimensionless wave numbers do not take into account the nature of the material from which the plate is made, nor its thickness, and only the aspect ratio, length and width;

- eigenvalues and dimensionless wave numbers values increase as the vibration modes n increase and as the vibration modes m increase, the eigenvalues $K_{n,m}$ decrease;

- regardless of the mode of vibration, for ratios a/b<1, the eigenvalues K_n show a small increase, while the dimensionless wave numbers show a pronounced increase, a phenomenon that reverses for a/b>1;

- it can be seen that the dimensionless wave numbers λ_2 have a maximum for a/b=1 (a square shaped plate), after which they start to decrease.

BIBLIOGRAFIE

[1] Soedel W., Vibration of Shells and Plates, Third Edition, Revised and Expanded, Marcel Dekker, Inc., New York, USA, 2005

[2] Leissa A.W., Vibration of Plates, National Aeronautics and Space Administration, NASA SP-160, USA, 1969

[3] Hațiegan C, Tufiși C., Identificarea și evaluarea defectelor în plăci elastic subțiri prin analiză modală, Eurostampa, Timișoara, România, ISBN 978-606-32-1172-0, 2022

[4] Gillich G.R., Negru I., Protocsil C., Stanciu E., Minda F.P., Evaluarea integrității structurilor mecanice, Ed. Eftimie Murgu, Reșița, ISBN 978-606-631-081-9, 2018

[5] Praisach Z.I., Tufiși C., Dinamica structurilor, Vibrații transversale la grinzi simple, Modelul Euler-Bernoulli, Eurostampa, Timișoara, România, ISBN 978-606-32-1373-1, 2023

COMAT The 10th International Conference on ADVANCED COMPOSITE MATERIALS ENGINEERING

Transilvania University of Brasov
FACULTY OF MECHANICAL ENGINEERING

22-23 October 2024

Changing the normalized natural frequencies for a rectangular plate with a damage

Zeno-Iosif Praisach[1], Gigi Atinge*[2], Patric Timotei Stan[3], Cristian Tufiși[4]

1. Babeș-Bolyai University, Cluj-Napoca, Faculty of Engineering Reșița Romania, zeno.praisach@ubbcluj.ro
2. Babeș-Bolyai University, Cluj-Napoca, Faculty of Engineering Reșița Romania, gigi.atinge@stud.ubbcluj.ro
   *Corresponding author: nicoleta.bacescu@stud.ubbcluj.ro
3. Babeș-Bolyai University, Cluj-Napoca, Faculty of Engineering Reșița Romania, patric.stan@ubbcluj@ubbcluj.ro
4. Babeș-Bolyai University, Cluj-Napoca, Faculty of Engineering Reșița Romania, cristian.tufiși@ubbcluj.ro

Abstract: *The paper presents the analytical results obtained for a thin rectangular plate with a damage from the point of view of the dynamic behavior. The damage can occupy any position on the plate surface, and the change in natural frequencies is presented for the normalized values by the ratio between the natural frequency of the damaged plate and the natural frequency of the healthy plate. The paper presents two cases of analysis: the rectangular plate simply supported on all sides and the plate simply supported on two opposite sides and clamped on the other two. Changes in natural frequencies are illustrated as 3D surfaces and provide an overview of the dynamic behavior of the plate when the damage can occupy any position on the plate.*

Keywords: *rectangular plate, damage, natural frequencies, mode shape*

1. INTRODUCTION

Damage detection is a major problem that concerns many researchers, who use analytical and experimental methods [1]. Structure monitoring methods can be global or local. Global methods evaluate the conditions of the entire structure simultaneously, while local methods provide information about a relatively small region of the structure [2].

The paper presents a global analytical method for the detection of damages in thin rectangular plates by comparing the normalized strain energy with the ratio of natural frequencies for the structure with the damage and the healthy structure.

The paper presents two cases of support of an equal-sides, namely: the plate simply supported on two opposite sides and clamped on the other two (denoted as SS-C-SS-C, and the plate simply supported on all sides (denoted SS-SS-SS-SS).

2. SUPPORTED RECTANGULAR PLATE TYPE: SS-C-SS-C

Let's consider a thin rectangular plate (fig. 1), simply supported (SS) along the y direction at: x=0 and x=a.

The thickness of the plate is denoted by h, and the other two dimensions are denoted by a and b, along the x and y directions. The plate is fixed (C) along the x direction at: y=0 and y=b. The ratio a/b=1, i.e. the plate is square.

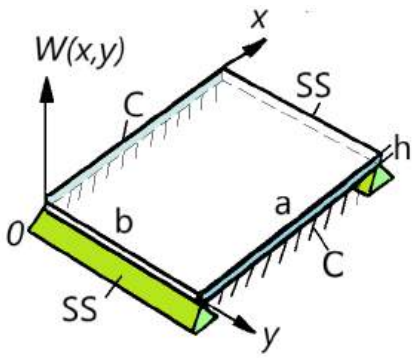

Figure 1: Rectangular plate simply supported (SS) along two opposing edges and clamped (C) on the other two.

In the case of flat plates, the normalized modal shape function is [3, 4]:

$$W_{m,n}(x,y) = \left\{ cos\left(\rho_{2_n}\frac{y}{b}\right) - cosh\left(\rho_{1_n}\frac{y}{b}\right) - \frac{cos(\rho_{2_n}) - cosh(\rho_{1_n})}{\frac{\rho_{1_n}}{\rho_{2_n}} sin(\rho_{2_n}) - sinh(\rho_{1_n})} \cdot \left[\frac{\rho_{1_n}}{\rho_{2_n}} sin\left(\rho_{2_n}\frac{y}{b}\right) - sinh\left(\rho_{1_n}\frac{y}{b}\right)\right] \right\} sin\left(\frac{m\pi x}{a}\right) \quad (1)$$

where,

ρ_1, ρ_2 are the dimensionless wave numbers;

m, n are the vibration modes numbers along the x and y directions.

Considering the relationship [5, 6] deduced from the beams that allows us to calculate the natural frequencies for the beam with a damage (f_D) as a function of the natural frequencies of the healthy beam (f_U) and the normalized strain energy:

$$f_D = f_U \left[1 - \gamma \left(\frac{\partial^2 W(x)}{\partial x^2}\right)^2\right]; \quad (2)$$

where, γ is the severity of the damage.

For the considered case, it can be deduced that the ratio of these frequencies, considering that the severity γ=1, and taking into account the strain energy of the thin plate, gives:

$$\frac{f_D}{f_U} = 1 - \gamma \left\{ \left(\frac{\partial^2 W_{m,n}(x)}{\partial x^2} + \frac{\partial^2 W_{m,n}(y)}{\partial y^2} \right)^2 - 2(1-\nu) \left[\frac{\partial^2 W_{m,n}(x)}{\partial x^2} \cdot \frac{\partial^2 W_{m,n}(y)}{\partial y^2} - \left(\frac{\partial^2 W_{m,n}(x,y)}{\partial x \partial y} \right)^2 \right] \right\}^2 \in [0, \dots, 1]; \quad (3)$$

where, ν is the Poisson coefficient.

3. SUPPORTED RECTANGULAR PLATE TYPE: SS-SS-SS-SS

Let's consider a thin rectangular plate simply supported (SS-SS-SS-SS) all around.

The normalized modal shape function [3, 4] is:

$$\frac{\partial^4 W_{m,n}(x,y)}{\partial x^2 \partial y^2} = \pi^4 \left(\frac{mn}{ab}\right)^2 \cdot sin\left(\frac{m\pi x}{a}\right) \cdot sin\left(\frac{n\pi y}{b}\right) \quad (4)$$

The ratio between natural frequencies for the rectangular plate with a damage and the natural frequencies of the healthy rectangular plate considering that the severity γ=1, is given by relationship (3).

4. RESULTS

Based on relations (1), (3) and (4), figures 2-7 show the modal shapes and natural frequency changes for the rectangular plate when a damage appears on the plate regardless of the location of the damage.

Figures 2, 3 and 4 show on the left side the modal shapes for vibration modes m=1, n=1; m=1, n=2; m=3, n=1 for the rectangular plate with the aspect ratio a/b=1, simply supported on two opposite sides and clamped on the other two (SS-C-SS-C), and on the right side of the figures, are illustrated the evolution of the normalized natural frequencies by the ratio f_D/f_U, according to the relationship (3), regardless by the location of the defect.

For the same vibration modes (m=1, n=1; m=1, n=2; m=3, n=1), for comparison, figures 5, 6 and 7, show on the left side the modal shapes for the rectangular plate with the aspect ratio a/b=1, simply supported on all sides (SS-SS-SS-SS), and on the right side of the figures, are illustrated the evolution of the normalized natural frequencies by the ratio f_D/f_U, according to the relationship (3), regardless by the location of the defect.

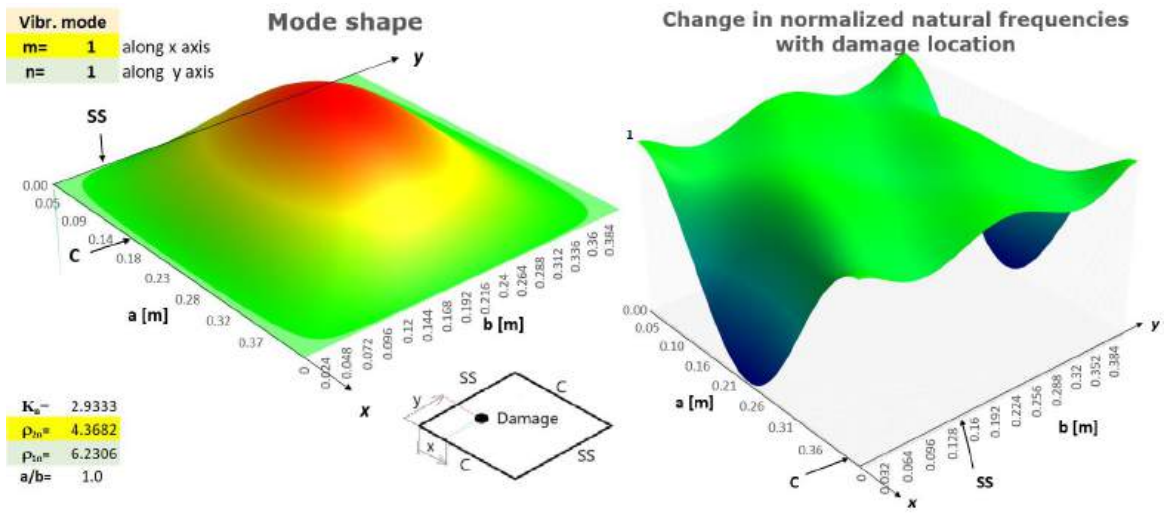

Figure 2: Vibration mode shape (left) for m=1, n=1 of the rectangular plate SS-C-SS-C and the changes in the normalized natural frequencies with the location of the damage (right).

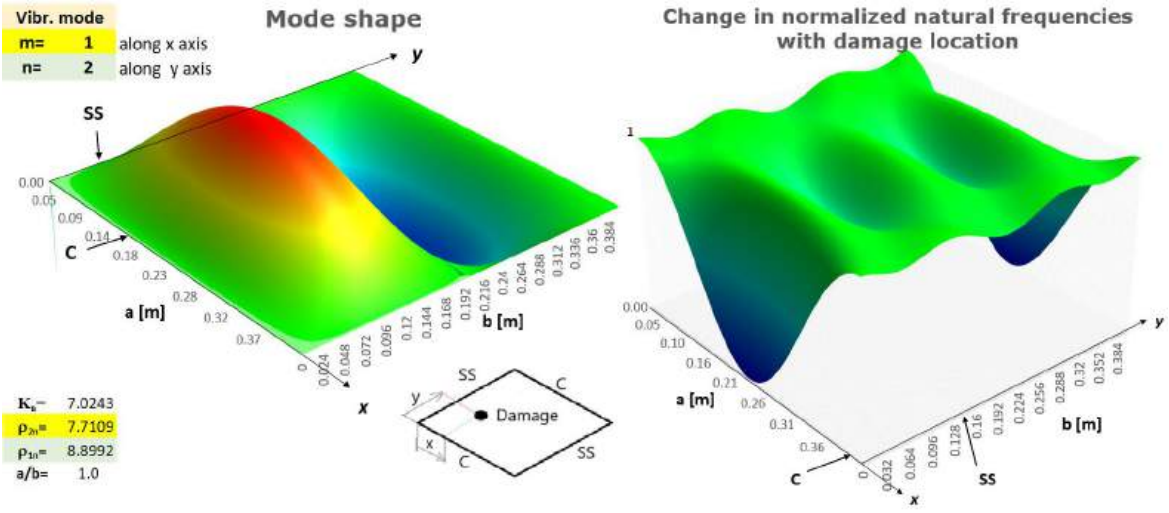

Figure 3: Vibration mode shape (left) for m=1, n=2 of the rectangular plate SS-C-SS-C and the changes in the normalized natural frequencies with the location of the damage (right).

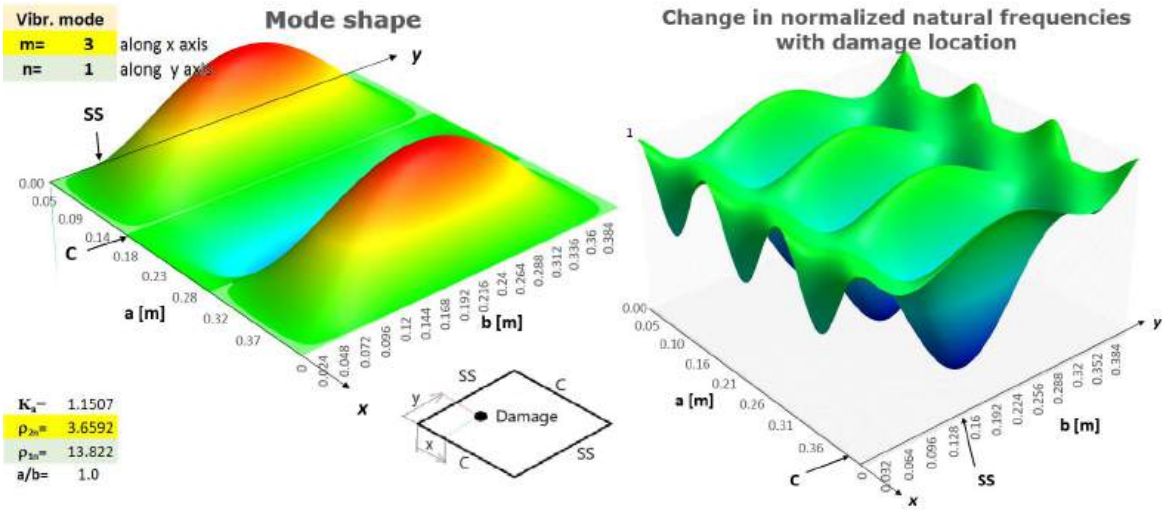

Figure 4: Vibration mode shape (left) for m=3, n=1 of the rectangular plate SS-C-SS-C and the changes in the normalized natural frequencies with the location of the damage (right).

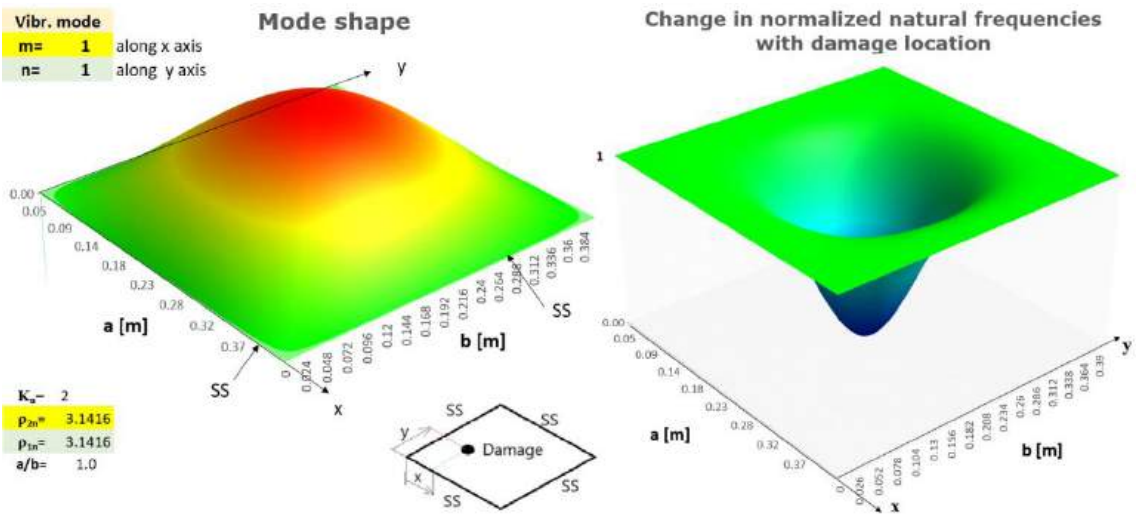

Figure 5: Vibration mode shape (left) for m=1, n=1 of the rectangular plate SS-SS-SS-SS and the changes in the normalized natural frequencies with the location of the damage (right).

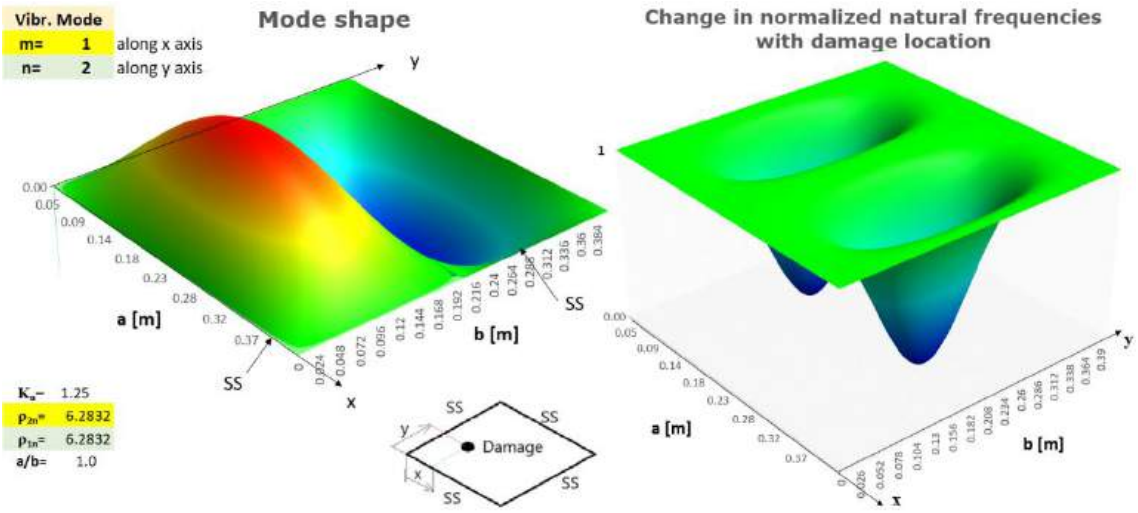

Figure 6: Vibration mode shape (left) for m=1, n=2 of the rectangular plate SS-SS-SS-SS and the changes in the normalized natural frequencies with the location of the damage (right).

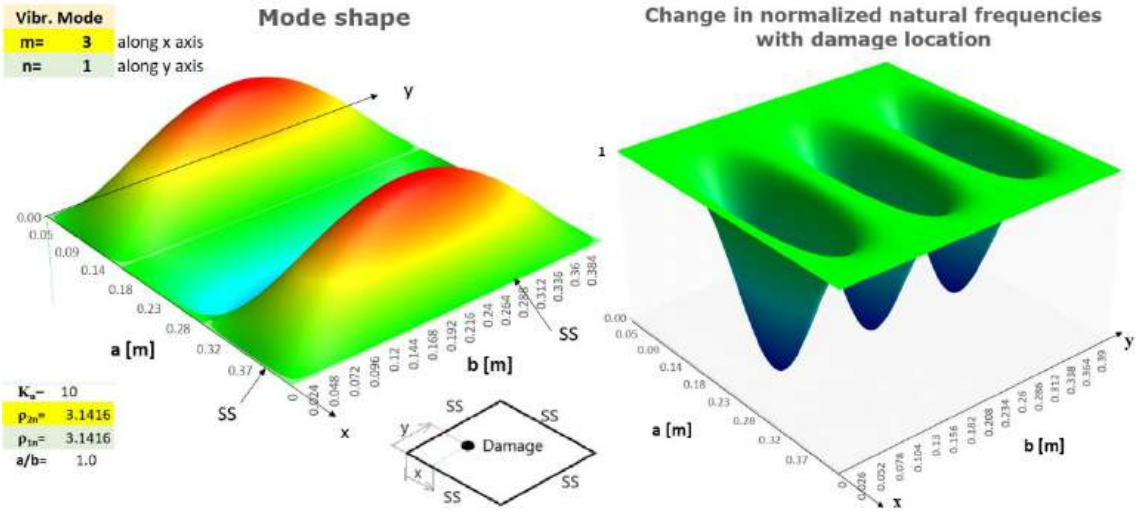

Figure 7: Vibration mode shape (left) for m=3, n=1 of the rectangular plate SS-SS-SS-SS and the changes in the normalized natural frequencies with the location of the damage (right).

5. CONCLUSIONS

For the considered thin rectangular plate model, with the ratio a/b=1 of the sides, the following conclusions can be drawn from the modal analysis of the obtained results, it can be concluded that:

- The normalized modal functions (1) and (4) for rectangular plates represent the product of the modal functions from the beams in the two directions x and y for which the same boundary conditions are imposed;

- For the two types of supports of the rectangular plate, the modal shapes illustrated in figures 2 – 7, do not show significant differences in terms of appearance, although the modal functions (1) and (4) are totally different;

- Relation (3) presents a general form for obtaining the natural frequencies when a plate is damaged depending on the natural frequency of the healthy plate, regardless of the location of the damage;

- For the two types of supports of the rectangular plate, the changing of the natural frequencies of the damaged plate shows a significant difference in terms of appearance for the same vibration mode, although the relationship (3) is the same.

- From the point of view of the dynamic behavior, at the occurrence of a damage on the plate, the influence of the clamped sides (figures 2 – 4) for the SS-C-SS-C plate is much more pronounced compared to (figures 5 – 7) the case of the plate simply supported on all sides (SS-SS-SS-SS).

The paper presents an analytical solution for detecting and localization of a damage in a rectangular thin plate by using a global method considering the dynamic behavior of the structure.

BIBLIOGRAFIE

[1] Gillich G.R., Negru I., Protocsil C., Stanciu E., Minda F.P., Evaluarea integrității structurilor mecanice, Ed. Eftimie Murgu, Reșița, ISBN 978-606-631-081-9, 2018

[2] Hațiegan C, Tufiși C., Identificarea și evaluarea defectelor în plăci elastic subțiri prin analiză modală, Eurostampa, Timișoara, România, ISBN 978-606-32-1172-0, 2022

[3] Soedel W., Vibration of Shells and Plates, Third Edition, Revised and Expanded, Marcel Dekker, Inc., New York, USA, 2005

[4] Leissa A.W., Vibration of Plates, National Aeronautics and Space Administration, NASA SP-160, USA, 1969

[5] Gillich G.R., Praisach Z.I., Modal identification and damage detection in beam-like structures using the power spectrum and time-frequency analysis, Signal Processing, Volume: 96, Special Issue: SI, Pages: 29-44, Part: A; 2014

[6] Gillich N., Tufiși C., Săcărea C., Rusu C., Gillich G.R., Praisach Z.I., Ardeljan M., Beam damage assessment using natural frequency shift and machine learning, Sensors, 22(3), 1118; https://doi.org/10.3390/s22031118, 2022